Jenő Takács

WILEY-VCH

Mathematics of Hysteretic Phenomena

The T(x) Model for the Description of Hysteresis

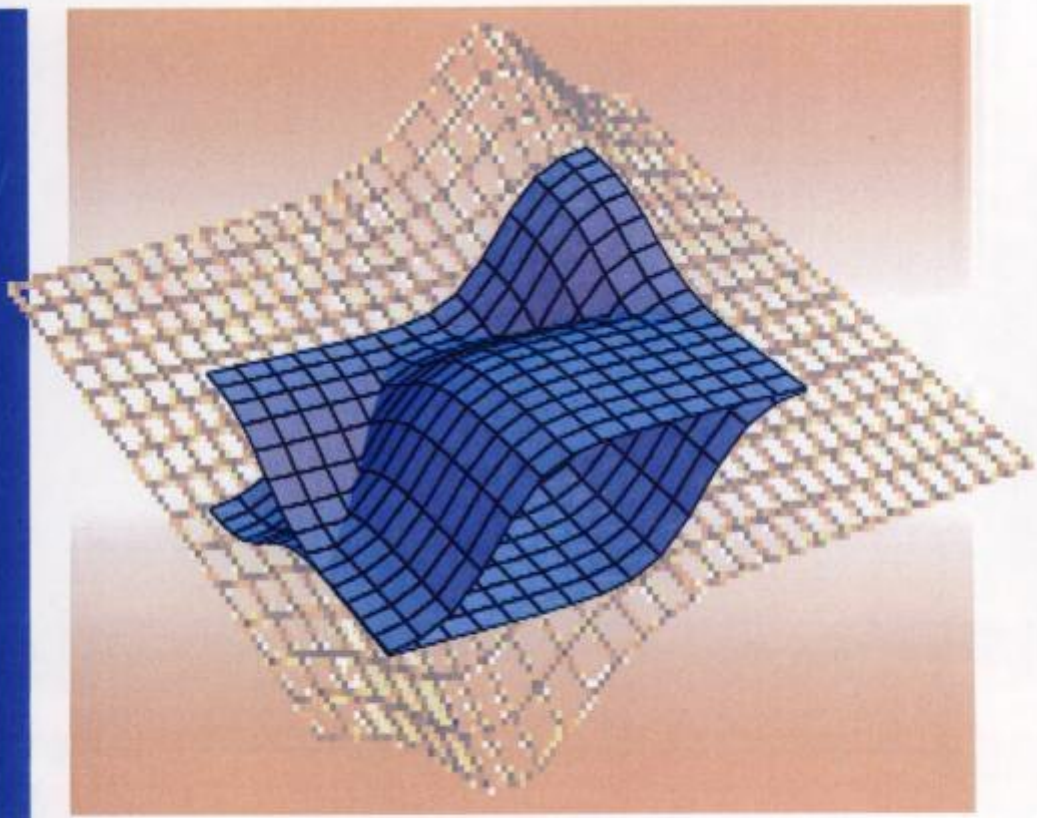

Jenő Takács

Mathematics of Hysteretic Phenomena

The T(x) Model for the Description of Hysteresis

Mathematics of Hysteretic Phenomena. Jeno Takács

ISBN: 3-527-40401-5

Jenő Takács

Mathematics of Hysteretic Phenomena

The T(x) Model for the Description of Hysteresis

WILEY-VCH GmbH & Co.

Author:

Dr. Jenő Takács
University of Oxford, Department of Engineering Science
jenotakacs@aol.com

Library of Congress Card No. applied for

British Library Cataloguing-in-Publication Data
A catalogue record for this book is available from the British Library.

Bibliographic information published by

Die Deutsche Bibliothek

Die Deutsche Bibliothek lists this publication in the Deutsche Nationalbibliografie; detailed bibliographic data is available in the Internet at <http://dnb.ddb.de>.

ISBN 3-527-40401-5

Printed on acid-free paper.

Printing: Strauss-Offsetdruck GmbH, Mörlenbach
Bookbinding: Großbuchbinderei J. Schäffer GmbH & Co. KG, Grünstadt

Printed in the Federal Republic of Germany

Foreword

This book on the Mathematics of Hysteretic phenomena deals with one of the most challenging topics in the theory and applications of magnetic materials. Although a number of important texts on this subject have appeared in recent years, generously referred to here in this book, the approach adopted by the present author is to develop the subject from a set of axioms concerning the geometric shape of Hysteretic trajectories governed by the mathematics of the hyperbolic tangent. Nevertheless his treatment is also shown to be soundly based on the physical principles, with the connections with Boltzman statistics and classical electromagnetism firmly established.

Over several introductory chapters the reader is guided through the steps of how the tangent hyperbolic curve can be transformed to describe saturation effects, hysteresis loops, and the difficult area of reversal loops. This is followed by such central issues as remanent magnetism, permeability and susceptibility, magnetic energy and losses and time varying magnetisation. The later chapters deal with a range of important subjects of practical importance including transient effects, magnetic recording, magnetic viscosity and magnetostriction.

It is self evident that hysteresis plays a central role in all physical phenomena; nature is fundamentally non-linear and hysteretic. Practical applications abound; sometimes the effects are negative, as with losses in power systems, and other times positive, as with magnetic recording applications. The process of reaching a good design in either case requires mathematical, physical and computational modelling. The first stage is that described in this book and is fundamental but before meaningful and robust computations can be carried out, verifiable parameters representing the physical behaviour of magnetic materials have to be obtained by measurement. The results from any software that optimises a practical device will only be as good as the material modelling data it is given and it is encouraging that we now have a body of work dealing with these basic modelling concepts of which this book is an important contribution.

Throughout the text the author has taken great care to set each topic in its historical context giving extensive literature citation and attribution for each step as it unfolds. I believe this book adds to our understanding of the subject and will fulfil an important niche in the tools needed by engineers and educators alike.

Bill Trowbridge
15 May, 2003

Egy kis független nyugalmat
Melyben a dal megfoganhat,
Kértem kérve:
S õ halasztá évrül-évre.
J. Arany

Preface

The idea presented here in this book is not "new". To explain this understatement I have to take the reader back in history. Not in world history perhaps only the history of my professional career. The idea of modeling ferromagnetic phenomena by using the $T(x)$ function came to me in the late 1950s while working on ferromagnetic projects for a small research company called Epsylon Research. On the list of projects were, for instance, pulse data recording, the forerunner of digital data recorders (at the time the word "digital data recording" had not been invented yet) for the British space programme called Woomera (after the place where it was based in Australia). Further projects were the first prototype "black box" for BA, which still makes me shudder every time an aeroplane drops out of the sky. But the long list would be far from complete without mentioning the pocket tape recorder, the first ever (it is the first *to my knowledge*), which became probably the biggest flop in my professional life. The general view, including that of my fellow professionals, was at the time, that the bigger recorder was better and nobody yet dreamt of putting a tape recorder into his pocket or her handbag. Even the thought was extraordinarily absurd and for all practical purposes ridiculous. The mildest professional opinion was that "there is no point in wasting money on the patent, for it will never catch on". The idea was unsellable and was soon forgotten. The "wheel", however, has been reinvented a few times in human history and it took Mr "Walkman" quite a long time, some decades in fact, to reinvent this wheel.

With the change of times my ferromagnetic notes were shelved and I left the field for other pastures. Without the help of the present computer power at my disposal I could not have taken this problem to the present conclusion. The idea surfaced again decades later, when I decided to clear out my old desk and in a file marked "Unfinished " I came across a folder with " Magnetic phenomena" written on its front with large red letters.

The rest was *easy*. It took only a *few years* to resuscitate my *old idea* in this form and to come to the point of publishing it in a book. So, as I said at the beginning, the theory presented here is not new but certainly novel.

At the start of writing this book I set myself an aim to satisfy the curiosity of those connoisseurs who out of sheer scientific interest wanted to see a solutions to long-outstanding problems, the puritans who have no interest in practical applicability. As I progressed through the first chapter I began to see the importance of this theory not only as a pure mathematical description of the phenomena but also as a significant tool in physics,

engineering, and technology, in magnet and magnetic component design as well as in other fields of natural sciences. The realization of this made me write this book for a large spectrum of the scientific public not only those involved in physics and engineering but also others involved in other fields of science where the phenomenon of hysteresis exists.

The Introduction leads the reader through the history of magnetism as a natural physical phenomenon and its development into one of the important fields of physical sciences.

In Chapter 2 the reader is introduced to the various functions namely the $B(x)$, $L(x)$, $M(x)$ and $T(x)$ functions, developed in the last hundred years, for the purpose of describing the saturation phenomenon as a part of the magnetization process. Although the various approaches resulted in different functions, it has been shown that each of them describes the relationship between the exciting field and the resulting magnetization very closely.

Chapter 3 describes the $T(x)$ mathematical model of the hysteresis loop in general form and its variants like the major and minor loops, biased loops and finally it describes the model developed for the inverse hysteresis at the first time in mathematical form.

In Chapter 4 the model described in Chapter 3 is applied to the anhysteretic phenomena, namely the process of virgin and the anhysteretic magnetization.

Chapter 5 describes the reversal process in periodic magnetization. Starting with the first-order reversal it progresses to the mathematical description of the higher-order reversals and the reversals with changing amplitude. By using the Mayergoyz relationship it establishes a relationship between the T distribution and the other two distributions, Gaussian and Lorentzian, used by other mathematical models.

The remanent magnetization is one of the important areas of the magnetization processes and one of the most difficult phenomena to describe in mathematical form due to the double nonlinear process. In Chapter 6 a mathematical description is given not only to the generation of the remanent loop but also to the reversal of the process leading to the accurate mathematical prediction of the multivalued process. The model of the anhysteretic remanence is also included in this chapter.

Permeability, susceptibility, shearing, stored magnetic energy, and hysteresis loss are the important concepts of the practical magnet and magnetic component designer. Graphs, tabulations and rules backed up by experimental results guide those working in this field with very little mathematical verification of the design processes used. In Chapters 7 and 8 this missing link is given to the designer including the first mathematical description of unshearing.

Most of the magnetic components used in electrical or electronic circuitry are subjected to time-varying magnetization processes, normally periodic excitation. In Chapter 9 the distortion due to the double nonlinearity is discussed. The approach to the Fourier analysis of these distortions and the Laplace transform of some of the distorted wave forms are described by the use of the exponential model. Special attention is paid both in the Fourier and the Laplace transformations to the Rayleigh region and the mathematical criterion for the "small"-signal excitation is given. The Fourier analysis and Laplace transform of the distorted waveform resulted from anhysteretic magnetization process is also described in this chapter using the same model.

Magnetic transients or accommodation as it is often called in the literature, theoretically is one of the least explained effects in magnetism. Although this effect is analogous to the transients in electrical circuits most (if not all) of which is mathematically fully formulated, in magnetism the modeling of these transients eluded researchers so far. In Chapter 10 a number of examples are given for the application of the $T(x)$ model to solve the problem of magnetic transients (accommodation) under different starting conditions.

Chapter 11 is devoted to the modeling of the process of analogue magnetic recording.

So far all the phenomena modeled were supposed to be static, i.e. not influenced by the rate of change in the excitation signal. Often, however, the magnetic effects are not independent of the rate of change, leading to more complicated formulation of the hysteresis loop as shown in Chapter 12. When two hysteresis loops interact they form a coupled system as can be seen in the formation of the wasp-waisted and the Perminvar-like hysteresis loops. The mathematical model of these are also given in this chapter.

In some physical phenomena, showing hysteresis, the response is independent of the direction of the excitation. A typical example is the effect of magnetostriction. This kind of hysteresis lead to butterfly-like hysteresis loops. These and similar phenomena showing the same effect are formulated in Chapter 13.

I had and enjoyed the support and encouragement of a number of people in writing this book for which I am grateful. I feel I have to single out Amália Iványi for special thanks. Our long discussions, her comments and suggestions helped me greatly to make this book more readable and enjoyable to my fellow scientists and students. My gratitude goes to Bill Trowbridge for introducing this book.

Finally I am grateful to my wife Judith, for her patience during the time of writing this book.

Oxford, March 2003
JT

Mathematics for Hysteretic Phenomena

1. Introduction

1.1 Introduction

The purpose of this book is not to repeat the well-documented facts about magnetic phenomena or introduce the reader to the elementary knowledge of magnetism but to describe a new model, which gives a mathematical formulation to, so far as one can tell, most known magnetic phenomena. To study the fundamentals there are a number of excellent text books with long lists of publications, which enable the reader to access the latest literature on the subject and learn the basics necessary to read, understand and enjoy the following chapters [1–5].

This book is intended for a wide range of professional people. Some of the chapters are written with the practical magnet designer in mind, giving analytical solutions to practical problems. Other chapters may appeal to the theoretician whose interest is to find the mathematical description of a physical phenomenon. In either case the mathematics is kept at a relatively simple but professional level. I have tried to make the results more expressive to the reader by using graphs wherever possible. The shape of most of these curves is well known to the reader, therefore it will make the judgment easy on the applicability of the model presented here in this book.

Magnetism is one of the most difficult areas of physical science. The phenomenon of magnetism itself has been known in antiquity from its familiar property – its power of attracting iron – since the time of Thales. In China magnets have been used as compasses in navigation since about 4000 BC. Its name originated from the place named Magnesia in Asia Minor, where the substance magnetite or lodestone (known for its magnetic properties) was found in abundance. The Greeks used it as a crude compass as well, before artificial magnets were employed for that purpose and they also provided probably the first documentation of the magnetic effect in 800 BC. The first known description, in "modern" times, of the magnetic behaviour is attributed to Petrus Peregrinus (Peregrinus de Maricourt) a French military engineer and scientist, who in 1269 described the study of magnetism in his "Epistola de magnete". Later, at the turn of the 16th century, William Gilbert's "De Magnete" describes the Earth as a large magnet (giant lodestone) of a spherical shape.

After a humble and slow beginning great scientists like Gilbert (or Gylberde), Oersted, Gauss, Faraday and Weber, amongst others, contributed to the better understanding of magnetism. Weber [5] suggested that every magnet was composed of magnetized domains, little magnets randomly fitted into substances that could be magnetized. These magnetic particles are now believed to be of molecular dimensions. According to Alfred Ewing's theory [6] of mutual interaction between magnetic particles, developed from Weber's suggestion, an ordinary piece of magnetisable iron is composed of molecular magnets arranged in a haphazard fashion so that the vectorial sum of the their magnetic moments appears to be zero on the macroscopic scale. In this state they neutralize each other and the specimen appears to be magnetically neutral, i.e. they show no magnetic attraction or

Mathematics of Hysteretic Phenomena. Jeno Takács

ISBN: 3-527-40401-5

repulsion on external bodies. Although the atomic moments show some order, even before magnetization, inside the domains, it is the domains that are randomly oriented in the demagnetized state. When the magnetically neutral specimen is placed in a magnetic field however, the disorder disappears and more elementary magnetic particles line up in the direction of the applied field with their axes parallel to the field. Poles appear at the ends of the magnet, while the central portions exhibit only weak magnetic powers where equal and opposite poles neutralize each other's effects. This theory primarily explains the fact that when a magnetized iron is broken or cut each of the parts show the same magnetic properties and new free poles are created. This process can be repeated over and over again with the same effect. Secondly, when all the domains are arranged in order and their axes all parallel with the applied field and no more domains are left unturned, the magnet reaches the state of saturation. The magnetic order inside a ferromagnetic substance on the atomic scale also gives a possible explanation as to why it is that the initial permeability (before any magnetization) is not zero for most ferromagnetic materials. This is the quantity represented by the first derivative of the virgin magnetization curve at zero field excitation. For further explanation and details on this subject see Chapters 4 and 7.

At the beginning of the 20th century, Pierre Weiss [7,8] postulated the existence of the elementary magnet, called magneton, analogous to the elementary electrical charge the electron and defined it as the unit of magnetic moment. The idea fitted the Bohr model well and later the existence of the magneton was experimentally verified by Gerlach and Stern [9].

Whilst the explanation of the magnetic phenomena progressed steadily with experimental verification, its mathematical modeling was lagging behind. There was and still remains the difficult task to model and formulate the double nonlinearity in mathematical form, characteristic of these magnetic processes. First, over a certain strength of the applied field the magnetic state of the specimen will not alter, irrespective of how much the field is increased. That is to say that when all the domains are forced to line up with the field and no more change can be expected in the magnetic state of the material, the specimen has reached a state of saturation. Secondly, when the field is reversed, the magnetized sample will not take up the expected state, which was determined by the original value of the field, but a different one, showing that the magnetic state of the specimen is not a single-valued function of the applied magnetic field. The same field, depending on whether it is increasing or decreasing will produce two magnetic states within the sample. Up and down cycling with the field will produce repeatable results but each field will produce two magnetic states exhibiting the phenomenon called hysteresis (Greek: hysteros = later). The word hysteresis to describe this phenomenon was introduced by Ewing in 1881 [10,11].

These nonlinearities, the saturation and the hysteresis, are discussed and formulated in details in Chapters 2 and 3, respectively, by using the model defined and formulated in Chapters 1 and 2.

Within the confines of a hysteresis loop bordered by the major loop there is a field whose geometry is governed by laws of tangent hyperbolic nature. Lines, belonging to this field must be of a specific shape and the movements of points are restricted to trajectories determined by a set of rules. As in other systems there are the axioms upon which the geometry is built. These are the general rules of the "game" that all elements of the field will obey. If we are to study the lines and their behaviour patterns in the field of hysteresis and to draw conclusions concerning the physical phenomena they represent, then these

axioms governing the behaviour must be defined before our study begins. The following axioms are necessary to describe the field within the hysteresis loop.

Axiom 1. The field is confined to the area bordered by the major hysteresis loop.
Axiom 2. Inside the area of a hysteresis loop all lines are of tangent hyperbolic shape.
Axiom 3. Through one point inside a hysteresis loop an infinite number of tangent hyperbolic curves can be drawn whose individual shape and behaviour is predetermined by one particular past history.
Axiom 4. On every point, within the confines of a major loop, lies one and only one unbiased symmetrical minor loop. Therefore, every point can be characterized by one x_m value representing the crossover point of the up and down going part of that particular minor loop.
Axiom 5. Within the field, through two points only two tangent hyperbolic curve can be drawn. One is a member of the ascending the other of the descending family of the lines forming the field. As a consequence, the two points determine one and only one closed minor hysteresis loop, which belongs to the field. That is to say that the shortest line between two points is a tangent hyperbolic curve in the field but the path is direction dependent (The name "closed loop" above emphasizes the fact that there are "open loops" as well in the system as we will see in Chapter 5, which conform, to different rules.) This Axiom is equivalent in other models to the congruency property.
Axiom 6. All upwards going lines mimic parts of the ascending leg of the major hysteresis loop and similarly all down-going lines mimic the descending leg of the major loop.
Axiom 7. All "constants" (like the ones marking shifts of lines within the enclosed field) shall change according to the tangent hyperbolic rule.

The model is not based solely on geometrical axioms. Other rules come from the nature of magnetism and are confirmed by observations and experiments. These were recognized long ago and some models incorporated them in order to fit their results to observations and experimental data. The properties incorporated into this model are the "return-point-memory" property and the "wiping-out" property [12].

The first of these properties attributed to magnetic materials, the "return-point-memory" makes the cyclically magnetized sample remember the peak value, positive or negative, of the magnetization where the process has been previously stopped and/or reversed. Due to this property combined with Axiom 3, the magnetized sample remembers that symmetric minor loop the state of magnetization moved to, characterized by a single x_m value before it was reversed.

The second, "wiping-out" property makes the medium remember the last extreme (minimum or maximum) where the magnetization stopped or changed direction, whilst all the others preceding the last maximum or minimum are wiped out from the memory of the substance.

The recognition and the first description of these effects are attributed to Madelung who published his paper on his observations as early as 1905 [13]. These attributes formulated by Madelung make the ferromagnetic hysteresis a Markovien nonlinearity[1].

[1] Markov Andrei Andreyevich (1856–1922). Russian mathematician, formulator of the stochastic (random) process.

The model presented in this book is essentially an attempt to describe experimental facts in general mathematical terms and makes some attempt to explain the physical causes of either the saturation or the hysteresis. It is not a wholly phenomenological approach [14] since it has its foundations rooted in the Boltzmann model of magnetic saturation as shown in Chapter 3.

Although the model illustrated in this book is primarily intended to describe the hysteretic behaviour of ferromagnetic substances, its basic principle should be applicable to other fields of science, manifesting effects similar or identical to the hysteretic phenomena in Magnetics. Hysteresis is observed in other scientific disciplines such as biology, control engineering, semiconductor physics and superconductivity [15] to name just a few.

References

[1] S. Chikazumi, *Physics of Magnetism* (Robert E. Krieger Publ. Co., Malabar, Florida, 1986).
[2] S. Chikazumi, *Physics of Ferromagnetism* (Clarendon Press, Oxford, 1997).
[3] A. H Morrish, *The Physical Principles of Magnetism* (John Wiley and Sons Inc., N.Y., 1965).
[4] G. Bertotti, *Hysteresis in Magnetism* (Academic Press, London, 1998).
[5] W. Weber, Uber den zuzammenhang er lehre vom diamagnetismus mitter lehre von dem magnetismus und der elektricitat. Ann. Phys. Chem. (Pogg. Ann). LXXXVII. **No. 10.** pp.145–189 (1852).
[6] J.A. Ewing, *Magnetic Induction in Iron and Other Metals* (The Electrician Publishing Co., London, 1893).
[7] P.E. Weiss, La variacion du ferromagnetisme avec la temperature. Comptes Rendus **143**, pp.1136–1139 (1906).
[8] P.E Weiss, L'Hypothese du champ moleculare et la propriete ferromagnetique. J. de Phys. **VI**, pp. 661–690 (1907).
[9] W. Gerlach and O. Stern, Uber die richtungsquantelung im magnetfeld. Ann. Phys. (Leipzig) **74. No.16**, pp.673–699 (1924).
[10] J.A. Ewing, Effects of stress on the thermoelectric quality of metals. Proc. Roy. Soc. **XXXII**, pp. 399–402 (1881).
[11] J.A. Ewing, On the production of transient currents in iron and steel conductors by twisting when magnetised or by magnetising them when twisted. Proc. Roy. Soc. **XXIII**, pp. 21–23 (1882).
[12] I.D. Mayergoyz, Mathematical Models of Hysteresis (Springer-Verlag N.Y., USA, 1991).
[13] E. Madelung, Uber magnetisierung durch schnellverlaufende strome und die wirkungweise der Rutherford-Markoni magnetodetektors. Ann. Phys. **l.1. no. 5**, pp. 861–863 (1905).
[14] J. Takács A phenomenological mathematical model of hysteresis. COMPEL Int. J. Comp. Math. E. E. Eng. **20 No.4**, pp. 1002–1014 (2001).
[15] I.D. Mayergoyz and T.A. Keim, Superconducting hysteresis and the Preisach model. J. Appl. Phys. **67. No.9**, pp. 5466–5468 (1990).

2. Saturation Effect

2.1 L(x), B(x), T(x) and M(x) Functions

A certain characteristic temperature, above which their properties suddenly change, sets the magnetic behaviour of ferromagnetic materials. This behaviour is governed by Curie's law and the critical point on the temperature scale is called the Curie temperature [1]. Above the Curie point these substances show paramagnetic behaviour but the Curie points of most materials, particularly those used for practical application are in the range of hundreds of °C. Below this temperature in the ferromagnetic region, the relationship between applied field and magnetization is highly nonlinear. When a ferromagnetic substance is subjected to an increasing magnetic field its magnetic induction only increases to a point above which its state will not change and it becomes independent of the applied magnetic field. This is an other way of expressing the physical phenomena, that inside a magnetic specimen, there are a finite number of mobile elementary magnetic dipoles, called domains, which can line up in the direction of the field applied. When all the domains are turned with their axes parallel with the field then the sample runs into magnetic saturation and no further change will occur in its magnetic state.

In 1905 Langevin [2] produced a theory describing paramagnetism, which was initially applied by Weiss to [3] ferromagnetic materials as well. Although strictly speaking it is only applicable to gaseous paramagnetic substances, while solids obey the Curie–Weiss law [4], his results eventually culminated in the Langevin function (L(x)), shown in normalized for in (2.1). This also describes the ferromagnetic saturation effect.

$$\mathrm{L}(x) = C_1 \coth x - C_2/x. \tag{2.1}$$

Brillouin later improved Langevin's theoretical approach. His mathematical solution to this phenomenon, the Brillouin function (B(x), see (2.2) [5] describes the effect by using similar hyperbolic functions. In fact, it is the quantum-mechanical analogue of the Langevin function. Under some conditions (see below) the two functions approach each other and become the same. Other theoretical approaches to ferromagnetism, since the introduction of these theories, have also greatly improved the understanding of the physics of magnetic behaviour but the shape of the saturation curve is not described any better than initially done by Langevin,

$$\mathrm{B}(x) = C_3 \coth C_3 x - C_4 \coth C_4 x. \tag{2.2}$$

On a large macroscopic scale with the appropriate choice of constants, both functions describe the saturation effect well. The reader has to be warned, however, that both functions show singularity around $x = 0$ therefore they require extreme caution in applications.

Mathematics of Hysteretic Phenomena. Jeno Takács

ISBN: 3-527-40401-5

When $C_3 = C_1$ and $C_2 \rightarrow 0$ then $B(x) \rightarrow L(x)$ as a limit.

Let us now consider the case of the single electron, when the atom has only one unpaired electron similar to Ni. As the spin (s) of the electron can only be $\pm$ ½ the electron moment as the result of quantization, can have only two possible states. It can only align its moment parallel ($s = +1/2$) or antiparallel ($s = -1/2$) to the direction of the applied field. As a result the magnetization by using Boltzman statistics, will be [6]

$$M(x) = C_5 \tanh C_6 x, \tag{2.3}$$

representing the irreversible magnetization. For further details on this theory refer to Chapter 3. The Brillouin function will also approach this function in the single electron case.

The $T(x)$ function, on which the model introduced here is based, is the combination of a hyperbolic and a linear function as shown in (2.4), where the two terms are well matched to the reversible and the irreversible components of the magnetic induction, respectively.

$$T(x) = A_0 x + B_0 \tanh C_0 x. \tag{2.4}$$

Unlike the $L(x)$ and $B(x)$, the $T(x)$ function, is only partially based on existing theories. Nevertheless, it describes the saturation effect as well as the other two functions and makes the formulation of the hysteresis easier, as we will see in Chapter 3. One has to be aware of the fact that mathematical solutions to problems in physics are often formulated in different mathematical expressions, depending often on the intermediate steps taken during calculation, but describe the physical phenomenon equally well. In fact, I would not be surprised at all if one day a theoretician produced a full mathematical solution to the magnetic saturation effect, based on the Boltzmann statistics, in the form of the $T(x)$ function. Since this approach is not exactly heuristic but based on the Boltzman approach, when it happens this model may become the sole legitimate noncurve-fitting mathematical model that formulates not only the saturation and the hysteresis but also other magnetic phenomena as well on a macroscopic scale.

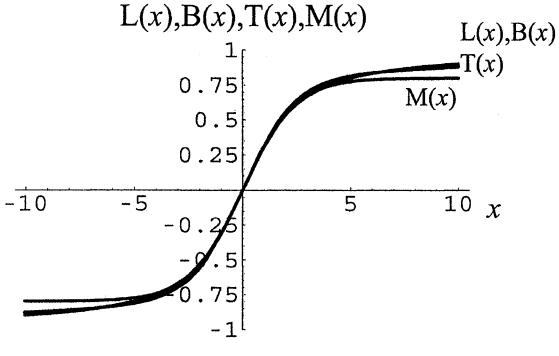

Figure 2.1: The Langevin $L(x)$, Brillouin $B(x)$, $T(x)$ and $M(x)$ functions

Figure 2.1 depicts all four functions, L(x), B(x), M(x) and T(x). For the plotting calculations the following numerical values were used: $A_0 = 0.008$, $B_0 = 0.8$, $C_0 = 0.4167$, $C_1 = C_2 = 1$, $C_3 = 1.02$, $C_4 = 0.1$, $C_5 = 0.8$ and $C_6 = 0.4167$.

The graph shows a good fit of the L(x), B(x) and T(x) functions for all x values including the deep saturation region. Where the process does not drive the magnetic specimen into deep saturation as it is in most practical applications, the linear term in T(x) can mostly be neglected ($A_0 \approx 0$) leaving the always dominant tangent hyperbolic term on its own. The T(x) function then goes into the M(x) function.

2.2 The T(x) Model

Let us consider a simple model of a solid in equilibrium whose molecules possess magnetic moment. We will assume, for simplicity that each molecule of the solid is a dipole with the same magnetic moment **m**. Let us apply now a uniform magnetic field **H** to the solid. In quantum mechanics only discrete energy states are allowed, which in this case is limited to two possible states. One is when **m** the magnetic moment is aligned parallel to the magnetic field representing the energy state of $\varepsilon_p = \mathbf{mH}$ and the other is the when the moment is antiparallel to the field with energy state of $\varepsilon_a = -\mathbf{mH}$. This corresponds to the case in practice when the dipole has two possible spin values of $\pm$ 1/2 [7]. Under the influence of the applied magnetic field some of the dipoles will change their orientations and will point in the direction of the field. When the field is weak only a small number of the dipoles will point in this direction. When only half of the total number of dipoles aligns up parallel to the field, then the effect of the field will be zero on the sample since the other dipoles in equal number will align antiparallel to the field. In between the minimum and the maximum energy states the number of dipoles will change following the Boltzmann distribution [8–10]. When n_0 number of dipoles has zero energy and n have energy ε, the relation between n and n_0 is determined by the Boltzmann factor in the following form.

$$\frac{n}{n_0} = \exp\left(-\frac{\varepsilon}{kT}\right). \tag{2.5}$$

Here k is the Boltzmann constant and T is the absolute temperature.

When the solid is at a temperature of T the occupation numbers n_1 and n_2 of the two energy levels ε_1 and ε_2 can be written as

$$n_1 = \exp\left(-\frac{\varepsilon_1}{kT}\right), \; n_2 = \exp\left(-\frac{\varepsilon_2}{kT}\right), \tag{2.6}$$

where $n_1 + n_2 = N$ the total number of dipoles, then

$$n_1^* = \frac{n_1}{N} = \frac{\exp\left(-\frac{\varepsilon_1}{kT}\right)}{\exp\left(-\frac{\varepsilon_1}{kT}\right) + \exp\left(-\frac{\varepsilon_2}{kT}\right)}, \tag{2.7a}$$

$$n_2^* = \frac{n_2}{N} = \frac{\exp\left(-\frac{\varepsilon_2}{kT}\right)}{\exp\left(-\frac{\varepsilon_1}{kT}\right) + \exp\left(-\frac{\varepsilon_2}{kT}\right)}. \tag{2.7b}$$

The total energy of the system

$$E = n_1^* \varepsilon_1 + n_2^* \varepsilon_2, \tag{2.8}$$

where

$$\varepsilon_1 = -\mathbf{mH} \text{ and } \varepsilon_2 = \mathbf{mH}, \tag{2.9}$$

corresponding to the two distinct energy states.

After the substitution of (2.7) and (2.9) into (2.8) we can rewrite the total energy in the following form

$$E = -\frac{\exp\left(-\frac{\varepsilon_1}{kT}\right)}{\exp\left(-\frac{\varepsilon_1}{kT}\right) + \exp\left(-\frac{\varepsilon_2}{kT}\right)} \mathbf{mH} + \frac{\exp\left(-\frac{\varepsilon_2}{kT}\right)}{\exp\left(-\frac{\varepsilon_1}{kT}\right) + \exp\left(-\frac{\varepsilon_2}{kT}\right)} \mathbf{mH}. \tag{2.10}$$

The total energy, in the equilibrium state, is the product of the total magnetic moment and the field [11], therefore

$$E = -\mathbf{MH}, \tag{2.11}$$

and the total magnetic moment of the sample **M** can be written in the form

$$\mathbf{M} = \frac{E}{\mathbf{H}} = \mathbf{m}\frac{\sinh\frac{mH}{kT}}{\cosh\frac{mH}{kT}} = \mathbf{m}\tanh\frac{mH}{kT}. \tag{2.12}$$

Here **M** depends on the average dipole moments. Adding a linear term to (2.12) representing the reversible magnetization will take us to (2.4) (see T(x) function) [12].

2.3 Other Models

As we can see, the various approaches produced different functions to describe the saturation effect, which characterizes the ferromagnetic materials. Amongst the best known models the various Preisach models are the most widely used. A crucial factor in any model is the mathematical description of the interaction between the magnetic moments and the applied field in both the interaction and the saturation regions. The statistical distribution of the magnetic moments or probability density, describing this relationship is a bell-shaped function, as we know from experience. This function, which for the Preisach model is

called the Preisach function, is often chosen to be Lorentzian or Gaussian, which is usually referred to as normal distribution [13] (for more on the Preisach function see Section 5.3). The choice of the Gaussian function over and above any other is normally justified on two grounds. The first is that normal distribution is often used to describe probability density in other natural phenomena. The second is that the integral of a Gaussian function can be evaluated in closed form. These two attributes however are not unique to the Gaussian function and other functions can also be selected on these grounds or derived from given criteria.

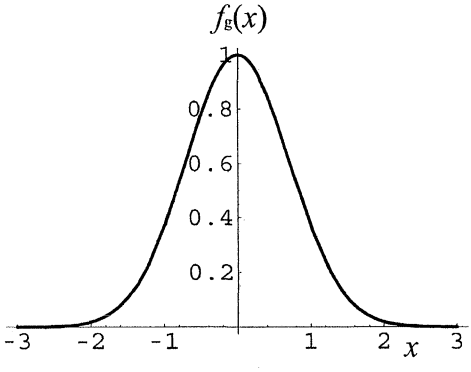

Figure 2.2: Gaussian distribution function $f_g(x)$ for $C_7 = 1$ and $a = 1$

The Gaussian function $f_g(x)$ in simple form is given in (2.13) and plotted in Figure 2.2

$$f_g(x) = C_7 \exp\left[-\left(\frac{x}{a}\right)^2\right]. \tag{2.13}$$

The integral of $f_g(x)$ between the limits of 0 and x, is known as error function erf(x), and defined as

$$erf(x) = \frac{2}{\sqrt{\pi}} \int_0^x \exp(-x^2)\, dx\,. \tag{2.14}$$

This function in (2.14) is plotted in Figure 2.3.

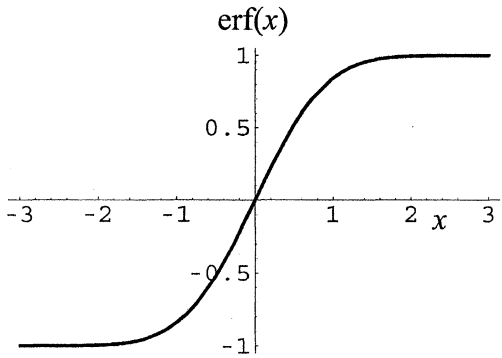

Figure 2.3: The error function erf(x) calculated from (2.14)

This function can be closely matched by the T(x) function by choosing the appropriate parameters as shown in Figure 2.4.

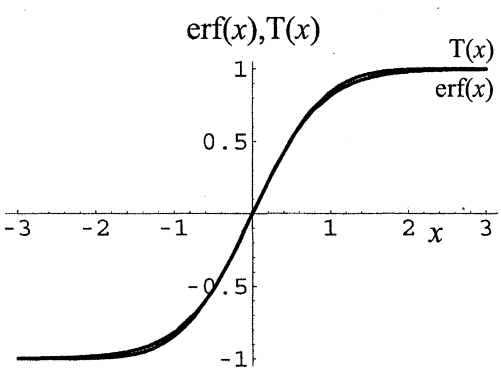

Figure 2.4: The erf(x) and the T(x) functions

The description of the saturation effect in mathematical form by using any of the functions mentioned above is an approximation. The most important factor in choosing the right function is its closeness to match the physical phenomena of saturation.

As we have seen, the first derivative by x of the distribution function is the distribution density function, [11] which in the case of the T(x) function (see (2.4)) is

$$\frac{\mathrm{d}}{\mathrm{dx}}\mathrm{T}(x) = B_0 C_0 \ (\mathrm{sech}\ C_0\ x)^2 + A_0 . \tag{2.15}$$

When $A_0 = 0$ this function shows not only a striking similarity to the Gaussian function shown in Figure 2.2, but by selecting the constants B_0 and C_0 appropriately this function, shown in Figure 2.5, can be made very close to the so-called normal probability distribution function.

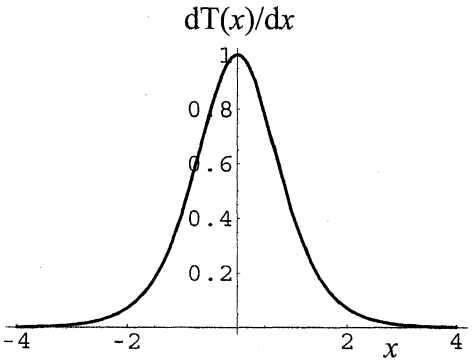

Figure 2.5: The probability density of the T(x) function

When the reversible magnetization is not negligible then the probability density function differs only by the A_0 constant from the bell-shaped curve shown in Figure 2.5.

References

[1] P. Curie, Magnetic properties of bodies at various temperatures. Ann. Chim. Phys. **V**, pp.289–405 (1895).
[2] M.P. Langevin, Magnetisme et theorie des electrons. Ann. Chim. Phys. **V**, pp. 70–127 (1905).
[3] P.E. Weiss, La variacion du ferromagnetisme avec la temperature. Comptes Rendus. **143,** pp.1136–1139 (1906).
[4] P.E. Weiss, L'Hypothese du champ moleculare et la propriete ferromagnetique. J. de Phys. **VI**, pp.661–690 (1907).
[5] M.L. Brillouin, Les moments de rotation et le magnetisme dans la mechanique ondolatoire. J. Phys. Radium **VIII**, pp.74–84 (1927).
[6] J.S. Dugdale, Entropy and its Physical Meaning (Taylor and Francis, London, 1996).
[7] Y.-K. Lim, Problems and Solutions on Thermodynamics and Statistical Mechanics (World Scientific, Singapore, 1995).
[8] L. Boltzmann, Vorlesungen uber Gastheorie (J.A. Burth., Leipzig, 1896–98).
[9] L. Boltzmann, Lectures (California University Press, Berkley, 1962).
[10] E.H. Kennard, Kinetic Theory of Gases (McGraw-Hill, NY., 1938).
[11] D.G. Rees, Foundation of Statistics (Chapman and Hall, London, 1987).
[12] J. Takács, A phenomenological mathematical model of hysteresis. COMPEL Int. J. Comp. Math. E. E. Eng. **20. No. 4**, pp. 1002–1014 (2001).
[13] E. Della Torre, Magnetic Hysteresis (IEEE Press, N.Y., 1999).

3. Hysteretic Phenomena

3.1 Hysteresis

When a ferromagnetic specimen is subjected to a cyclic magnetic field the magnetic state of the sample will not follow the magnetizing field but it will lag behind it. This phenomenon was observed and published by Warburg as early as 1881 [1]. This sluggishness of the induction in the magnetizing process is called hysteresis and the curve it follows, describing the relationship between the applied field and induction, is referred to as the hysteresis loop, derived from the Greek word of hysterein, meaning to be behind. The term "hysteresis" was introduced in magnetism by Ewing also in 1881 [2]. This relationship, between field and induction, is irreversible everywhere inside the hysteresis loop, except on one specific line namely the anhysteretic magnetization curve. Although empirical evidence for a long time pointed to irregularities, dislocations, and impurities in the magnetic material as to the cause of this effect, the theoretical verification of this hypothesis is still missing and all these should be regarded as assumptions. It appears, however, that the internal friction due to the presence of these imperfections in the metal gives rise to hysteresis. Similarly the anisotropic nature of the crystalline structure of the ferromagnetic substance can lead to jumps, a form of switching of the magnetic moments, causing lag between the magnetic state of the substance and the applied field. We can assume, based on this generally accepted view, that an isotropic magnetic sample void of imperfections would follow a reversible magnetization curve represented by a single-valued function between induction and the applied magnetizing field. The process would then be anhysteretic, which, with its representative curve, will be discussed in Section 4.2 in detail. The presence of lag in the induction versus field relationship represents the second nonlinearity in the magnetizing process.

The mathematical modeling of the hysteresis loop is one of the classic problems of magnetism and its history goes back to the early part of the 20th century. During that time a large number of attempts were made to fit mathematical expressions to magnetic data, often with some dubious results. In general terms all the different approaches fall into two categories. One, but not necessarily the first category is theoretically based, as the theory of micromagnetics of Aharoni [3,4] and Brown [5–8]. The work of others, like Jiles and Atherton [9] is based on wall movement and domain rotation following Kersten [10,11], Becker and Doring's earlier works [12], which also fall into this first category. The results of these models produced by this approach are overcomplicated and difficult to apply. In spite of all this and other contributions to this field (like Bertotti [13,14]) it is not very likely that a general and accurate analytical model is going to emerge in the near future. All the curve-fitting approaches falls in the second category, which are effectively no more than mathematical curve-fitting exercises to known magnetic data. A great number of attempts

Mathematics of Hysteretic Phenomena. Jeno Takács

ISBN: 3-527-40401-5

were made to fit the hysteresis loop with functions, including the simplest approach of power series by Brauer [15], $\tan^{-1}$ function by Karlqvist in 1954 [16], rational polynomials like Rivas et al. [17] and earlier Fisher and Moser in 1956 [18]. Trutt et al. in 1968 [19] applied piecewise linear approximation to fit the hysteresis loop and Widger proposed rational fraction approximation in 1969 [20].

Presently there are a few models left that can be regarded as classical. The names and numbers are debatable depending on one's preference but on the ground of general acceptance the following three models can be listed that fall into the first category: Stoner–Wohlfarth (S–W) model [21] a theory based on crystalline anisotropy, Jiles–Atherton (J–A) model [22] based on isotropic polycrystalline structure with domain wall motion and the Globus model [23–25] postulating ring-shaped polycrystalline structure for the magnetic substances.

One of the most remarkable contributions to hysteresis modeling was made by Preisach in 1935 [26]. His model, to my knowledge, is the only survivor of almost seven decades of scientific scrutiny. Although it is only a complex curve-fitting program, therefore falling into the second category, it does not give much of an insight into the physical phenomena of magnetization nor into the magnetic properties of the ferromagnetic substances, though in the knowledge of the hysteresis data it can give a reasonable prediction of the magnetic behavior of the substance. In those long years it has been modified, added to and updated by a number of people [27–29] so now a number of variants exist, for instance, the accommodation, wiping-out property, vector, moving model, etc. By including certain new properties into the model or tailoring towards specific applications, particular models have been developed based on the classical Preisach model. After so long its usefulness and popularity is still high amongst theoreticians and the practical users alike.

The list of approaches given here to describe the hysteresis loop in mathematical form is far from complete and only a small number of references, those that I personally regarded as "milestones" in the history of the development of this subject, are given.

3.2 Major and Minor Hysteresis Loops

The well-known regular shape of the hysteresis loop is the starting point of this model based on the functions specified below. By using certain functions, mimicking the sigmoid shape of the hysteresis loop, as it is often called, one can formulate the phenomena of saturation and hysteresis. We recall here (2.4), which describes the saturation effect in a mathematical expression in the hysteresis [30]. The reader has to remember that by an appropriate normalization we can convert the physical quantities like magnetic induction and field into dimensionless quantities in order to conform to the rules of "pure" mathematics. In the rest of the book in all calculations, although their physical names are going to be used for description, the symbols refer to normalized dimensionless concepts. This can be done without affecting the general validity of the model and the following calculations.

In order to describe the hysteresis with the $T(x)$ function it is necessary to shift it in a horizontal as well as vertical direction symmetrically as it physically happens in a hysteresis loop. When $T(x)$ is shifted once in a horizontal direction by a_0 and in vertical direction by b_1, we come to a set of equations describing the ascending and descending part of a loop like a hysteresis one (see (3.1)). The two curves run between two limits that will be marked as x_m (positive extremum) and $-x_m$ (negative extremum). At these two points they cross over and this crossing provides the mathematical criteria for finding the value of b_1 as shown in (3.2)

$$f_+ = \tanh(x - a_0) + A_0 x + b_1 \quad \text{for increasing } x \text{ values} \tag{3.1a}$$

$$f_- = \tanh(x + a_0) + A_0 x - b_1 \quad \text{for decreasing } x \text{ values} \tag{3.1b}$$

At the crossover point when $x = x_m$, and $f_+ = f\,b_1$ can be calculated from (3.1) as

$$b_1 = [\tanh(x_m + a_0) - \tanh(x_m - a_0)] / 2 \tag{3.2}$$

When A_0 is negligibly small, much smaller than unity, the maximum value of the first term, as in most of the practical cases, the expressions in (3.1) go into (3.3) while b_1 in (3.2) remains the same.

$$f_+ = \tanh(x - a_0) + b_1 \quad \text{for increasing } x \text{ values} \tag{3.3a}$$

$$f_- = \tanh(x + a_0) - b_1 \quad \text{for decreasing } x \text{ values}. \tag{3.3b}$$

When the maxima (positive and negative) are increased the hysteresis loop stretches up to a certain size beyond which it will not change irrespective of the further increase in the exciting field. The largest loop achieved in this way is by definition, the major hysteresis loop of the magnetic substance. Inside this major loop an infinite number of minor loops can exist whose shape and size are determined by the amplitude of the field applied to the substance.

Figure 3.1 depicts a major loop calculated from (3.3) for $a_0 = 1.5$ and $x_m = 4$. Symmetrical minor loops, members of the set, are also shown for x_m values of 2 and 1.

The loops calculated from (3.1) when the reversible magnetic induction is not negligible (in the calculation $A_0 = 0.05$) are shown in Figure 3.2. The other numerical parameter values used in the calculation are the same as before. As one can see, the loci of the crossover points of the minor loops lie on the curve running in the middle of the major loop. This curve is called the anhysteretic induction or magnetization curve f_s and its significance and definition will be discussed in detail in Chapter 4.

At this point we can rightly ask the question, how many free parameters are needed to fully define the hysteresis loop, which characterizes the properties of a ferromagnetic material? In other words how many degrees of freedom do we have to describe a regular sigmoid-like hysteresis loop, encountered in most practical cases.

When considering the symmetrical major hysteresis loops two points seem to be obvious. One is where the loop cuts the horizontal and the other where it cuts the vertical axis. The first is called coercivity, which is the value of the field needed to reduce the induction to zero from saturation. In the T(x) model here this quantity is represented by the symbol a_0. The second is known as the remanence f_r and this is the value the induction shrinks to, when the field of excitation is switched off at or above saturation level. This is a remarkable feature of the hysteresis that one can get a flux density even in the absence of an external field. Permanent magnets are based on this phenomenon. Although as one can see this is an important parameter, but as far as the model is concerned it is more convenient to specify the point x_m where the up and down going parts of the hysteresis loop intersect. Through the condition of $f_+(0) = f_r$ the two parameters are linked as shown in (3.4). Here $f_+(0)$ represents the value of f_+ at $x = 0$, which is the remanence, marked f_r, by definition.

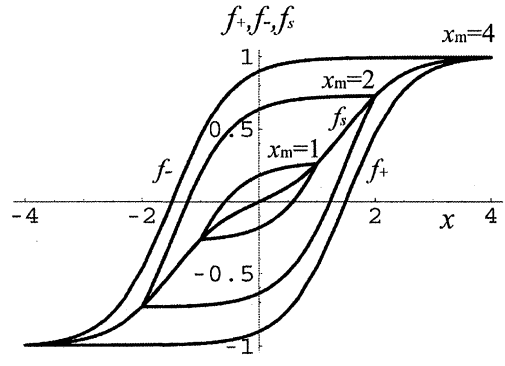

Figure 3.1: Major and symmetrical minor hysteresis loops and the anhysteretic induction curve when the reversible magnetization is negligible ($A_0 = 0$) for a_0 =1.5, x_m = 4, 2, and 1

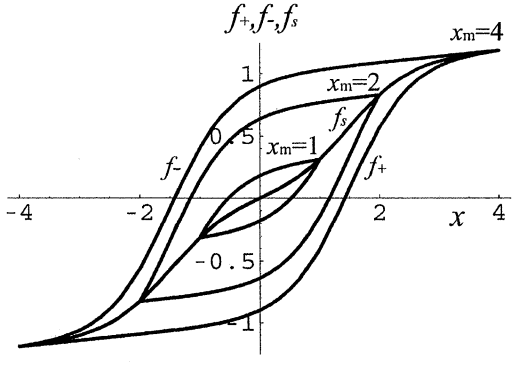

Fiure.3.2: Major and minor hysteresis loops and the anhysteretic induction curve when the reversible magnetization is not negligible ($A_0 = 0.05$) for a_0 =1.5, x_m = 4, 2, and 1

Let us substitute $x = 0$ into the first expression of (3.1), which leads us to

$$f_r = \tanh a_0 - b_1 \quad . \tag{3.4}$$

After substituting b_1 expressed in (3.2) into (3.4) and solving (3.4) for x_m we arrive to the following results:

$$x_m = \operatorname{arcth}\sqrt{\frac{f_r}{\tanh a_0 \,[f_r \tanh a_0 - (\tanh a_0)^2 + 1]}} \quad \text{from the ascending side} \tag{3.5a}$$

and

$$x_m = \operatorname{arcth} \sqrt{\frac{f_r}{\tanh a_0 \, [f_r \tanh a_0 + (\tanh a_0)^2 - 1]}} \quad \text{from the descending side, (3.5b)}$$

where the following condition must be satisfied:

$$f_r \geq \tanh a_0 - \frac{1}{\tanh a_0} .$$

These expressions in (3.5) show an unambiguous relationship between the maximum magnetic field x_m and the remanence f_r for both the ascending and the descending part of the hysteresis loop, giving a full justification for using x_m as a free parameter in place of f_r in further calculations. These two parameters are convertible, therefore, they give a free choice to the reader in practical calculations.

By selecting B_0 and C_0 scaling factors to match the measured data (see (2.4)) we can dispense with the third and fourth independent parameters. The third represents the maximum value of the magnetic induction, induced by the saturation field. The fourth parameter determines the angle of the hysteresis curve to the horizontal axis at the coercive point that can also vary independently from the other parameters. This parameter, which represents the relative permeability at this point and influences the shape of the hysteresis loop, will be discussed in detail in Chapter 7. In addition to the parameters listed above, initial permeability (the first derivative of the virgin magnetization curve at $x = 0$) is also independent of all the others. This parameter with the virgin magnetization curve and their significance is discussed in Chapter 4 in detail. When the linear term, i.e. the reversible magnetization, becomes significant, its slope represented by coefficient A_0 becomes an additional independent parameter that can vary independently of the other five.

As can be seen, for a magnetic material with reversible magnetic property ($A_0 \neq 0$) six parameters will define the hysteresis loop described by this model. When properties of ferromagnetic substances are given in tabulated form, these are the parameters specified in order to describe its magnetic properties in practical terms. The only exception is f_r the remanent magnetism as we have seen earlier. Instead of the f_r remanence as a practical parameter in the further calculations x_m the saturation excitation field will be used as an independent parameter. The two parameters, however, are unambiguously related to each other as shown in (3.5). This choice was made solely on the ground of convenience to ease the mathematical calculations in the later chapters and has no relevance to the relation of the model to practical cases.

It is important to remember that in practical calculations of magnetic phenomena the expressions in (3.3) will take up the following normalized form.

$$f_+ = B_0 \tanh [C_0 \, (x - a_0)] + A_0 x + b_1 \qquad \text{for increasing } x \text{ values} \qquad (3.6a)$$

$$f_- = B_0 \tanh [C_0 \, (x + a_0)] + A_0 x - b_1 \qquad \text{for decreasing } x \text{ values} \qquad (3.6b)$$

and

$$b_1 = B_0 \, \{\tanh [C_0 \, (x_m + a_0)] - \tanh [C_0 (x_m - a_0)]\} / 2 \quad . \qquad (3.7)$$

With the following choice of normalization (3.6) and (3.7) will go into (3.3) and (3.4).

$$B_0 = \frac{B}{B_{sat}}, \; C_0 = \frac{H}{H_{sat}} \text{ and } A_0 = A\frac{H_{max}}{B_{max}},$$

where B and B_{sat} are the amplitude and the saturation values of the induction respectively, measured in units of kg A^{-1} s^{-2}. H and H_{sat} are the amplitude of the field and the saturation field, respectively, in A m^{-1} and A the magnitude of the reversible magnetization whose dimension is kg m A^{-2} s^{-2}.

In the following, in order to simplify the calculations, the normalized expressions shown in (3.2) and (3.3) are going to be used and we refer back to (3.6) and (3.7) only when it is absolutely necessary. All quantities plotted in the graphs in this book are also dimensionless normalized quantities.

3.3 Biased Hysteresis Loops

As often happens in practice, ferromagnetic materials are subjected to a combination of steady (DC) and varying (AC) magnetic field. The effect of this is a change in the shape of the hysteresis loop. Depending on the relative direction of the constant field the hysteresis loops will shift either towards the first (positive bias) or the third (negative bias) quadrant of the coordinate system.

When the ferromagnetic sample is driven into deep saturation, depending on how deep the saturation is, the major hysteresis loop may not change at all when DC bias is applied. In the following we are going to investigate the conditions when the induction is below the saturation level and it is moving along on one of the minor loops. Minor loops are by definition those that have at least one of the extrema below the value of the saturation field.

Let us suppose we apply a constant field of d_0 magnitude to the specimen in the positive direction. Due to the DC bias the intersections in the first and the third quadrant between the ascending and the descending part of the hysteresis loop will not be the same as in (3.2) and (3.3) but it will be shifted to different points. The crossover points of the hysteresis loop up and down going parts will not sit symmetrically in the first and the third quadrant of the coordinate system therefore the constant b_1 could not be used. Let us call the shift in the first quadrant b_3 and the one in the third quadrant b_4. With reference to (3.2) we can calculate the expressions for b_3 and b_4 shifting the crossover points x_m and $-x_m$ by the magnitude of the DC field d_0 as shown in (3.8) and (3.9).

$$b_3 = [\tanh(x_m + d_0 + a_0) - \tanh(x_m + d_0 - a_0)]/2 \tag{3.8}$$

and

$$b_4 = [\tanh(-x_m + d_0 + a_0) - \tanh(-x_m + d_0 - a_0)]/2 \; . \tag{3.9}$$

During one cycle, while the AC field is changing from x_m to $-x_m$ and back, the shifting constant will change from b_3 to b_4 and back again to b_3 (see Axiom 7 in Chapter 1). Applying the rule that every change inside the area of the major hysteresis loop will follow

the tangent hyperbolic law, the change between b_3 and b_4 can be described by (3.10a) for the ascending and by (3.10b) for the descending part. Here b_u represents now the ascending and b_d the descending final shifting constants in the process.

$$b_u = b_3 \frac{\tanh(-x_m + d_0 - a_0)}{\tanh(-x_m + d_0 - a_0) - \tanh(x_m + d_0 - a_0)} + b_4 \frac{\tanh(x_m + d_0 - a_0) - \tanh(x - a_0)}{\tanh(x_m + d_0 - a_0) - \tanh(-x_m + d_0 - a_0)} \tag{3.10a}$$

$$b_d = b_3 \frac{\tanh(-x_m + d_0 + a_0) - \tanh(x + a_0)}{\tanh(-x_m + d_0 + a_0) - \tanh(x_m + d_0 + a_0)} + b_4 \frac{\tanh(x_m + d_0 + a_0) - \tanh(x + a_0)}{\tanh(x_m + d_0 + a_0) - \tanh(-x_m + d_0 + a_0)}. \tag{3.10b}$$

As we can see the two expressions will differ depending whether the field is increasing or decreasing, in other words the b_u and b_d "constants" will mimic the corresponding part of the hysteresis loop and will be different in every point (see Axiom 7 in Chapter 1).

After the replacement of b_1 in (3.1) by b_u and b_d we can express f_+ and f_- describing the ascending and the descending part of any biased minor hysteresis loop in the following form.

$$f_+ = \tanh(x - a_0) + b_u + A_0 x \tag{3.11a}$$

$$f_- = \tanh(x + a_0) - b_d + A_0 x. \tag{3.11b}$$

First let us take the easier case and assume that the reversible magnetization makes no significant contribution to the process, i.e. $A_0 = 0$, then (3.11) is reduced to a simpler form as shown below

$$f_+ = \tanh(x - a_0) + b_u \tag{3.12a}$$

$$f_- = \tanh(x + a_0) - b_d. \tag{3.12b}$$

A set of positively DC biased minor hysteresis loops are depicted in Figure 3.3. The major loop and the anhysteretic magnetization curve (for details see Chapter 4) are also shown. We can see that all crossover points, i.e. anhysteretic points, of the minor loops are lying on the anhysteretic curve as we have seen previously in Chapter 3. The curves were calculated from (3.11) and the following parameter values were used in the calculation: $a_0 = 1.5$, $d_0 = 0.75$ and $x_m = 5, 3, 2, 1$. In Figure 3.4 four hysteresis loops have been plotted with the following parameters values: $a_0 = 1$, $d_0 = 0.75$ and $x_m = 4, 2.5, 2, 1$.

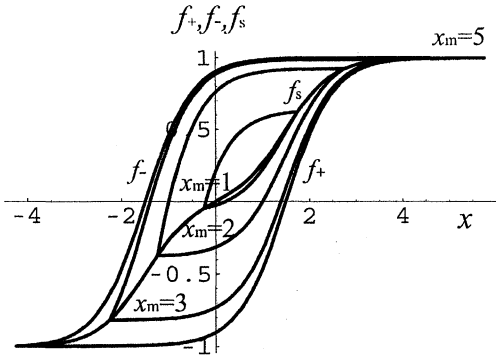

Figure 3.3: Major, minor biased hysteresis loops and the corresponding anhysteretic curve for $x_m = 5$, 3, 2, and 1, $a_0 = 1.5$, $d_0 = 0.75$, $A_0 = 0$

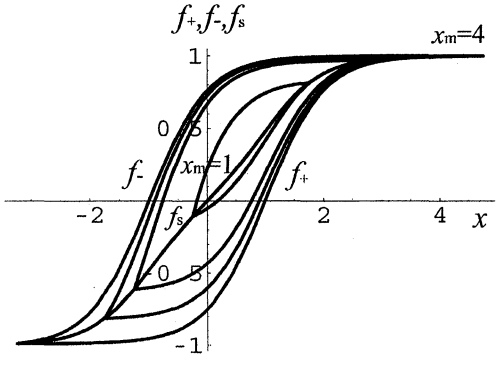

Figure 3.4: Major, minor biased hysteresis loops and anhysteretic curve for $x_m = 4$, 2.5, 2, and 1, $a_0 = 1$, $d_0 = 0.75$, $A_0 = 0$

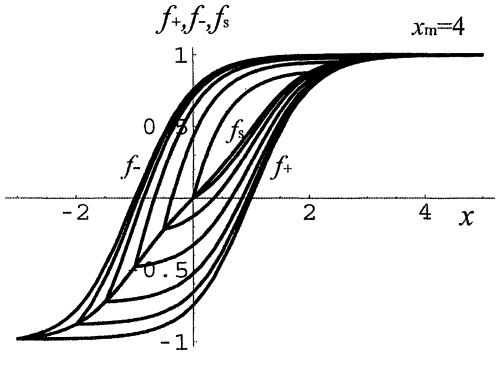

Figure 3.5: Major and minor biased hysteresis loops for $x_m = 4$, 3, 2.5, 2, 1.5, and 1, $a_0 = 1$, $d_0 = 0.75$, $A_0 = 0$

In Figure 3.5 a set of curves are shown where the parameters used in the calculation were as follows: $a_0 = 0.75$, $d_0 = 0.5$ and $x_m = 4, 2.5, 2, 1.5, 1$, and 0.5.

The differences between the curves in Figures 3.3, 3.4, and 3.5 are indicative of the hysteresis loop dependence on a_0 the coercive force and on the magnitude of the DC bias d_0.

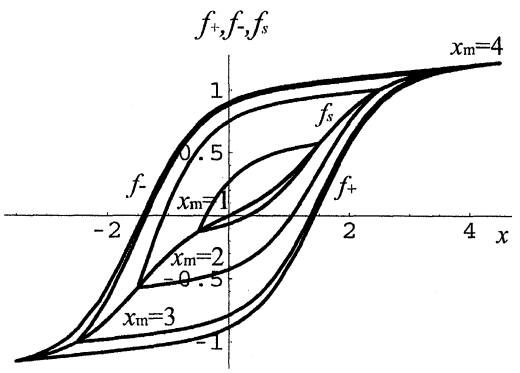

Figure 3.6: Major, minor biased hysteresis loops, and the corresponding anhysteretic curve with reversible magnetization for $x_m = 4, 3, 2, 1$, $a_0 = 1.5$, $d_0 = 0.5$, and $A_0 = 0.05$

Let us take now the slightly more complicated case when $A_0 \neq 0$ and the effect of the reversible magnetization cannot be ignored. It is obvious that the transition between b_3 and b_4 constants will not be changed by the presence of the reversible magnetization, therefore (3.10) will apply. By using (3.11) a set of hysteresis loops, major and minor loops included, were plotted as shown in Figure 3.6. The value of A_0 used in the calculation was 0.05 with the following additional parameter values: $a_0 = 1.5$, $d_0 = 0.5$, and $x_m = 4, 3, 2, 1$, and 0.5.

3.4 Inverse Hysteresis

As often happens in industrial applications the field, which is exciting the magnetic components, is a subject of unexpected distortions due to outside interference. This is quite normal in cases of periodic excitation. The induction is the monitored quantity normally, therefore instead of the usual $B = f(H)$ function its inverse $H = f(B)$ is needed to find out the distortion in the exciting waveform. Since any deviation from the sinusoidal shape, in harmonic excitation for instance, can have an undesirable effect on the magnetic components, it is often necessary to find out the distortion in the source. So far the only way to find the distorted excitation function has been the graphical method. By projecting the recorded induction waveform backward onto the hysteresis loop one could reconstruct the shape of the exciting wave [31]. This process is obviously tedious, involves the accurate knowledge of the hysteresis curve in a graph form and the conversion of a large number of points for a reasonable accuracy. The T(x) model [30] described here provides an analytical tool for the calculation of the inverse function to determine the excitation from the recorded induction waveform.

Let us recall (3.2) and (3.3) and express x the normalized excitation as a function of the induction, in other words let us form the inverse hysteresis. The solution to this task is shown in (3.13a and b) for the ascending and the descending part of the inverse hysteresis loop, respectively

$$x = \text{arcth}\,(f_+ - b_1) + a_0 \qquad \text{for the ascending part} \tag{3.13a}$$

$$x = \text{arcth}\,(f_- + b_1) - a_0 \qquad \text{for the descending part,} \tag{3.13a}$$

where b_1 is defined in (3.2

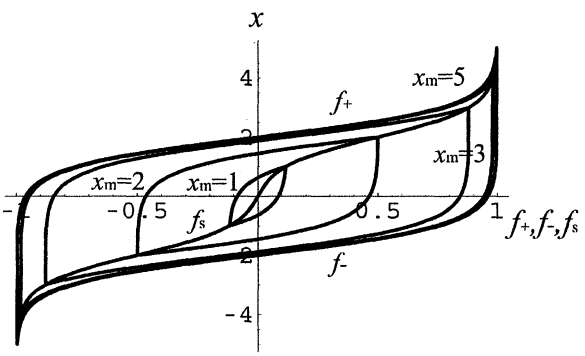

Figure 3.7: Inverse hysteresis loops for $a_0 = 2$ and $x_m = 1, 2, 3, 4$, and 5.

A set of reversed hysteresis loops are depicted in Figure 3.7 for $a_0 = 2$ and the x_m values of 1, 2, 3, 4, and 5. The loops are plotted between the two limits of f_m where

$$f_m = \tanh\,(x_m - a_0) + b_1\,. \tag{3.14}$$

In the graph, the inverse of the anhysteretic magnetization curve is also plotted, representing the loci of the crossover points at f_m. The inverse of the anhysteretic curve x_s is formulated in (3.15)

$$x_s = \text{arctanh}\left[\frac{-[1-(\tanh a_0)^2] + \sqrt{[1-(\tanh a_0)^2]^2 + 4f_+^2(\tanh\ a_0)^2}}{2f_+(\tanh\ a_0)^2}\right]. \tag{3.15}$$

3.5 The Hysteroid

Hysteresis is not restricted to the field of magnetism and to ferromagnetic materials. These phenomena are present in the elastic and electromagnetic behavior of materials, in which a lag occurs between the application and the removal of a force or field and its subsequent

effect. Similar behavior can be seen in some materials when varying electric fields are applied (electric hysteresis). Elastic hysteresis occurs when a varying force repeatedly deforms an elastic material. The deformation produced does not completely disappear when the force is removed, and this results in energy loss on repeated deformations. When within a family of hysteresis loops every symmetrical minor loop is given a place on its own, in three dimensions, they form a closed space called a hysteroid. In this formation parallel with the field-induction plane lie the minor loops with decreasing x_m values. Figure 3.8 shows a hysteroid.

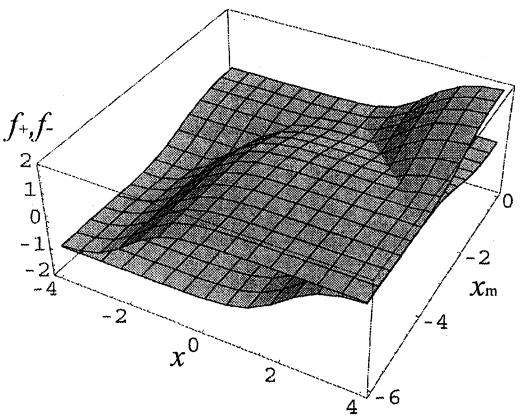

Figure 3.8: The hysteroid

References

[1] E. Warburg, Magnetische untersuchungen. Ann. Physik. **13**, pp.141–164 (1881).
[2] J.A. Ewing, On the production of transient electric currents in iron and steel conductors by twisting them when magnetised or by magnetising them when twisted. Proc. Roy. Soc. **XXXIII**, 21–23 (1881).
[3] A. Aharoni, Some recent developments in micromagnetics at the Weizman Institute of Science. J. Appl. Phys. **30**, 70S–78S (1959).
[4] A. Aharoni, Magnetization curling. Phys. Stat. Sol **16**, 3–42 (1966).
[5] W.F. Brown, Micromagnetics domains and resonances. J. Appl. Phys. **30**, 62S–69S (1959).
[6] W.F. Brown, *Micromagnetics* (J. Wiley, N.Y., 1963).
[7] W.F. Brown, *Micromagnetics* (Robert Krieger, Malabar, Florida, 1978).
[8] W.F. Brown and A.E. LaBonte, Structure and energy of one-dimensional domain walls in ferromagnetic films. J. Appl. Phys. **36, No. 4**,1380–1386 (1965).
[9] D.C. Jiles and D.L. Atherton, Theory of ferromagnetic hysteresis J. Appl. Phys. **55(6)15**, 2115–2120 (1984).
[10] M. Kersten, *Problem der Technischer Magnetisirungscurve* (Springer, Berlin, 1938).
[11] M. Kersten, *Grundlagen Theorie der Ferromagnetischer Hysterese und der Koerzitivkraft* (Hirzel, Berlin, 1943).
[12] R. Becker and W. Doring, *Ferromagnetismus* (Springer, Berlin, 1939).
[13] G. Bertotti, Energetic and thermodynamic aspects of hysteresis. Phys. Rev. Lett. **76, No 10**, 1739–1742 (1996).

[14] G. Bertotti, V. Basso and G.J. Durin, Randomfree energy model for the description of hysteresis. J. Appl. Phys. **79**, 5764–5766 (1996).
[15] J.R. Brauer, Simple equations for the magnetization and reluctivity curves of steel. IEEE Trans. Magn. **MAG-11**, **No.1**, 81 (1975).
[16] O. Karlqvist, Calculation of the magnetic field in the ferromagnetic layer of a magnetic drum. Trans. of Roy. Inst. of Techn. Stockholm **86**, 1–27 (1954).
[17] J. Rivas, L.M. Zamarro, E. Martin and C. Pereira, Simple approximation for magnetization curves and hysteresis loops. IEEE Trans. Magn. **MAG-17**, **No.4**, 1498–1502 (1981).
[18] J. Fisher and H. Moser, Die nachbildung von magnetisierungscurven durch einfache algebraishe oder transzendente funktionen. Archiv fur Electrotechn. **XLII**, **5**, 286–299 (1956).
[19] C.F. Trutt, E. A. Erdélyi and R.E. Hopkins, Representation of the magnetization characteristic of DC machines for computer use. IEEE Trans. Power Apparat. Sys. **PAS-87**, 665–669 (1968).
[20] G.F.T. Widger, Representation of magnetisation curves over extensive range by rational fraction approximations. Proc. IEE **116**, 156 (1969).
[21] E.C. Stoner and E.P. Wohlfarth, A mechanism of magnetic hysteresis in heterogeneous alloys. Phil. Trans. Roy. Soc. A **240**, 599–642 (1948).
[22] D.C. Jiles and D.L. Atherton, Theory of ferromagnetic hysteresis. J. Magn. Magn. Mater. **61**, 48–60 (1986).
[23] A. Globus, Influence des dimensions des parois sur la permeabilite initiale. Comptes Rendus Acad. Seances, **255**, 1709–1711 (1962).
[24] A Globus and P. Duplex, Separation of susceptibility mechanisms for ferrites of low anisotropy. IEEE Trans. Magn. **2**, 441–445 (1966).
[25] A. Globus and M. Guyot, Wall displacement and bulging in magnetizatiom mechanism of the hysteresis loop. Phys. Stat. Sol. B **52**, 427–431 (1972).
[26] F. Preisach, Über die magnetishe nachwirkung. Zeit. Physik. **94**, 277–302 (1935).
[27] I.D. Mayergoyz, *Mathematical Models of Hysteresis* (Springer-Verlag, N.Y., 1991).
[28] E. Della Torre, *Magnetic Hysteresis* (IEEE Press, N.Y., 1999).
[29] A. Iványi, *Hysteresis Models in Electromagnetic Computation* (Akademiai Kiado, Budapest, 1997).
[30] J. Takács, A Phenomenological mathematical model of hysteresis. COMPEL Int. J. Comp. Math. E. and E. Eng. **20**, **No. 4**, 1002–1014 (2001).
[31] P. Del Vechio, A. Salvini, I. Carrarini and G.M. Veca, Ferromagnetic materials excited by a distorted periodic field source. COMPEL Int. J. Comp. E. and E. Eng. **17**, **No. 3**, 398–491 (1998).

4. Nonhysteretic Processes

4.1 Virgin Magnetization Curve

Ferromagnetic materials in their virgin state (before magnetization) will contain domains with strong magnetic moments. Each moment, however, varies in direction from domain to domain. The overall vectorial result is therefore the cancellation of the magnetic effect, the material as a whole has no magnetic moment and shows no external magnetic influence. When, however, an external magnetic field is applied, domains, with moments in the direction of the applied field, increase their size at the expense of their neighbors and the internal magnetic field effect increases greatly over that of the external field. When the external field is removed the domain alignment usually is not wholly returned to the original random state and a residual or remnant dipole field remains in the macroscopic structure. The fact that the magnetic moment of the material is different after the field has been removed and that the magnetic state of the material is a function of its previous magnetic history, is called hysteresis (see Chapter 3).

A magnetization curve starting from the demagnetized state – that is, zero magnetization at zero field – and going into saturation is called an initial or virgin magnetizing curve. One can return a specimen into its "virgin" state by demagnetizing the material. The name virgin magnetizing curve will be reserved for the curve that starts from the state before magnetization or when the specimen was demagnetized by applying an AC field, initially large enough to saturate the material and its amplitude slowly reduced to zero. This technique of obtaining a demagnetized state is called AC demagnetization (see Chapter 10).

When a specimen is magnetized in its virgin state for the first time, or magnetized for the first time after a total AC demagnetization, the curve representing the relationship between induction and applied field (virgin magnetization curve) will be different from the normal hysteresis curve of the material. At zero fields the initial tangent (i.e. first derivative) of the virgin curve, in general, can vary and for most ferromagnetic materials this initial slope is not zero.

Let us recall now the T(x) function from (2.4) in a normalized form and differentiate it twice by x. By adding the second derivative multiplied by a factor C_3 to the T(x) function we can model the virgin magnetization curve. The mathematical expression, which models the virgin magnetization, is given in (4.1).

$$f_v = \tanh x \left[1 - 2C_3 \, (\operatorname{sech} x)^2\right]. \tag{4.1}$$

By using (4.1) a set of curves were calculated and plotted as shown in Figure 4.1 for the following values $C_3 = 0$, 0.2, 0.4, and 0.5.

Mathematics of Hysteretic Phenomena. Jeno Takács

ISBN: 3-527-40401-5

The first derivative of f_v by x represents the differential permeability (see Chapter 7) of the virgin magnetization curve. Its value at $x = 0$ is a free parameter whose value is independent of the other parameters and it changes from one magnetic material to another as it was pointed out in Chapter 3 without affecting any other properties of the specimen. Its value is linked to C_3 in (4.1). After differentiating f_v by x and substituting $x = 0$ into the equation, we find the following relationship between the initial permeability and the value of C_3.

$$\frac{\mathrm{d}}{\mathrm{d}x} f_v = \mu_d = 1 - 2C_3 \text{ at } x = 0. \tag{4.2}$$

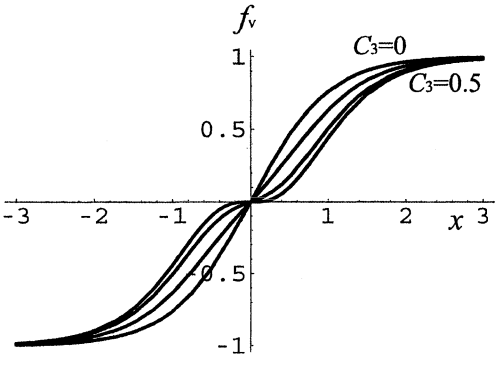

Figure 4.1: The virgin magnetization curves for C_3 values of 0, 0.2, 0.4, and 0.5 and when the reversible magnetization is negligible, $A_0 \approx 0$

As shown before, the first derivative can change between zero and unity therefore the corresponding C_3 values, which can be selected independently of the other free parameters, will be between

$$C_3 = ½ \text{ for } \frac{\mathrm{d}f_v}{\mathrm{d}x} = 0$$

and

$$C_3 = 0 \text{ for } \frac{\mathrm{d}f_v}{\mathrm{d}x} = 1.$$

As we can see these two C_3 values represent the two limits as shown in Figure 4.1. It also indicates that the angle of the tangent at zero can only vary between 0 and 45°. The virgin and initial permeabilities and associated problems will be discussed in detail in Chapter 7. The definition and a detailed explanation of the concept of permeability are also given in the same chapter.

Rayleigh observed in 1887 [1] that at low magnetization the character of the magnetization curve followed a quadratic character, with good approximation as a function

of the excitation. In his approximation a linear term represents the reversible while a quadratic term represents the irreversible magnetization. He has approximated the hysteresis loop, at low magnetization, with parabolic curves. That approximation found its use in hysteresis-loss calculations (see Chapter 8) and also for finding the distortion caused by the hysteresis (see for instance Chapter 9) when ferromagnetic materials were subjected to periodic magnetization as for instance in a transformer. At higher magnetization, however, this relationship breaks down. The high field, near saturation behavior was modeled in a form of an infinite series by Becker and Doring [2], later Bozorth [3].

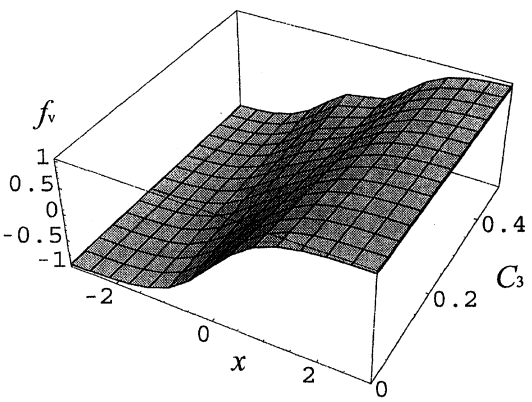

Figure 4.2: Surface map of the virgin magnetization curves shown in Figure 4.1 f_v against x ($-3 < x < 3$) and C_3 ($0.05 < C_3 < 0.5$)

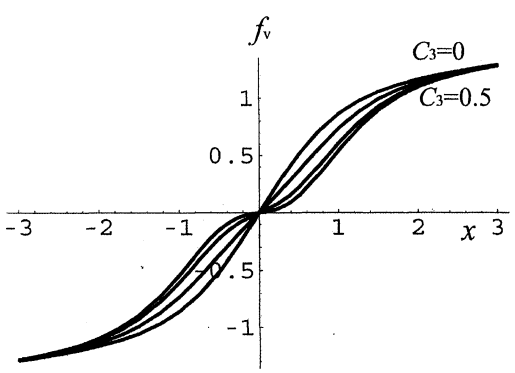

Figure 4.3: The virgin magnetization curve for C_3 values of 0, 0.2, 0.4, and 0.5. When the reversible magnetization is not negligible, $A_0 = 0.008$.

When A_0 is not negligible the linear term has to be taken into account and the expression in (4.1) can be rewritten into the form as in (4.3) below,

$$f_v = \tanh x \left[1 - 2C_3 \, (\operatorname{sech} x)^2\right] + A_0 x \,. \tag{4.3}$$

The presence of the reversible component in the magnetization will also change the value of the initial permeability as shown in (4.4) and it will be greater by A_0

$$\mu_d = 1 - 2C_3 + A_0 \quad \text{at } x = 0. \tag{4.4}$$

Figure 4.3 depicts a set of virgin magnetization curves calculated by using the expression in (4.3) for the same C_3 and A_0 values as before. The two sets of curves show marked differences, which is due to the presence of the reversible magnetization.

4.2 Anhysteretic Magnetization

According to the presently accepted view, a ferromagnetic specimen, without imperfections, anisotropy or interactions between domain walls, would not show any effect of hysteresis. The magnetization would follow a single-valued function of the applied field, presumably the anhysteretic magnetization curve, and the same induction would be produced with the same exciting field irrespective of whether it has an increasing or decreasing tendency. Therefore the whole process of magnetization and the curve describing the process would be reversible and free of hysteresis.

Unfortunately, the elimination of the imperfections and the anisotropy from the ferromagnetic materials is usually far too difficult; therefore it is not practical, so anhysteretic magnetization has to be achieved by other means. When a cyclic magnetizing field is applied so that the magnetization is moving on minor loops and the field extrema are changed then the loci of the crossover points between the up-going and down-going parts of the hysteresis loop will describe the anhysteretic magnetization curve (see Chapter 3). The changes in the magnitude of the field can be intermittent or continuous, both ways we come to the same result. People were tempted for a long time to describe the magnetization process with a single-valued function. Similarly, in the same way a number of approaches have been made to describe the saturation curve, by using power series, hyperbolae like Frõhlich [4], various transcendental functions [5] and Fourier series [6]. Lehman [7] even suggested that sections of the curve in calculations should be represented by a number of approximations selected from a large range of functions. A great contribution was made to the mathematical description of the magnetization curve for field values considerably greater that the coercivity by Lamont in 1867 (Lamont's law) [8]. Frõhlich and Kenelly followed his footsteps in the last decade of the nineteenth century [4,9]. Their approaches still provide a useful tool in magnetic calculations. Needless to say that the anhysteretic magnetization and the hysteresis free magnetization are not the same process, therefore they will not produce the same physical effect, their character will be vastly different, and require distinctly different mathematical modeling. People very often mix up these two entirely different concepts in magnetism.

For the mathematical modeling of the anhysteretic phenomenon we have to recall again (3.1) and (3.2). The crossover points between the up- and down-going part of the hysteresis loop in the first quadrant occur at $x = x_m$ therefore the loci of these points can be calculated by substituting $x = x_m$ into the first expression of (3.1) as shown below

$$. f_+(x_m) = \tanh(x_m - a_0) + A_0 x_m + [\tanh(x_m + a_0) - \tanh(x_m - a_0)]/2 \quad (4.5)$$

From this equation we can express the function the anhysteretic magnetization f_s in the following form, by replacing x_m with x:

$$f_s = A_0 x + [\tanh(x + a_0) + \tanh(x - a_0)]/2 . \quad (4.6)$$

When A_0 is approaching zero and the linear term is negligible, then the expression in (4.6) goes into a simpler form

$$f_s = [\tanh(x + a_0) + \tanh(x - a_0)]/2 . \quad (4.7)$$

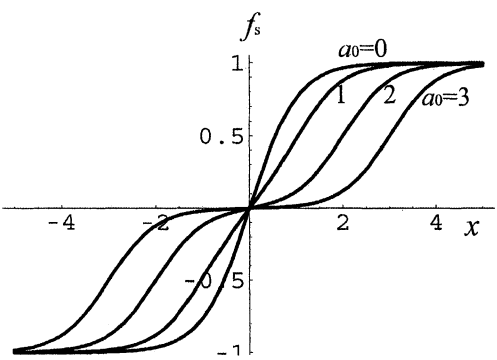

Figure 4.4: Anhysteretic magnetization curves for $A_0 = 0$ and $a_0 = 0$, 1, 2, and 3

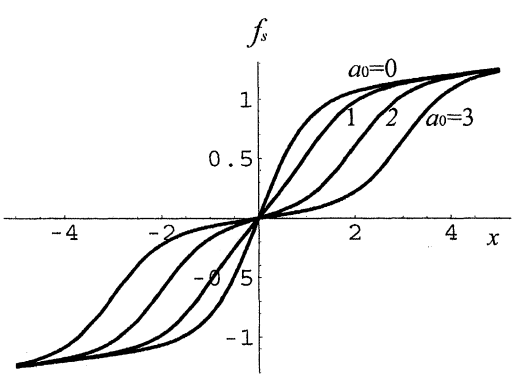

Figure 4.5: Anhysteretic magnetization curves for $A_0 = 0.05$ and $a_0 = 0$, 1, 2, and 3

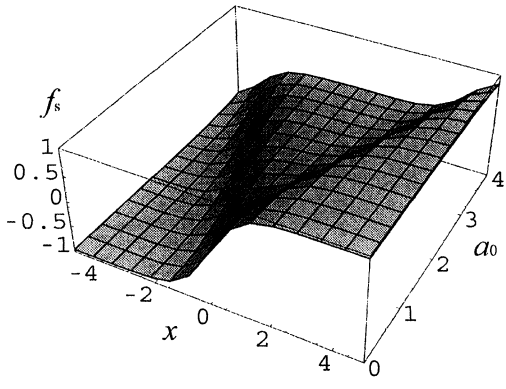

Figure 4.6: Surface plot of the anhysteretic magnetization shown in Figure 4.4 as a function of the field excitation ($-5 < x < 5$) and coercivity ($0 < a_0 < 4$)

In both cases (when $A_0 = 0$ and $A_0 \neq 0$) the relationship between the anhysteretic magnetization curve and a set of corresponding hysteresis loops is unique. Every set of hysteresis loop has its anhysteretic curve, which belong to one and only one set of loops. In the knowledge of the major hysteresis loop the anhysteretic behavior of the magnetic specimen can be determined. The reverse is also true, a given anhysteretic behavior determines the hysteresis loop of the magnetic material. When the loops are normalized, the link between the two is a_0, the coercivity. Anhysteretic magnetization curves calculated from (4.7) and (4.6) are plotted in Figures 4.4 and 4.5, respectively for $A_0 = 0$ and $A_0 = 0.05$ with a_0 the coercivity as parameter for the values of 0, 1, 2, and 3.

The need for describing this anhysteretic relationship between induction and field in mathematical form, at least in a quantitative form was always great. Two empirical approaches that gained general acceptance were worked out independently by Frõhlich in 1881 [4] and Kennelly in 1891 [9]. Although they expressed the induction–field relationship in two different mathematical forms, ultimately the two expressions converged into the same formula. It can also be shown that, when Frõhlich's formula is expanded into a power series, it becomes the same as the series used by Weiss [10] to calculate the induction at saturation point. Recent approaches formulated the full range of this anhysteretic relationship including the saturation region [11,12].

References

[1] J.W. Lord Rayleigh, On the Behavior of Iron and Steel under the Operation of Feeble Magnetic Force. The Philosophical Magazine 5, **XXIII, No. 142**, 225–245 (1887).
[2] R. Becker and W. Doring, *Ferromagnetismus* (Springer, Berlin, 1938).
[3] R.M. Bozorth, *Ferromagnetism* (Van Nostrand, N.Y., 1951).
[4] O. Frõhlich, Investigations of Dymoelectric Machines and Electric Power Transmission and Theoretical Conclusions Therefrom. Electrotech. Z. **2**, 134–14 (1881).
[5] J. Fisher and H. Moser, Die Nachbildung von Magnetisierungscurven durch einfache algebraishe oder transzendente Funktionen. Archiv für Elektrotechnik. **4**, 286–299 (1956).

[6] F.C. Trutt, E.A. Erdélyi and R.E. Hopkins, Representation of the Magnetization Characteristic of DC Machines for Computer Use. IEEE Trans. on Power A and Sys. **87**, **No.3**, 665–669 (1968).
[7] S. Lehman, Elektronische Datenverarbeitungen. **I.6**, 165–172 (1964).
[8] J. Lamont, *Handbuch des Mgnetismus* (Voss, Leipzig, 1867).
[9] A.E. Kennelly, Magnetic Reluctance. Trans. Am. IEE. **8**, 485–517 (1891).
[10] P. Weiss, Absolute Value of Intensity of Magnetization at Saturation. J. Phys. **9**, 373–393 (1910).
[11] J. Rivas, J.M. Zamarro, E. Martin and C. Pereira, Simple Approximation for Magnetisation Curve and Hysteresis Loop. IEEE Trans. on Magn. **17**, 1498–1502 (1981).
[12] J. Takács, A Phenomenological Mathematical Model of Hysteresis. COMPEL Int. J. for Comp. and Math. in E. and E. Eng. **20**, **No.4**, 1002–1014 (2001).

5. Reversal Loops

5.1 First-Order Minor Reversal Loops

When the exciting field is interrupted and reversed during the process of magnetization, the direction of the induction will also be reversed and, as practical experience shows, it will move on to a different return path. Assuming that the original amplitude of the excitation remains the same, it returns eventually to a value set by the extreme of the exciting field. The shape of the return path, which is the subject of this chapter is one of the classic problems of magnetism. People recognized the similarity between parts of the return path and the major hysteresis loop and tried to apply this similarity in modeling as part of the of the reversal loop. These attempts lead to various approaches. Zirka and Moroz [1,2] used transplantation of parts of the major hysteresis loop to approximate the return path, with some dubious results. Some authors introduced differential equations for solving the problem [3] others turned to numerical refinement for improvement. All these attempts failed to satisfy the basic requirement of closing the minor loop at reversal and at maximum induction. In order to improve on this model scaling [4,5], transformation was applied, however, without success. The rule of congruency proposed by Madelung [6] and Mayergoyz [7] was also tried with limited results and Preisach's model was modified to include congruency for this very purpose.

The recognition of the similarity between parts of the minor and the major hysteresis loops was a step in the right direction, but to model the return path this recognition on its own was not enough, other additional rules were needed to complete the mathematical picture [8]. It will be shown here that the rules introduced at the beginning of this book will bring this problem to a satisfactory solution.

The rules applied in building up the model for closed minor return loops are going to be reviewed here briefly to the benefit of the reader. The first two rules come from the geometry governing the field within the space enclosed by the major hysteresis loop and state the fact that all lines in the enclosed field mimic either the up- or the down-going major hysteresis paths. The third rule tells us that all changes in this field will be of tangent hyperbolic in character and will be described by such a function. The last rule, which is confirmed by observations and also applied by other models, is the local memory rule. This rule tells us that the shape of a return path as part of the minor loops is predetermined by the magnetic history of the sample and in particular the last path and extremum (positive or negative maximum) of the magnetization. In the following we are going to build up a mathematical description of these minor reversal loops by recalling the basic equations of the model and applying the rules above.

Let us assume that the magnetization process is interrupted and reversed at an arbitrary x_r point either on the ascending or the descending part of the hysteresis loop. For the

Mathematics of Hysteretic Phenomena. Jeno Takács

ISBN: 3-527-40401-5

formulation we recall (3.12a and b), then the relationship between the induction f_+, f and the excitation field x can be described by the following expressions:

$$f_+ = \tanh\ (x\ -\ a_0) + b_1 + c_u \qquad \text{for increasing } x \text{ values} \tag{5.1a}$$

$$f_- = \tanh\ (x + a_0) - b_1 + c_d \qquad \text{for decreasing } x \text{ values} \tag{5.1b}$$

We must remember that every time a line moved as part of a set, a shifting "constant" that has a hyperbolic character, facilitates this move. Although the two sets of equations (3.12) and (5.1) look alike, we can see that they differ in the constants c_u and c_d. The u and d subscripts signify the up- and the down-going characters of the constants, respectively. The expressions for these new constants will be calculated below giving a step-by-step account of the calculation.

Let us consider the case when the magnetization is stopped and reversed on the ascending part of the hysteresis curve, where the horizontal field coordinate is marked with x_r. At this point, in order to maintain the continuity of the process of reversal, the value of the function describing the return path must be equal to that of the up-going induction function f_+ given in (3.1a). The return path will mimic the f_- function, shifted by c_{1d} as shown on the left side of (5.2). The subscript 1d signifies the first down-going step in the process. The new loop will start from x_{r1} (first reversal) and must end up at $-x_m$ the last negative maximum before the reversal, according to the rule. From the equality of the two functions we can write

$$\tanh\ (x + a_0) - b_1 + c_{1d} = \tanh\ (x - a_0) + b_1 \tag{5.2}$$

when $x = x_{r1}$ from (5.2) c_{1d} can be expressed as shown in (5.3),

$$c_{1d} = \tanh\,(x_r - a_0)\ -\ \tanh\,(x_r + a_0) + 2\ b_1 \tag{5.3}$$

The constant c_d in the return path shown in (5.1b) will change between two limits; x_r and $-x_m$ obeying the following two cardinal rules. The first is that the new "constant" will change, point to point, as a tangent hyperbolic function, between the two limits (see Axiom 7 in Chapter 1). The second is the local memory law, which compels the reverse path to return to its original value at $-x_m$ representing the last negative extreme. All this is formulated in (5.4),

$$c_d = c_{1d}\,\frac{\tanh\ (-x_m + a_0) - \tanh\ (x + a_0)}{\tanh\ (-x_m + a_0) - \tanh\ (x_r + a_0)} \tag{5.4}$$

After the substitution of c_d into (5.1b) we arrive at an expression describing the return path of the interrupted and reversed minor loop starting from point x_{r1} and finishing at $-x_m$ in the following form:

$$f_- = \tanh\ (x + a_0) - b_1 + c_{1d}\,\frac{\tanh\ (-x_m + a_0) - \tanh\ (x + a_0)}{\tanh\ (-x_m + a_0) - \tanh\ (x_r + a_0)} \tag{5.5}$$

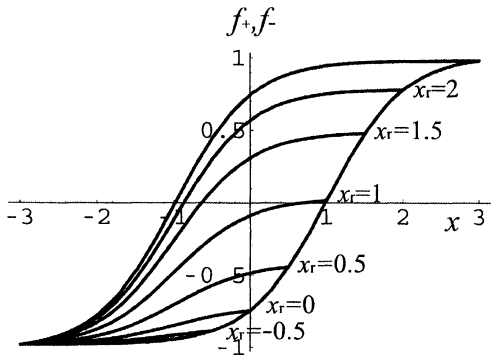

Figure 5.1: First-order minor reversal loops reversing at x_r = 2, 1.5, 1, 0.5, 0, and –0.5

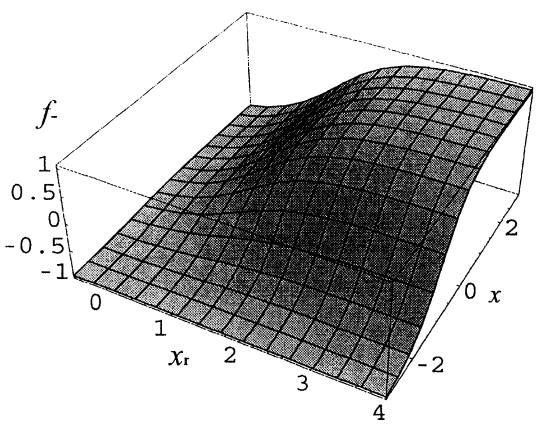

Figure 5.2: Surface map of the first-order reversal loops shown in Figure 5.1 f_- against x_r ($0 < x_r < 4$) and x ($-3 < x < 3$)

Based on this formulation a calculated set of first-order return curves is shown in Figure 5.1. They start at the points of reversal field coordinates of x_r = 2, 1.5, 1, 0.5, 0, and –0.5.

When the point of reversal is on the descending part of the hysteresis curve, naturally the model gives a different mathematical expression for the return path. Due to the law of similarity all changes and lines will now mimic the ascending part of the hysteresis loop. Taking all this into consideration we can write down the expression for c_u the shifting constant as shown in (5.6). By substituting this expression of c_u into (5.1a) we can formulate the up-going return path. The full mathematical expression for this process is given in (5.8). Here, similarly to (5.4) the subscript u signifies the up-going process after reversal and the subscript 1 signifies the first reversal.

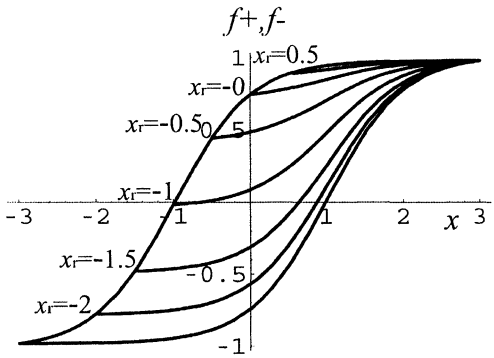

Figure 5.3: First-order reversal loops with reversing points at $x_r = 0.5, 0, -0.5, -1, -1.5$, and -2

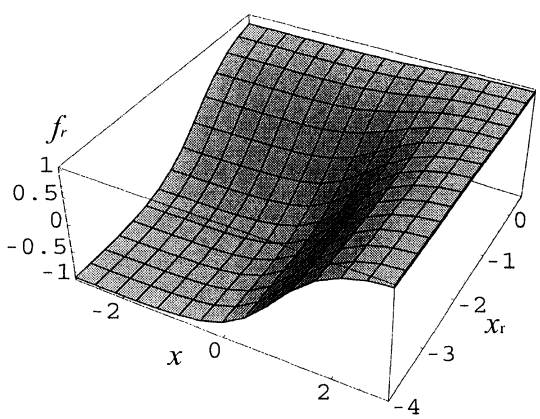

Figure 5.4: Surface map of the first-order reversal loops shown in Figure 5.3, f_+ against x_r ($0 < x_r < -4$) and x ($-3 < x < 3$).

$$c_{1u} = \tanh\ (x_r + a_0) - \tanh\ (x_r - a_0) - 2b_1 \tag{5.6}$$

$$c_u = c_{1u} \frac{\tanh\ (x_m - a_0) - \tanh\ (x - a_0)}{\tanh\ (x_m - a_0) - \tanh\ (x_r - a_0)} \tag{5.7}$$

$$f_+ = \tanh\ (x - a_0) + b_1 + c_{1u} \frac{\tanh\ (x_m - a_0) - \tanh\ (x - a_0)}{\tanh\ (x_m - a_0) - \tanh\ (x_r - a_0)} \tag{5.8}$$

Similarly to Figure 5.1 a set of return curves, starting from the descending part of the hysteresis loop, is shown for the point of reversal field coordinates of $x_r = 0.5, 0, -0.5, -1, -1.5$, and -2 in Figure 5.3, calculated by using (5.8). Figures 5.2 and 5.4 show the surface

maps of the return curves starting from the ascending and the descending side of the hysteresis loop, respectively, using the same data as for Figure 5.1 and Figure 5.2.

5.2 Open Reversal Loops with Monotonically Changing Amplitude

In practical applications it is often the case that a ferromagnetic substance is subjected to an AC excitation of changing magnitude. A typical example of this is the process of AC demagnetization, when the AC field amplitude is gradually reduced to zero in order to achieve demagnetization, i.e. the condition when induction is zero at zero field values. As it was described in Chapter 4, this process creates the right state for the anhysteretic magnetization. Like other problems associated with magnetism this was also the subject of study and a number of people tried to model it with various mathematical approaches [1,7]. All approaches have found it difficult to satisfy the two basic conditions, which are to close the loop at the point of reversal and transplant the right shape for the return path as we said before. As before in the attempt to solve other magnetic problems, transplantation, differential equations and numerical methods have been the major approaches without much progress. In the following we will investigate the case when the magnitude of the AC field is monotonically reduced in time, during magnetization and apply the mathematical model, presented here, to describe the induction, as a function of the field, resulted from the process [8]. For the sake of simplicity in the first instant we assumed that the maximum starting amplitude x_m changes linearly with the field, i.e. it is a first-order function of x. It is not difficult to see, however, that the model is also applicable when other higher-order functions or harmonic time functions are assumed or substituted in (5.9). It is worth noting that shape of the induction path only depends on the end value of the exciting field and independent of the way in time how it was produced.

When a ferromagnetic specimen is cycled around the hysteresis loop with diminishing amplitude of excitation, then x_m the maximum excitation field coordinate during one half of the cycle will change in the following manner:

$$-x = x_{m0}(1-\Delta)+\Delta x \tag{5.9}$$

here x_{m0} is the amplitude of the normalized field at start and Δ represents the linear decrement in the amplitude as specified above. This equality will satisfy the conditions that $x_m = x_{m0}$ when Δ is zero and also when $x = -x_{m0}$. The finishing amplitude at the end of every half-cycle will be the new reversing point and every successive reversal point will be the new starting point of the starting return curve in the next half-cycle. After the substitution of $x = x_{m,1}$ into (5.9), the normalized reversing field amplitude can be expressed mathematically in a general form as

$$x_{n,n} = -x_{m,n-1}\left(\frac{1-\Delta}{1+\Delta}\right)^n \tag{5.10}$$

where n represents the number of steps taken (starting from n = 1), $x_{m,n}$ is the field (horizontal) coordinate of the nth reversal point and Δ is the decrement as before. The model works equally well when the amplitude is incremented i.e. when the value of Δ is negative.

After the substitution of $x_{m,1}$ expression in (5.10) into (3.1) and (3.2) we arrive to the following equations for the first reversed leg

$$f_+ = \tanh\ (x - a_0) + b_1 + A_0 x \qquad \text{up-going} \tag{5.11a}$$

or

$$f_- = \tanh\ (x + a_0) - b_1 + A_0 x \qquad \text{down-going,} \tag{5.11b}$$

where b_1 after the substitution of expression for $x_{m,1}$ in (5.9) into (3.2), will be as

$$b_1 = \left\{\tanh\ \left[-x_{m,0}(1-\Delta) + \Delta x + a_0\right] - \tanh\ \left[-x_{m,0}(1-\Delta) + \Delta x - a_0\right]\right\}/2\,. \tag{5.12}$$

As a first step, the case, when the reversible magnetization is negligible, i.e. $A_0 = 0$, will be investigated, therefore we can use (3.3) as a starting equation.

When x_{m0}, the coordinate of the first reversal point is positive and falls into the first quadrant, the first return curve will mimic the descending major hysteresis path described by (3.3b). In the second step the next reversal loop will follow the ascending part formulated in (3.3a). From then on as the coordinates of the reversal points alternate between the upper and the lower values, the mathematical model will alternate between the two equations (5.13a) and (5.13b), changing over at every point of reversal. When the starting point is negative and starts in the third quadrant the process is reversed.

The two equations describing f_+ and f_- the up- and down-going paths of the minor open loop respectively, in full are as follows:

$$\begin{aligned} f_+ &= \tanh\ (x - a_0) \\ &+ \left\{\tanh\ \left[-x_{m,n-1}(1-\Delta) + \Delta x + a_0\right] - \tanh\ \left[-x_{m,n-1}(1-\Delta) + \Delta x - a_0\right]\right\}/2 \end{aligned} \tag{5.13a}$$

$$\begin{aligned} f_- &= \tanh\ (x + a_0) \\ &- \left\{\tanh\ \left[-x_{mn}(1-\Delta) + \Delta x + a_0\right] - \tanh\ \left[-x_{mn}(1-\Delta) + \Delta x - a_0\right]\right\}/2 \end{aligned} \tag{5.13b}$$

So far we have described of the first step in the process. The amplitudes in the following steps can be calculated by replacing $x_{m,0}$ with the coordinate of the first point of reversal $x_{m,1}$ whose value can be calculated from the expression in (5.9). A number of open minor loops are shown in Figure 5.5 with diminishing amplitude, where Δ the numerical value of the decrement is 0.1. The value of a_0 coercivity used in the calculation was 0.7 and the reversal started in the third quadrant at the value of $x_{m,0} = -1$.

It has to be pointed out that here the reversal starts from the anhysteretic magnetization curve and all points of reversals are located on it, as can be seen from Figure 5.3. The anhysteretic magnetization is described in detail in Chapter 4. Although the calculation here was carried out for a constant decrement, the model is also applicable to any set of piecewise monotonic inputs with both positive (decreasing) and negative (increasing) change in amplitude. The reader has to be reminded that the reversal points do not depend on the shape of the path, only their maximum excitation values at the ends of every cycle. Although in these calculations we assumed a first-order change in amplitude. It is possible to apply a complicated time function with changing amplitude, but the reversal points can still be calculated from (5.9) and (510). In most cases the path of magnetization between the two extrema is set by the magnetic properties of the sample under investigation and makes no contribution to the solution of the magnetic problem.

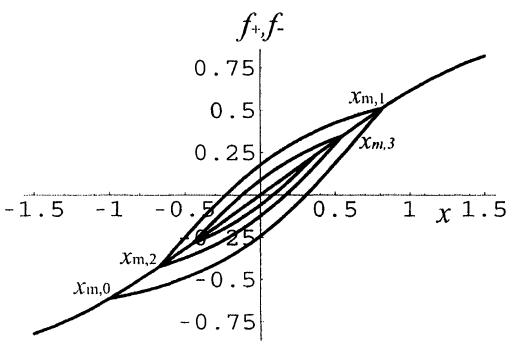

Figure 5.5: Open reversal loops with decreasing amplitude. $A_0 = 0$ and the decrement $\Delta = 0.1$

When the reversible magnetization is not negligible and the linear term has a finite but significant contribution to make to the induction, then we have to use the full expression of the induction given in (5.11), which includes the linear term of reversible magnetization. The inclusion of this term does not affect the value of b_1 as we have seen before, therefore its total effect is limited mathematically to an additional linear term in the expressions of f_+ and f_-. The mathematical formulation of the magnetic induction now is shown below in (5.14),

$$f_+ = A_0 x + \tanh\ (x - a_0) + \frac{1}{2}\left\{\tanh\ \left[-x_{mn}(1-\Delta) + \Delta x + a_0\right] - \tanh\ \left[-x_{mn}(1-\Delta) + \Delta x - a_0\right]\right\} \quad (5.14a)$$

and

$$f_- = A_0 x + \tanh\ (x + a_0) - \frac{1}{2}\left\{\tanh\ \left[-x_{mn}(1-\Delta) + \Delta x + a_0\right] - \tanh\ \left[-x_{mn}(1-\Delta) + \Delta x - a_0\right]\right\} \quad (5.14b)$$

for the ascending and the descending sections, respectively.

The calculation procedure from now on follows the steps as described before.

Figure 5.6 depicts a magnetization curve calculated from (5.14) with the following numerical values: $A_0 = 0.05$, $a_0 = 2$ and the process started in the first quadrant at the field coordinate of $x_{m,0} = 2$.

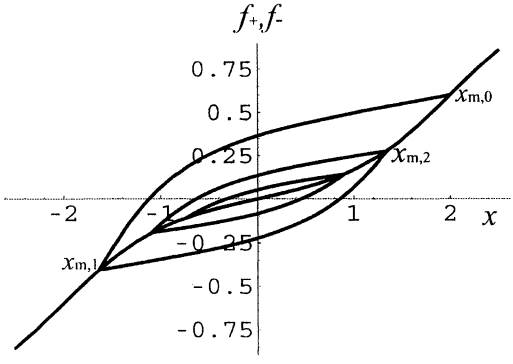

Figure 5.6: Open reversal loops with decreasing amplitude for $A_0 = 0.05$ and the decrement $\Delta = 0.1$

It has to be emphasized that the solutions given here are unique. As a consequence of the hyperbolic rules laid down in Chapter 1 there is one and only one hyperbolic line either ascending or descending that is allowed to go through the given points within a set of hysteresis loops, defined by a_0 and x_m parameters. The model obeying these rules yields the only unique solution possible.

5.3 The Preisach Distribution Function

The Preisach model has been so far the most popular model in the field of magnetics for the description of the hysteretic phenomena in ferromagnetic materials [7,9]. In the classical scalar Preisach model the hysteresis can be described in the following mathematical expression:

$$M(t) = \iint^{\alpha\,\beta} H(t)\, \gamma_p(\alpha,\beta)\, d\alpha\, d\beta \tag{5.15}$$

where M signifies the magnetization, H is the exciting magnetic field, γ_p is the distribution function of the elementary magnetic parts and α and β are switching values of the elementary rectangular loops. Mayergoyz showed in 1986 [10,11] that the γ_p distribution function can be calculated from two given values M_α and $M_{\alpha,\beta}$ of one of the first-order reversal curves, determined experimentally at points α and β. He formulated his findings in the following mathematical expressions. When function F is defined as

$$F(\alpha,\beta) = M_{\alpha} - M_{\alpha\beta}, \tag{5.16}$$

then the $\gamma_{P}(\alpha,\beta)$ distribution function can be described as

$$\gamma_{P}(\alpha,\beta) = -\frac{1}{2}\frac{\partial^2 F(\alpha,\beta)}{\partial\alpha\,\partial\beta}, \tag{5.17}$$

where M_{α} and $M_{\alpha\beta}$ are the magnetization values at field coordinates points α and β respectively measured on the same minor magnetization loop

This formulation looks simple in principle, however, in practice the determination of function $F(\alpha,\beta)$ usually represents a lot of complicated approximations or curve fittings. Because of this difficulty, in most practical calculations $\gamma_{P}(\alpha,\beta)$ is substituted by either a Lorentzian $\gamma_{L}(\alpha,\beta)$ or a Gaussian $\gamma_{G}(\alpha,\beta)$ distribution function. Although either of these functions gives a reasonably good approximation, they are only approximations and all approximations are prone to errors and seldom if ever lead to absolute accuracy. By using Mayergoyz' formulation, however, and substituting the mathematical expressions of M_{α} and $M_{\alpha\beta}$ from (3.2, 3,3) and (5.4, 5.5), respectively into (5.17), we can express the $\gamma_{T}(\alpha,\beta)$ distribution function in an analytical form from the T(x) function. Here x_r and x takes the place of α and β, respectively. There are the two expressions, the first is the ascending (5.18) and the second is for the descending part (5.19) of the hysteresis loop. First it was assumed that the return point is on an ascending major loop and the return loop is descending towards the negative maximum, hence the subscript of the negative sign (–),

$$M_{\alpha+} = \tanh(x_r - a_0) + b_1 \tag{5.18}$$

$$M_{\alpha\beta-} = \tanh(x_r + a_0) - b_1 + \left[\tanh(x_r - a_0) - \tanh(x_r + a_0) + 2b_1\right]\frac{\tanh(-x_m + a_0) - \tanh(x + a_0)}{\tanh(-x_m + a_0) - \tanh(x_r + a_0)}. \tag{5.19}$$

After forming $F(x_r, x)$ (see (5.16)), and differentiating it by x_r and x successively, we can express $\mu_{T}(x_r,x)$ in an analytical form. The calculation of function $F_{+}(x_r, x)$ starting from the descending part of the hysteresis loop and following the same steps, will yield similar expressions to $M_{\alpha-}$ and $M_{\alpha\beta+}$ in the following form:

$$M_{\alpha-} = \tanh(x_r + a_0) - b_1 \tag{5.20}$$

$$M_{\alpha\beta+} = \tanh(x_r - a_0) + b_1 + \left[\tanh(x_r + a_0) - \tanh(x_r - a_0) + 2b_1\right]\frac{\tanh(x_m - a_0) - \tanh(x - a_0)}{\tanh(x_m - a_0) - \tanh(x_r - a_0)} \tag{5.21}$$

In Figure 5.7 the bell-shaped μ_{T} distribution function calculated from (5.17) is depicted. As the graphs show, the μ_{T} distribution gives a nearly perfect fit to the μ_{G} Gaussian distribution near to the centerline of the curve but the fit is better to the μ_{L} Lorentzian distribution curve

far from the center line. Figure 5.8 shows the surface map of the distribution functions $\mu_{T+}(x_r,x)$ and $\mu_{T-}(x_r,x)$ as a function of x the excitation and x_r the reversal point coordinates.

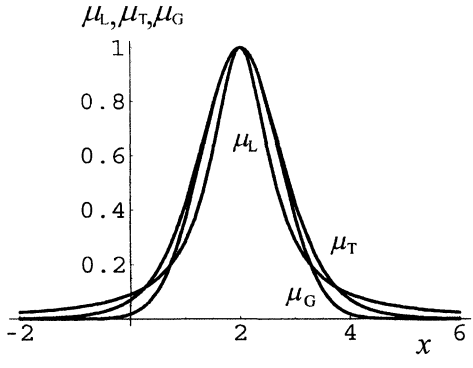

Figure 5.7: Distribution functions: Lorentzian μ_L, T model μ_T, and Gaussian μ_G

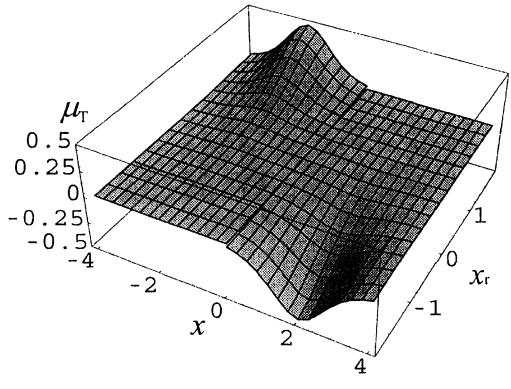

Figure 5.8: The surface map of the distribution function calculated from the T(x) model as a function of field excitation x ($-4 < x < 4$) and the coordinates of field interruption x_r ($-2 < x_r < 2$)

The reader must remember that although the distribution functions are plotted for wide limits to show the full bell-shaped curves, in reality they only have physical meanings between the limits of $\pm x_{m2}$ therefore for $|x| \geq |x_m|$ $\mu_+(x_r,x) = 0$ and $\mu_-(x_r,x) = 0$. It also has to be emphasized that the x_r field interruption coordinates can only have physical meanings while they are sitting on the hysteresis loop.

5.4 Higher-Order Reversal Loops

Mathematical models of any physical phenomena always represent an approximation of the process in question. Its goodness or accuracy can be measured by its ability to predict experimental results. In some case, for instance multiple reversals, the possible deviation between experiments and the model is cumulative. A small error, which in one step might be negligible, will be magnified at the end of the process particularly after a large number of steps. The investigation of the higher-order reversal loops and their comparison with experimental data could be a good measure of the accuracy of the model and its usefulness in practical applications [12–15].

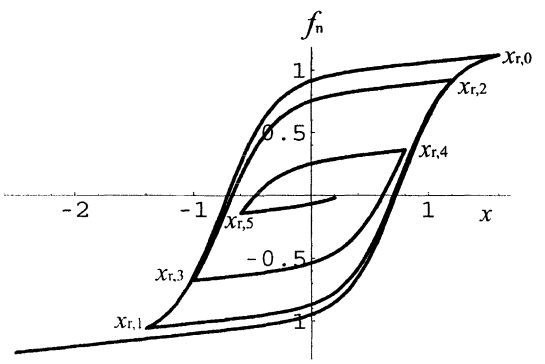

Figure 5.9: Open loops modeled up to six reversals with the field amplitude reduced by $\Delta x = 0.2$ after every reversal for $B = 2.4$ and $A_0 = 0.1$

As the first step in this process, a good match has to be found to the major hysteresis loop from which the characteristic free parameters can be calculated [16,17] (see Chapter 3). To demonstrate the process up to seven reversals loops have been calculated by using the T(x) model, assuming that $B_0 = 1$, $C_0 = 2.4$, and $A_0 = 0.1$ give the best parametric fit in (3.6) and (3.7). All seven calculated loops (six reversals) are depicted in Figure 5.9.

In Figure 5.10 another set of open loops are shown, modeled by using a different set of starting parameters ($B_0 = 1$, $C_0 = 2.2$, and $A_0 = 0.07$). The graph shows five reversals with six open loops. The decrement in amplitude was $\Delta = 0.2$ after every reversal.

Once the best fit has been found to the experimental data, as was said before, then the free parameters can be calculated (see Chapter 3). This will lead to a case when we have to abandon the normalized form of the model and use the full expressions of the model ((3.6) and (3.7)).

The nth ascending loop is described by the mathematical expression given in (5.22),

$$f_{+,n} = \tanh\left[C_0\,(x - a_0)\right] + b_{n-1} + c_n + A_0\,x \tag{5.22}$$

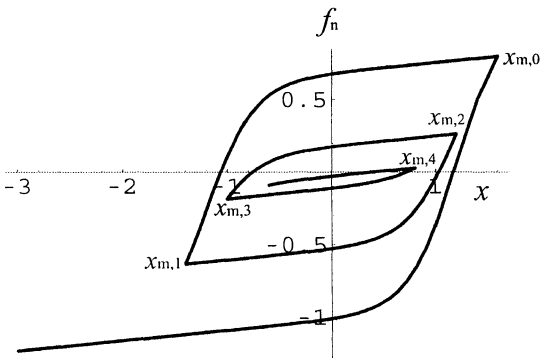

Figure 5.10: Calculated high-order (up to five reversals) reversal loops for $\Delta = 0.2$, $B_0 = 1$, $C_0 = 2.2$ and $A_0 = 0.07$

Here the c_n constant can be calculated from the criterion that at the nth and the $(n-1)$th loop at reversals f_{n-1} must be equal to f_n. This gives the two basic shifting constants c_{nu} and c_{nd}. The mathematical transition between the two constants, which is tangent hyperbolic in nature, is shown in (5.23),

$$c_n = c_{n,u} \frac{\tanh\ C_0\ (x_{r,\,n-1} - a_0) - \tanh\ [C_0\ (x - a_0)}{\tanh\ [C_0\ (x_{r,\,n-1} - a_0) - \tanh\ [C_0\ (x_{r,\,n} - a_0)} + c_{n,d} \frac{\tanh\ [C_0\ (x_{r,\,n} - a_0) - \tanh\ [C_0\ (x - a_0)}{\tanh\ [C_0\ (x_{r,\,n} - a_0) - \tanh\ [C_0\ (x_{r,\,n-1} - a_0)}. \tag{5.23}$$

Similarly for the $(n+1)$th descending loop we get the following expressions

$$f_{+,n+1} = \tanh\ [C_0\ (x - a_0)]\ + b_n + c_{n+1} + A_0\ x \tag{5.24}$$

where

$$c_{n+1} = c_{n+1,u} \frac{\tanh\ [C_0\ (x_{r,\,n} - a_0) - \tanh\ [C_0\ (x - a_0)}{\tanh\ [C_0\ (x_{r,\,n} - a_0) - \tanh\ [C_0\ (x_{r,\,n+1} - a_0)} + c_{n+1,d} \frac{\tanh\ [C_0\ (x_{r,\,n+1} - a_0) - \tanh\ [C_0\ (x - a_0)}{\tanh\ [C_0\ (x_{r,\,n+1} - a_0) - \tanh\ [C_0\ (x_{r,\,n} - a_0)}. \tag{5.25}$$

Here $x_{r,n-1}$,, $x_{r,n}$ and $x_{r,n+1}$ represent the field coordinates of the (n–1)th, the nth and (n+1)th reversal points, respectively, and the indices u and d represent the up- or down-going processes, respectively.

References

[1] S.E. Zirka and Y.I. Moroz, Hysteresis Modeling Based on Transplantation. IEEE Trans. Magn. **31**, 3509–3511 (1995).

[2] S.E. Zirka and Y.I. Moroz, Hysteresis Modeling Based on Similarity. IEEE Trans. Magn. **35**, **No. 4**, 2090–2096 (1999).

[3] N.A. Zolotariov, Mathematical modeling of Magnetic Hysteresis. Electrichestvo **No. 6**, 2–26 (1989).

[4] C.D. Jiles and D.L. Atherton, Theory of Ferromagnetic Hysteresis. Appl. Phys. **55**, 2115–2120 (1984).

[5] K.H. Carpenter, A Differential Equation Approach to Minor Loops in the Jiles-Atherton Hysteresis Model. IEEE Trans. Magn. **27**, 4404–4406 (1991).

[6] E. Madelung, Uber Magnetisierung durch schnellverlaufende Strome und die Wirkungweise der Rutherford-Markoni Magnetodetektors. Ann. Phys. 1905, **17**, **No. 5**, 861–863 (1905).

[7] I.D. Mayergoyz, *Mathematical Models of Hysteresis* (Springer-Verlag, N.Y., 1991).

[8] J. Takacs, A Phenomenological Mathematical Model of Hysteresis. COMPEL Int. J. Comp. and Math. for E. and E. Eng. **20 No.4**, 1002–1014 (2001).

[9] F. Preisach, Uber die magnetische Nachwirkung. Zeit. Physik. **94**, 277–302 (1935).

[10] I.D. Mayergoyz, (1986) Mathematical Models of Hysteresis. Phys. Rev. Lett. **56**, 1518–1521 (1935).

[11] I.D. Mayergoyz and T.A. Keim, Superconducting Hysteresis and the Preisach Model. J. Appl. Phys. **67**, **No. 9**, 5466–5468 (1990).

[12] I.D. Mayergoyz, G. Friedman and C. Salling, Comparision of the Classical and the Generalised Preisach Hysteresis Models with Experiment. IEEE Trans. Magn. **25**, 3925–3927 (1989).

[13] I.D. Mayergoyz, A.A. Adly and G. Friedman, New Preisach-type Models of Hysteresis and their Experimental Testing. J. Appl. Phys. **67**, 5373–5375 (1990)

[14] F. Ossart and T.A. Phung, Comparision between Various Hysteresis Models and Experimental Data. J. Appl. Phys. **67**, **No. 9**, 5379–5384 (1990).

[15] I.D. Mayergoyz and G. Friedman, Generalised Preisach Model of Hysteresis. IEEE Trans. Magn. **24**, 212–217 (1988) .

[16] E. Della Torre and F. Vajda, Parameter Identification of the Complete-moving Hysteresis Model Using Major Loop Data. IEEE Trans. Magn. Magn. **30**. 4987–5000 (1994).

[17] G. Friedman, New Formulation of the Stoner–Wohlfart Hysteresis Model and the Identification Problem. J. Appl. Phys. **67**, **No. 9**, 5361–5363 (1990).

6. Remanent Magnetism

6.1 The Loop of Remanent Magnetism

One of the riddles of the otherwise difficult subject is the mathematical description of the loop of remanent magnetism. Although most parts of the puzzle were available the rules to assemble the whole picture had eluded people. In the following, based on the rules given and the model described at the beginning in Chapter 1, a full mathematical description will be given of the process leading to the loop of remanent magnetism.

When the exciting magnetic field is interrupted at x_i the value of the normalized field during the process of magnetization, then the magnetic state of the specimen will not stay the same but it declines to a value below that determined by the field at the point of interruption. The shape of the path of decline following the interruption between $x = x_i$ and $x = 0$ has not been explained and all textbooks normally show an arbitrary line between the two points representing the excited and the remanent magnetic state. Some authors, realizing the similarity between the return path and part of the major loop, proposed the transplantation of part of the major loop [1,2]. Although this is a big step in the right direction, without applying the correct rules it will not lead to the right result. With this model, by applying the hyperbolic tangent rule, this return path can be expressed in an exact mathematical term [3]. Supposing the interruption of the field happened on the ascending side of the hysteresis loop then the field will decline on a path imaging the descending part of the loop shifted to the point of interruption. We know from practical experience that when the substance is brought into saturation and the magnetization is interrupted then the induction will follow the path of the hysteresis until the field drops to zero and the magnetization reaches the point of remanence [4]. The same rule applies to any point on the hysteresis loop, major or minor. By recalling the mathematical expression for the descending part of the hysteresis loop from (3.3), the return path $f_{r,-}$ shifted to the right position can be described as follows.

$$f_{r,-} = \tanh(x + a) - b_1 + c_4 . \tag{6.1}$$

The c_4 shifting constant can be calculated from the criterion, that the main loop and the descending minor loop share a common point at the point of interruption. By equating the expressions of the ascending part of the loop f_+ and $f_{r,-}$ above at $x = x_i$ we can get the constant as

$$c_4 = \tanh(x_i - a_0) - \tanh(x_i + a_0) + 2b_1 . \tag{6.2}$$

Mathematics of Hysteretic Phenomena. Jeno Takács

ISBN: 3-527-40401-5

The constant b_1 is defined in (3.2) and the $f_{r,-}$ function is limited to values between $x = x_i$ and 0. In the case when the magnetization is moving on the descending part of the hysteresis loop, by using the same logic and arguments, it is easy to see that the ascending return path will take the following form:

$$f_{r,+} = \tanh(x - a_0) + b_1 + c_5 \tag{6.3}$$

where, similarly to (6.2)

$$c_5 = \tanh(x_i + a_0) - \tanh(x_i - a_0) - 2\,b_1\,. \tag{6.4}$$

The full expressions describing both the ascending and the descending return paths are shown in (6.5).

$$f_{r,+} = \tanh(x - a_0) + \tanh(x_i + a_0) - \tanh(x_i - a_0) - b_1 \tag{6.5a}$$

$$f_{r,-} = \tanh(x + a_0) + \tanh(x_i - a_0) - \tanh(x_i + a_0) + b_1\,. \tag{6.5b}$$

All the curves are limited to values between $x = x_i$ and 0. Both the ascending and the descending sets of curves, showing the calculated return path, are depicted in Figure 6.1 for the interruption field coordinate values of $x_i = \pm 2,\ \pm 1.5,\ \pm 1$, and ± 0.5.

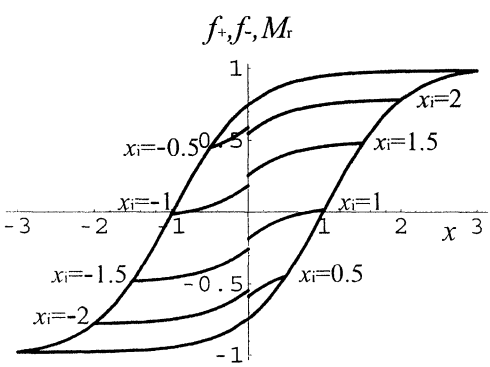

Figure 6.1: The ascending and descending return paths after the field excitation is turned off leading to remanent magnetism for the interruption field coordinates of $x_i = \pm 2,\ \pm 1.5,\ \pm 1$, and ± 0.5

The intersection between the return paths and the vertical axes marks the remanent magnetic state of the substance, i.e. the value of induction for $x = 0$. Its value is a function of the point of interruption x_i, the coercive force a_0 and x_m defining the loop on which the point of interruption was located.

Looking at Figure 6.1 it is obvious that in every loop there are two possible excitation field values for every state of remanent magnetism. One is corresponding to an ascending

and another to a descending return path. This is another way of stating the well-known multivalued relationship between the exciting field and residual flux. Although the remanent induction can be determined from the parameters of the hysteresis loop and the coordinates of the field of interruption, this is not so for the reverse. The knowledge of the remanent state is not enough to calculate the interrupted field value unambiguously. What is needed for determining the field values are the values of two parameters a_0 and x_m and also the direction of the field (up or down) at the point of interruption. It is possible to calculate both corresponding field values for a set of a_0 and x_m values, by equating the normalized field with zero i.e. $x = 0$ (no excitation) in (6.1). The remanent induction M_r can be described as the function of x_i the field of interruption in the following way

$$M_r = \tanh\ a_0 + \tanh\ (x_i - a_0) - \tanh\ (x_i + a_0) + b_l\,. \tag{6.6}$$

By solving (6.6) for x_i we can calculate x_{id} the field of interruption values for the set of descending return paths with the following result

$$x_{id} = \operatorname{arctanh}\sqrt{\frac{\tanh a_0 - M_r - b_l}{2\tanh a_0 - (\tanh a_0)^2 - (M_r + b_l)(\tanh\ a_0)^2}}\,. \tag{6.7}$$

Similarly, by doing the same mathematical steps to the expression of the ascending paths, we arrive to the following expression, where M_r the remanent magnetism is the same as in (6.6)

$$M_r = \tanh\ (-a_0) + \tanh\ (x_i + a_0) - \tanh\ (x_i - a_0) - b_l\,. \tag{6.8}$$

By solving (6.8) for x_i again we can get the expression for the values of the field of interruption x_{iu} for the ascending paths in the following form

$$x_{id} = \operatorname{arctanh}\sqrt{\frac{\tanh a_0 + M_r - b_l}{2\tanh a_0 - (\tanh a_0)^2 + (M_r - b_l)(\tanh\ a_0)^2}}\,. \tag{6.9}$$

We have to remember that M_r has the same numerical value in (6.7) as in (6.9).

Although the remanent magnetization curve has been measured and its shape has been explored experimentally, its mathematical modeling so far has proved very elusive. This model presented here, however, models the process mathematically as described in the following [3].

The remanent magnetization loop can be divided into four distinct regions. The first section in the first quadrant is associated with part of hysteresis curve running between saturation and zero field on the descending part of the loop. The second region is where the loop is running through the second and third quadrants into saturation. The third and the forth regions are the negative equivalents of the first and the second regions, respectively. Let us start by imagining that we are moving on the descending part of the hysteresis curve from the point of positive saturation. Any exciting field value between saturation and zero when interrupted will lead to a reduced remanent induction commonly known as remanence. The remanent magnetization in this region is independent of the field of magnetization and

its value is constant. This part of the remanent magnetization curve therefore is going to be represented by a line running between infinity and zero at the value of M_r. The second region runs from zero to the negative saturation field value. In the third region, similarly to the first one, the remanent magnetism is constant with the value of $-M_r$. Finally, the fourth region runs between zero and the positive saturation field value. In mathematical terms the first and the third region will be described by the $f_{r,-} = M_r$ and the $f_{r,+} = -M_r$ functions, respectively. The M_r remanent magnetism in the second region is described by the function in (6.6) and in the fourth region by (6.8).

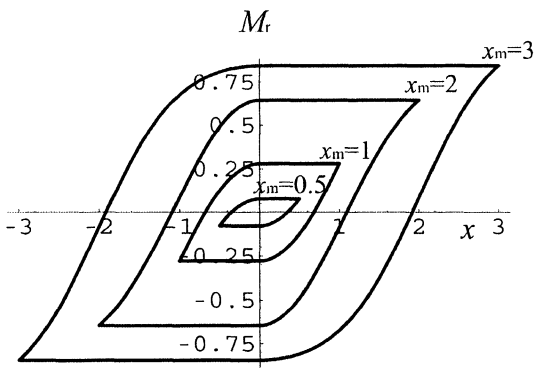

Figure 6.2: Remanent magnetization loops for coercivity of $a_0 = 2$, and the maximum field $x_m = 3$, 2, 1, and 0.5

A set of remanent magnetization loops constructed in the way as described above is depicted in Figure 6.2. The numerical values used in the calculation were $a_0 = 2$ and $x_m = 3$, 2, 1, and 0.5.

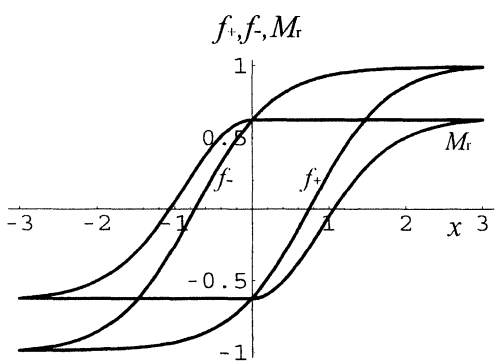

Figure 6.3: A set of curves showing the hysteresis and the corresponding remanent magnetization loops for $a_0 = 0.75$, $x_m = 3$, and $A_0 = 0$

In Figure 6.3 a hysteresis and its corresponding remanent magnetization curves are shown forming a set for the same numerical parameter values and belonging to the same family of hysteresis loops. At large a_0 values the two loops approach each other. Although the two curves, the induction versus field (hysteresis loop) and the remanent magnetization versus field (remanent magnetization loop), are fairly similar, in fact they represent completely different information. The full detailed knowledge of the hysteresis loop is necessary to calculate the loop of remanent magnetization, but the hysteresis loop can not be reconstructed with the full detailed knowledge of the remanent magnetization loop. A set of curves, showing the hysteresis and the remanent magnetization loops, depicted in Figure 6.3 calculated by using the numerical values of $a_0 = 0.75$, $x_m = 3$, $A_0 = 0$.

When the reversible magnetization can not be neglected then the equations shown in (6.10) should be used for the calculations. The expressions for the return paths only differs from (6.5) by an additional linear term,

$$f_{r,+} = \tanh\ (x - a_0) + \tanh\ (x + a_0) - \tanh\ (x_i - a_0) - b_i + A_0 x \qquad (6.10a)$$

$$f_{r,-} = \tanh\ (x + a_0) + \tanh\ (x - a_0) - \tanh\ (x_i + a_0) + b_i + A_0 x\,. \qquad (6.10b)$$

The equations for the remanent magnetization are the same as (6.6) and (6.8) for the descending and the ascending part, respectively.

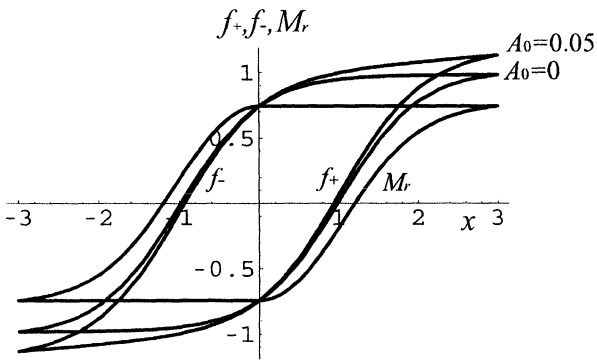

Figure 6.4: A set of curves showing the hysteresis loop with and without the reversible magnetization and the corresponding remanent magnetization loops for the parameter values of $a_0 = 0.75$, $x_m = 3$, $A_0 = 0$ and 0.05

In Figure 6.4 the set, formed by the hysteresis and remanent magnetization loops, is shown for the case when the relative magnitude of the reversible magnetization is $A_0 = 0.05$, with other parameter values same as before. The set also includes the hysteresis loop without the reversible magnetization ($A_0 = 0$). It is obvious that the two cases with and without the reversible magnetization lead to an identical remanent magnetization loop.

6.2 Biased Remanence Curves

It is often necessary in practical applications to combine two exciting fields, normally a slow changing or DC and a faster acting AC field as discussed in Chapter 3. When under these circumstances the AC exciting field is stopped, the resulting pattern of remanent magnetism will differ from the case shown in Section 6.1 due to the presence of the DC field component. In order to model these conditions (3.12), for the biased hysteresis loops, needs to be used as the starting equation of our modeling. Let us recall (3.12)

$$f_+ = \tanh\ (x - a_0) + b_u \tag{3.12a}$$

$$f_- = \tanh\ (x + a_0) - b_d\,. \tag{3.12b}$$

It has to be remembered that every remanent magnetism loop is composed of four distinct regions as described in Section 6.1. The first region extends from 0 to x_m and the return path can be described in mathematical form as

$$f_- = \tanh\ (x + a_0) - b_l + c_3 \qquad 0 \le x \le x_m \tag{6.11}$$

where b_l is given in (3.2).

Similarly to the shifting constant in Chapter 3, here c_3 can be calculated from the criteria, that the value of the down-going path in (3.12a) and the upward-going return path in (6.13) must be equal at the point of reversal. Therefore when $x = x_i$

$$c_3 = \tanh\ (x_i - a_0) - \tanh\ (x_i + a_0) + b_l + b_u \tag{6.12}$$

The second region, which also extends between the same two limits, can be described as

$$f_+ = \tanh\ (x + a_0) - b_l + d_3 \qquad 0 \le x \le x_m\,. \tag{6.13}$$

By using the same logic as before here d_3 can be calculated from (6.13) and (6.12b) as

$$d_3 = \tanh\ (x_i + a_0) - \tanh\ (x_i - a_0) + b_l - b_d\,. \tag{6.14}$$

The other two regions, the third and forth, running between $-x_m$ and 0, follow the same rules. Therefore the equation, describing the descending return path, will be

$$f_- = \tanh\ (x - a_0) + b_l + c_4 \qquad 0 \ge x \ge -x_m\,. \tag{6.15}$$

The expression in (6.16) below gives the c_4 shifting constant at $x = -x_i$,

$$c_4 = \tanh(-x_i + a_0) - \tanh(-x_i - a_0) - b_l - b_d . \tag{6.16}$$

Finally, the ascending return path in the forth quadrant can be described as

$$f_+ = \tanh\ (x - a_0) + b_l + d_4 \qquad 0 \geq x \geq -x_m \tag{6.17}$$

where d_4 can be expressed as

$$d_4 = \tanh\ (-x_i - a_0) - \tanh\ (-x_i - a_0) - b_l + b_u . \tag{6.18}$$

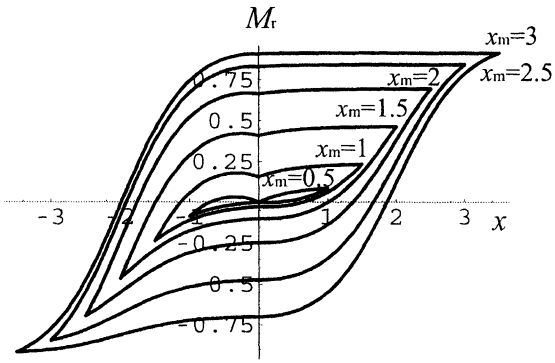

Figure 6.5: Biased remanent magnetization loops for $a_0 = 2$, $d_0 = 0.5$, and as a parameter $x_m = 0.5$, 1, 1.5, 2, 2.5, and 3

In order to complete the set of expressions, the formulae for b_3, b_4, b_u, and b_d are also listed here from Chapter 3 for the benefit of the reader

$$b_3 = [\tanh\ (x_m + d_0 + a_0) - \tanh\ (x_m + d_0 - a_0)]/2 \tag{3.8}$$

$$b_4 = [\tanh\ (-x_m + d_0 + a_o) - \tanh\ (-x_m + d_0 - a_0)]/2 \tag{3.9}$$

and

$$b_u = b_3 \frac{\tanh\ (-x_m + d_0 - a_0)}{\tanh\ (-x_m + d_0 - a_0) - \tanh\ (x_m + d_0 - a_0)}$$

$$+ b_4 \frac{\tanh\ (x_m + d_0 - a_0) - \tanh\,(x - a_0)}{\tanh\ (x_m + d_0 - a_0) - \tanh\ (-x_m + d_0 - a_0)} \tag{3.10a}$$

$$b_d = b_3 \frac{\tanh\ (-x_m + d_0 + a_0) - \tanh\,(x + a_0)}{\tanh\ (-x_m + d_0 + a_0) - \tanh\ (x_m + d_0 + a_0)}$$

$$+ b_4 \frac{\tanh\,(x_m + d_0 + a_0) - \tanh\,(x + a_0)}{\tanh\,(x_m + d_0 + a_0) - \tanh\,(-x_m + d_0 + a_0)} . \qquad (3.10b)$$

In Figure 6.5 a set of curves are shown representing the remanent magnetization curves with DC bias, calculated from (6.11), (6.13), (6.15), and (6.17). The numerical parameter values used for the calculation were: $a_0 = 2$, $d_0 = 0.5$, for the maximum field values of $x_m = 0.5$, 1, 1.5, 2.5, and 3.

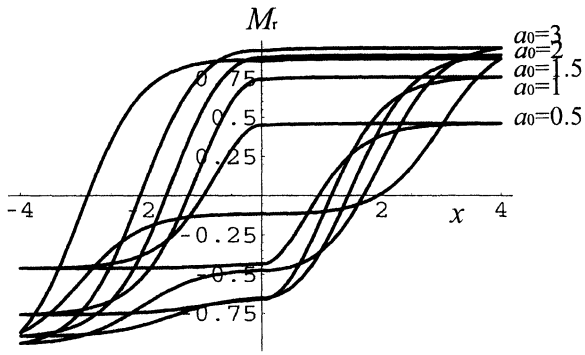

Figure 6.6: Biased remanent magnetization loops for $d_0 = 1$, $x_m = 3$, and as a parameter $a_0 = 0.5$, 1, 1.5, 2, and 3

Figures 6.6 and 6.7 depict the remanent magnetization loops dependence on the two other parameters namely a_0 (coercivity) and the DC bias d_0.

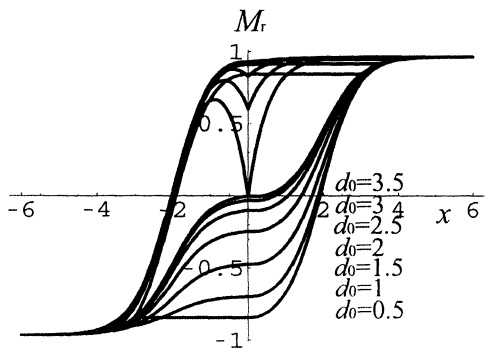

Figure 6.7: Biased remanent magnetization loops for $x_m = 3$, $a_0 = 2$, and as a parameter $d_0 = 0.5$, 1, 1.5, 2, 2.5, 3, and 3.5

The parameter values used for the calculations were for Figure 6.6 $d_0 = 1$, $x_m = 3$, and $a_0 = 0.5$, 1, 1.5, 2, and 3, for Figure 6.7 were $x_m = 3$, $a_0 = 2$, and $d_0 = 0.5$, 1, 1.5, 2, 3, and 3.5.

In the case when $A_0 \neq 0$ i.e. the reversible magnetization is not zero, the remanent magnetization loops will be unaltered, identical to the cases discussed above.

6.3 Anhysteretic Magnetization and Anhysteretic Remanence

As was pointed out in Chapter 4, anhysteretic magnetization by definition free of hysteretic effects so the relationship between exciting field and induction can be described by a single-valued function. Since this is the property of a perfect flawless material, it is difficult to achieve in practice. It leaves the second alternative to achieve the anhysteretic magnetization, namely the cyclic magnetization where the extremes of the minor loops, both positive and negative, will move on the anhysteretic curve. Section 4.2 is dedicated to the full explanation and the mathematical treatment of the anhysteretic magnetization and its representative curve. This single-valued function of the field-induction relationship is an important feature of the magnetization process and it has great practical significance. The reader must remember the difference between the hysteresis-free material and the anhysteretic magnetization process. While (2.4) describes the hysteresis free magnetization (4.6) formulates the anhysteretic process in a mathematical form. When, during this combined AC-DC magnetization the process is interrupted, the specimen is left in an anhysteretically magnetized state that will revert into a remanent state. In the following the mathematical description of the remanent magnetization resulting from the anhysteretic process will be given. A glance at the set of remanent magnetization loops shown in Figure 6.5 can convince the reader that the crossover points again form a continuous line between the positive and negative saturation. This, which that we will call anhysteretic remanent curve, is analogous to the anhysteretic magnetization curve. Its relation to the remanent magnetization and the hysteresis loop will be explained in this section. The procedure is similar to that of the hysteretic remanent magnetization described in detail in Section 6.1.

The expression for the anhysteretic magnetization curve f_s is given in (4.7) as

$$f_s = [\tanh\ (x + a_0) - \tanh\ (x - a_0)]/2\,. \tag{4.7}$$

For the description of the anhysteretic remanent magnetization we have to follow the logical steps described for the hysteretic remanent magnetization in Section 6.1. Let us suppose that the magnetizing field is decreasing from positive saturation and the process follows the anhysteretic curve. When the field is abruptly removed then the induction will decline until the return curve intersects the vertical axis where $x = 0$. We have seen in Chapter 3 that the extrema of all symmetric minor loops are located on the anhysteretic curve. Any point on the anhysteretic curve used as a point of interruption belong to one and only one minor loop whose extremum is the point of interruption. From this it will follow that the remanent magnetism will be determined by the intersections of the minor loops whose extrema lie on the anhysteretic magnetization curve with the vertical axis.

Since the return path for the point of interruption x_i will be a minor loop with the extremum of $x_m = x_i$ by substituting x_i for x_m in (3.2) we can formulate the return path in this form,

$$f_{-} = \tanh\ (x + a_0) - [\tanh\ (x_i + a_0) - \tanh\ (x_i - a_0)]/2 \tag{6.20a}$$

$$f_{+} = \tanh\ (x - a_0) + [\tanh\ (x_i + a_0) - \tanh\ (x_i - a_0)]/2\,. \tag{6.20b}$$

By substituting $x = 0$ into (6.20) we can formulate the function of the points of intersections with the vertical axis as the function of x_i representing the remanent magnetic state in the following form,

$$f_{r,-} = \tanh\ a_0 - [\tanh\ (x_i + a_0) - \tanh\ (x_i - a_0)]/2 \qquad \text{for}\ \ 0 \geq x_i \tag{6.21a}$$

$$f_{r,+} = \tanh\ (-a_0) + [\tanh\ (x_i + a_0) - \tanh\ (x_i - a_0)]/2 \qquad \text{for}\ \ 0 \leq x_i\,. \tag{6.21b}$$

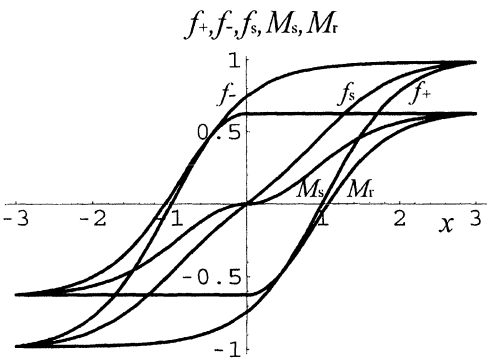

Figure 6.8: A set of curves showing the major hysteresis loop and the anhysteretic curve with the corresponding hysteretic remanent magnetization loop and its anhysteretic curve

Figure 6.8 shows a major hysteresis loop and the anhysteretic magnetization curve superimposed on the corresponding loop of remanent magnetism with the anhysteretic remanent magnetization curve.

In the knowledge of the remanent magnetization loop the anhysteretic remanent magnetization can also be determined. By applying the definition of the anhysteretic magnetization process, described in Section 4.2 and by using (6.20) we can express the function describing the positive-going part of the anhysteretic remanent magnetization curve in the first quadrant in the following form

$$f_r = [M_r + \tanh\ (-a_0) + \tanh\ (x_i + a_0) - \tanh\ (x_i - a_0) - b_l]/2$$

$$\text{for} \quad x_m \geq x_i \geq 0\,, \tag{6.22}$$

and similarly in the third quadrant

$$f_r = [-M_r + \tanh\ a_0 + \tanh\ (x_i - a_0) - \tanh\ (x_i + a_0) + b_l]/2$$

$$\text{for} \quad -x_m \le x_i \le 0 \tag{6.23}$$

We must remember that the remanent magnetism is constant for descending field values between zero and the positive maximum with the value of M_r . The same is true for the remanent magnetism for ascending field values between $-x_m$ and zero. Here the value of the remanence is $-M_r$.

At first sight the two approaches formulated in (6.21), (6.23), and (6.20) produced two different results. However, considering that

$$M_r = \tanh(-a_0) + b_1$$

therefore

$$-M_r = \tanh(a_0) - b_1 . \tag{6.24}$$

After substitution of M_r and $-M_r$ into (6.22) and (6.23) we arrive at an expression identical to (6.21). We can conclude that both approaches will lead to the same result.

As we expected the anhysteretic magnetization and the anhysteretic remanent magnetization are both single-valued functions of the normalized field, therefore in the knowledge of one the other can be calculated unambiguously.

References

[1] S.E. Zirka and Y.I. Moroz, Hysteresis modeling based on transplantation. IEEE Trans. Magn. **31**, 3509–3511 (1995).

[2] S.E. Zirka and Y.I. Moroz, Hysteresis modeling based on similarity. IEEE, Trans. Magn. **35, No. 4**, 2090–2096 (1999).

[3] J. Takács, A phenomenological mathematical model of hysteresis. COMPEL Int. J. Comp.and Math. for E. and E. Eng. **20, No.4**, 1002–1014 (2001).

[4] E. Della Torre, *Magnetic Hysteresis* (IEEE Press, N.Y., 1999).

7. Permeability and Shearing

7.1 Permeability and Susceptibility

So far we have talked about field excitation, induction and magnetization by using conventional notation H, B, and M, respectively. Now we are going to introduce two new closely related concepts, permeability and susceptibility. The relationship between these quantities above is usually written in the following form

$$B = \mu_0(H + M) \tag{7.1a}$$

or

$$B = \mu_0(H + \chi H) = \mu_0\mu_r H \tag{7.1b}$$

where susceptibility is defined as the ratio of magnetization to field

$$\chi = \frac{M}{H} \tag{7.2}$$

In physics and material science people like to use susceptibility, while in engineering particularly where magnetic materials are involved, permeability is preferred [1]. For most nonferrous materials permeability and susceptibility are independent of the field therefore they are both relatively small and constant, which makes an easy linear relationship between field, induction, and magnetization. Ferromagnetic materials are different, because their permeability and susceptibility are both large and field dependent, which makes the relationship between magnetic field and the other two quantities, induction and magnetization of a highly nonlinear nature.

One can often come across the term of relative permeability denoted by μ_r. This is defined as

$$\mu_r = \frac{\mu}{\mu_0} \tag{7.3}$$

here μ_0 represents the permeability of free space whose magnitude is $\mu_0 = 4\pi 10^{-7}$ H m^{-1}. The relative permeability of free space is unity. There is an easy relationship between relative permeability and susceptibility, which can be seen from (7.1b)

Mathematics of Hysteretic Phenomena. Jeno Takács

ISBN: 3-527-40401-5

$$\mu_r = 1 + \chi \tag{7.4}$$

Throughout this book we are going to use the preferred engineering term and concentrate on permeability.

There are a number of different kinds of permeabilities defined in practice:

- *The static permeability* μ_{st} is the ratio between induction and field this is often referred to as normal permeability.
- *The incremental permeability.*
- *The differential permeability* μ_d, which is the limit of the incremental permeability, when the change in field approaches zero, is also referred to as *reversible permeability.* It is defined as the first derivative of the virgin or the hysteresis curve (see also in Chapter 10, superimposed minor hysteresis loops.)
- *The initial permeability* μ_i is defined as the tangent to the virgin magnetization curve when the field is approaching zero.

By recalling the relationship between the normalized field and induction we can formulate the various permeabilities as shown below. The simplest, the static or normal permeability μ_{st}, which belongs to the virgin magnetization curve, with reference to the definition above, can be calculated by simply dividing f_s in (4.1) by x thus

$$\mu_{st} = \frac{f_s}{x} = \frac{(\tanh x)[1 - 4C_3(\operatorname{sech} x)^2]}{x} \tag{7.5}$$

For the calculation of the differential permeability we have to take the first derivative of f_s expression in (4.1) by x as shown in (7.6)

$$\mu_d = \frac{df_s}{dx} = (\operatorname{sech} x)^2 - 4C_3\,(\operatorname{sech} x)^4 + 8C_3\,(\operatorname{sech} x)^2\,(\tanh x)^2 \tag{7.6}$$

μ_d is the magnitude of the incremental permeability, i.e. the change in permeability when, for instance, the ferromagnetic material is subjected to a small AC magnetization force, normally superimposed onto a larger DC magnetization. It is the so-called reversible permeability because at the end of each cycle it returns repeatedly to the same value. In some applications magnetic substances are only used with low excitation field, therefore the initial permeability μ_i often plays an important role (at $x \sim 0$) in these applications. This permeability is represented by the first derivative or the tangent in the first quadrant of the virgin magnetization curve in the zero-field region. Its numerical value can be calculated from (7.6) by substituting $x = 0$. As we know for most ferromagnetic material μ_i is not zero at zero magnetic field. Its value is related to the constant C_3, which determines the shape of the virgin magnetization curve, as shown in (4.2). The static and the differential permeabilities, as defined in (7.5) and (7.6), are plotted in Figure 7.1 for $C_3 = 0.15$ and also for the two limiting values of $C_3 = 0$ and 0.25 (see Chapter 4).

So far we have formulated and plotted the permeabilities related to the virgin magnetization curve. When the magnetization process is moving on the hysteresis curve a different mathematical expression should be used for calculating their value, due to the fact that in the hysteresis loop the relationship between field and induction is formulated in a different form. For this, we can recall (3.3) and divide it by x to get the static permeability at any point of the hysteresis loop.

$$\mu_{st,+} = \frac{\tanh\ (x - a_0) + b_1}{x} \qquad \text{for increasing } x \text{ values} \tag{7.7a}$$

$$\mu_{st,-} = \frac{\tanh\ (x + a_0) - b_1}{x} \qquad \text{for decreasing } x \text{ values,} \tag{7.7b}$$

where b_1 is specified in (3.2).

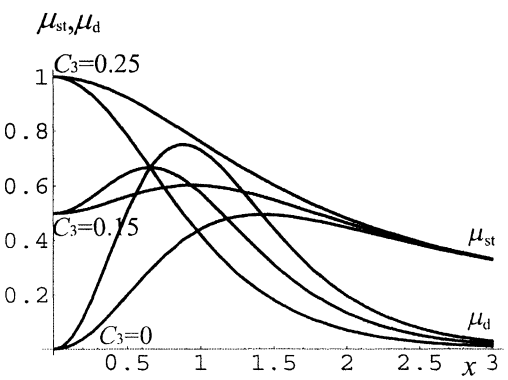

Figure 7.1: The static and differential permeabilities related to virgin magnetization for C_3 = 0, 0.15, and 0.25

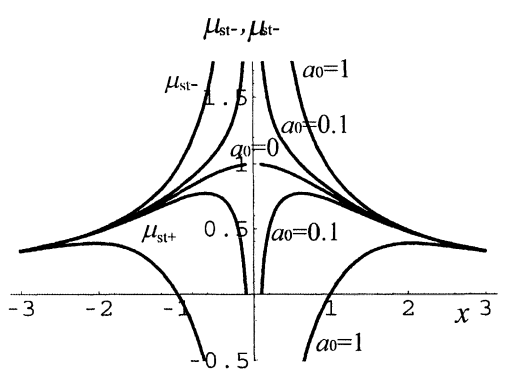

Figure 7.2: Static permeability of the hysteresis loop versus field, a_0 as parameter

The differential permeability can be calculated for the hysteresis loop by taking the first derivative of the expressions in (3.3) by x,

$$\mu_{d,+} = \frac{df_+}{dx} = [\text{sech}\,(x - a_0)]^2 \qquad \text{for increasing } x \text{ values} \tag{7.8a}$$

$$\mu_{d,-} = \frac{df_-}{dx} = [\text{sech}\,(x + a_0)]^2 \qquad \text{for decreasing } x \text{ values.} \tag{7.8b}$$

A set of static permeability curves of the hysteresis loop, calculated from (7.7) is shown in Figure 7.2. The static permeability goes to infinity as the field approaches zero because of the finite value of the induction at zero field.

The differential permeability calculated from (7.8) is depicted in Figure 7.3 for the coercivity as a parameter for the values of $a_0 = 0$, 1.5, and 3.

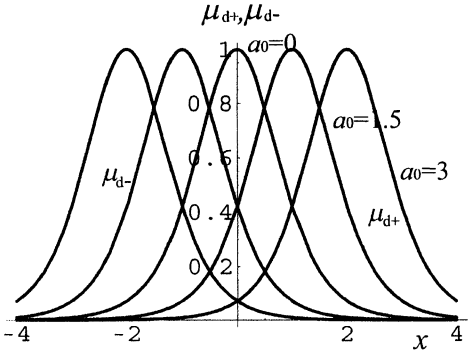

Figure 7.3: Differential permeability of hysteresis loops versus field for $a_0 = 0$, 1.5, and 3

It should be noted that each of the differential permeability curves will reach its maximum where the exciting field equals the value of coercivity, i.e. $x = a_0$.

When the linear term, representing the reversible magnetization, in (3.1) is not negligible both the static and the differential permeability will be different by the constant A_0. By using the same definitions as before and (3.1) for the case of $A \neq 0$ the static permeability can be formulated in the following form

$$\mu_{st,+} = \frac{\tanh\,(x - a_0) + b_1}{x} + A_0 \qquad \text{for increasing } x \text{ values} \tag{7.9a}$$

$$\mu_{st,-} = \frac{\tanh\,(x + a_0) - b_1}{x} + A_0 \qquad \text{for decreasing } x \text{ values.} \tag{7.9b}$$

Similarly the differential permeability is defined as

$$\mu_{d,+} = \frac{df_+}{dx} = [\text{sech}\,(x - a_0)]^2 + A_0 \qquad \text{for increasing } x \text{ values} \tag{7.10a}$$

$$\mu_{d,-} = \frac{df_-}{dx} = [\text{sech}\,(x + a_0)]^2 + A_0 \qquad \text{for decreasing } x \text{ values.} \tag{7.10b}$$

It can be seen that (7.9) and (7.10) only differ from (7.7) and (7.8) by a constant, therefore the shapes of permeability curves are the same in both cases and only subjected to a shift in the vertical direction by the additional constant term, represented by the amplitude of the reversible magnetization.

7.2 Shearing and Unshearing

In practical magnetic circuit design it is often necessary to combine ferromagnetic material and an air gap. Chokes and transformers often work with DC current passing through their windings. The inductance of the component is a strong function of the DC bias, which is a highly undesirable feature of DC-biased magnetic components. The presence of an air gap in the circuit, however, reduces the magnetic excitation, which shows up in the reduced dependence of the equivalent permeability of the circuit on bias. A suitably chosen gap in the magnetic circuit has a very significant linearizing effect on the effective permeability, therefore makes the inductance of the component less dependent on the amplitude of the DC bias. The mathematical equivalent of this process is the addition of a linear function to the hysteresis loop, whose parameter is dependent on the induction and proportional to the relative length of the air gap and the magnetic path. The effective result is that the hysteresis loop is stretched along the horizontal axis in opposite directions and the process is refereed to as "shearing". The mathematical description of the process of shearing is as follows.

In a closed magnetic circuit V_m the total magnetic potential (using conventional notations) can be written as the sum of the potential drop on the magnetic path and the air gap (the gap assumed to be small to other dimensions)

$$V_m = H_i l_i + H_a l_a = H_i l_i + \frac{B}{\mu_0} l_a \tag{7.11a}$$

$$H_i = H_{i0} - \frac{B}{\mu_0} \frac{l_a}{l_i} \tag{7.11b}$$

where H_i is the magnetic field in the magnetic material, H_a is the field in the gap and H_{i0} is the field in the circuit with no gap. The symbols l_i and l_a represent the ferromagnetic path length and the gap, respectively.

Let us return to our notation and call the new running coordinate (the new normalized field) of the sheared loop x_1. The relationship between the original coordinate x and x_1 according to the rules of coordinate transformation, can be described as follows

$$x_1 \pm a_0 = x \pm a_0 - \frac{B\, l_a}{\mu_0\, l_i} = (x \pm a_0)(1 - \mu_{ac} \frac{l_a}{l_i}) \tag{7.12}$$

Here, according to the definition of the process of shearing above, we added a term that is dependent on B the normalized induction and the ratio between the path lengths l_i and l_{ai}. The other parameters μ_0 and $\mu_{ac} \approx \mu_d$ are the permeability of air and that of the ferrous material, respectively, for small changes (see Section 7.1 for reversible permeability). By expressing the term $x \pm a_0$ from (7.12) and substituting into (7.11) we can write the induction in the sheared magnetic circuit as a function of the new normalized field x_1 as

$$f_+(x_1) = \tanh \frac{x_1 - a_0}{1 + \mu_{ac} \frac{l_a}{l_i}} + b_3 \tag{7.13a}$$

$$f_-(x_1) = \tanh \frac{x_1 + a_0}{1 - \mu_{ac} \frac{l_a}{l_i}} - b_3 . \tag{7.13b}$$

The b_3 constant can be calculated from the conditions same as the one set for b_1 in Chapter 3 and its expression is given in (7.14). For simplicity we assumed in the calculation that $d_0 = 0$, i.e. no DC bias, but the same mathematical process applies to the biased case as well.

$$b_3 = \left(\tanh \frac{x_1 + a_0}{1 - \mu_{ac} \frac{l_a}{l_i}} - \tanh \frac{x_1 - a_0}{1 + \mu_{ac} \frac{l_a}{l_i}} \right) / 2 . \tag{7.14}$$

Here x_{m1} represents the extreme of the new normalized field. Figure 7.4 depicts an unsheared and a sheared hysteresis loop calculated from (3.3) and (7.13) for the values of $\mu_{ac} \frac{l_a}{l_i} = 0.9$, $a_0 = 1$ and $x_{m1} = 4.73$.

The virgin induction curve can be sheared in the same way as the hysteresis loop for virgin or demagnetized circuit with an air gap. The expression for the sheared virgin magnetization is shown in (7.15) after the substitution of x expression from (7.12) into (4.1)

$$f_s(x_1) = \left(\tanh \frac{x_1}{1 + \mu_{ac} \frac{l_a}{l_i}} \right) \left[1 - 4C_3 \left(\operatorname{sech} \frac{x_1}{1 + \mu_{ac} \frac{l_a}{l_i}} \right)^2 \right] . \tag{7.15}$$

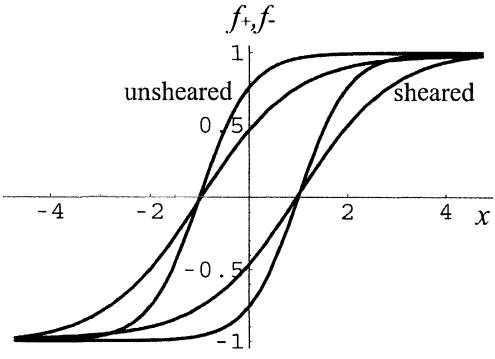

Figure 7.4: Sheared and unsheared major hysteresis loops

The unsheared and sheared virgin magnetization curves are depicted in Figure 7.5. The linear shearing function, represented by the additional term in expression (7.12) is also plotted. The C_3 value used in the calculation was 0.11 and the other parameters were the same as before.

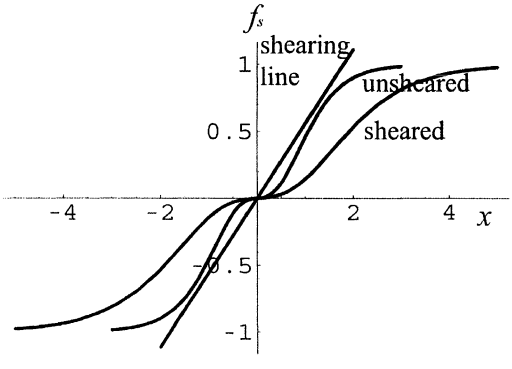

Figure 7.5: Sheared and unsheared virgin induction curves with the shearing line

In practice, it is often desirable to reconstruct the unsheared magnetization curves from the sheared loop. When in a magnetic specimen, for instance, the demagnetization factor is not negligible then its measured hysteresis loop requires correction or unshearing. So far this operation could only be done by graphically shifting the loop point by point by the amount indicated by the linear shearing function. The other alternative is the use of numerical methods. A modified version of the Preisach model has been developed [2,3] for the shearing and unshearing of hysteresis loops, however, this often produces spurious results and instabilities in the iterative computation. The model described here, with the knowledge of the linear shearing function, by the conversion from (7.13) to (3.3) and vice versa, gives, for the first time, the unique analytical method of shearing and unshearing hysteresis loops. The same applies to the virgin induction curves when (4.1) is used as a starting point.

The inductance of magnetic components, like a choke for instance, is linearly proportional to the μ_{ac} permeability of the magnetic core material used. When DC current is passing through its winding creating DC field in the ferrous material, the permeability will be dependent on the DC bias and drops rapidly with increasing DC field. Although the introduction of an appropriate air gap in the magnetic circuit, i.e. shearing the hysteresis loop, reduces the average value of the effective permeability, it also greatly reduces its dependence on the DC bias, hence linearizes the inductance within the design range of the DC field. By using the definitions of permeabilities in Section 7.1 we can express the static permeability of the sheared loop in the following form,

$$\mu_{st,+} = \left(\tanh \frac{x_1 - a_0}{1 + \mu_{ac} \frac{l_a}{l_i}} + b_3 \right) / x_1 \qquad \text{for increasing } x \text{ values} \tag{7.16a}$$

$$\mu_{s-} = \left(\tanh \frac{x_1 + a_0}{1 + \mu_{ac} \frac{l_a}{l_i}} - b_3 \right) / x_1 \qquad \text{for decreasing } x \text{ values.} \tag{7.16b}$$

Similarly we can express the differential permeability for the sheared loop after differentiating (7.13) by x_1 that comes to the following expression

$$\mu_{d+} = \frac{df_+(x_1)}{dx} = \left(\operatorname{sech} \frac{x_1 - a_0}{1 + \mu_{ac} \frac{l_a}{l_i}} \right)^2 \frac{1}{1 + \mu_{ac} \frac{l_a}{l_i}} \qquad \text{for increasing } x \tag{7.17a}$$

$$\mu_{d-} = \frac{df_-(x_1)}{dx} = \left(\operatorname{sech} \frac{x_1 + a_0}{1 + \mu_{ac} \frac{l_a}{l_i}} \right)^2 \frac{1}{1 + \mu_{ac} \frac{l_a}{l_i}} \qquad \text{for decreasing } x. \tag{7.17b}$$

The sheared and the unsheared differential permeabilities μ_{d+} and μ_{d-} calculated from (7.17) are plotted in Figure 7.6 for the values of $x_m = 3$, $a_0 = 1$ and the shearing factor of

$$\mu_{ac} \frac{l_a}{l_i} = 0.9.$$

The same permeabilities can also be calculated for the virgin magnetization curve as we have seen before. After the substitution of x from (7.12) into (7.5) we will come to μ_s the static permeability

$$\mu_s = \frac{f_s(x_1)}{x} = \left(\tanh \frac{x_1}{1+\mu_{ac}\frac{l_a}{l_i}} \right) \left[1 - 4C_3 \left(\operatorname{sech} \frac{x_1}{1+\mu_{ac}\frac{l_a}{l_i}} \right)^2 \right] / \frac{x_1}{1+\mu_{ac}\frac{l_a}{l_i}} . \qquad (7.18)$$

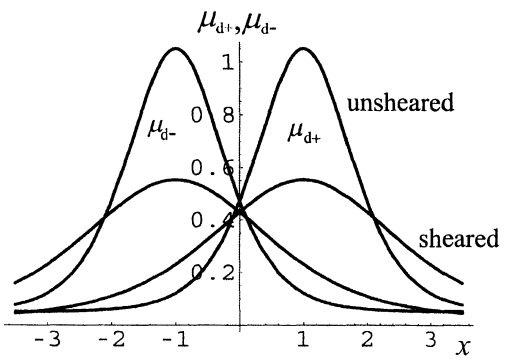

Figure 7.6: Sheared and unsheared differential permeabilities

One can also calculate an expression for the differential permeability by substituting

$$x = \frac{x_1}{1+\mu_{ac}\frac{l_a}{l_i}} \qquad (7.19)$$

into (7.6), which yields the following expression for μ_d

$$\mu_d = \frac{df_s(x_1)}{dx} = \left(\operatorname{sech} \frac{x_1}{1+\mu_{ac}\frac{l_a}{l_i}} \right)^2 - 2C_3 \left(\operatorname{sech} \frac{x_1}{1+\mu_{ac}\frac{l_a}{l_i}} \right)^4 . \qquad (7.20)$$

The sheared and unsheared virgin permeability curves calculated from (7.6) and (7.20) are depicted in Figure 7.7 for C_3=0.11 and $\mu_{ac}\frac{l_a}{l_i} = 0.9$.

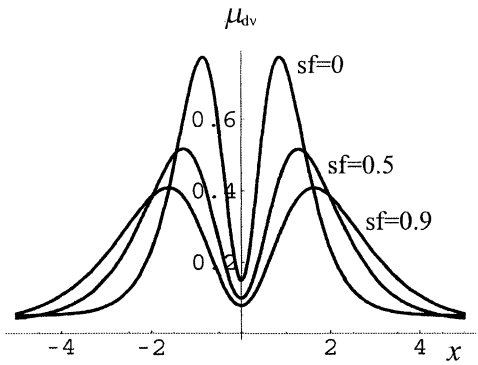

Figure 7.7: Differential permeabilities of the virgin magnetization curve. for $C_3 = 0.11$ and shearing factors of sf = 0, 0.5, and 0.9

When the reversible magnetization is not negligible i.e. $A_0 \neq 0$, by using (7.13) the starting equations can be written in the following form

$$f_+(x_1) = \tanh\frac{x_1 - a_0}{1 + \mu_{ac}\frac{l_a}{l_i}} + A_0\frac{x_1}{1 + \mu_{ac}\frac{l_a}{l_i}} + b_3 \qquad \text{for increasing } x \tag{7.21a}$$

$$f_-(x_1) = \tanh\frac{x_1 + a_0}{1 + \mu_{ac}\frac{l_a}{l_i}} + A_0\frac{x_1}{1 + \mu_{ac}\frac{l_a}{l_i}} - b_3 \qquad \text{for decreasing .} \tag{7.21b}$$

The differential permeability can be obtained after the differentiation of (7.21) by x_1. The plots of the sheared hysteresis loop calculated from (7.21) and the corresponding permeability curve are shown in Figure 7.8 for $x_m = 3$, $a_0 = 1$, $A_0 = 0.04$ and

$$\mu_{ac}\frac{l_a}{l_i} = 0.9$$

Similarly, the virgin magnetization with the reversible magnetization included can be expressed in the following mathematical form

$$f_s(x_1) = \left(\tanh\frac{x_1}{1 + \mu_{ac}\frac{l_a}{l_i}}\right)\left[1 - 4C_3\left(\operatorname{sech}\frac{x_1}{1 + \mu_{ac}\frac{l_a}{l_i}}\right)^2\right] + A_0\frac{x_1}{1 + \mu_{ac}\frac{l_a}{l_i}} \tag{7.22}$$

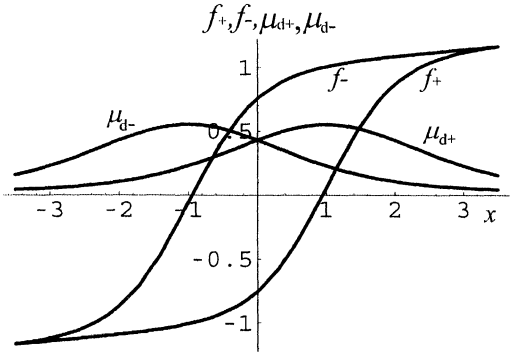

Figure 7.8: The virgin magnetization curve and the corresponding differential permeability for $A_0 = 0.04$

The differential permeability, same as before, is given by the first derivative of $f_s(x_1)$ in (7.22) by x_1. The two functions, the virgin magnetization and the corresponding differential permeability are depicted together in Figure 7.9. The shapes will be very similar to those shown in Figure 7.3.

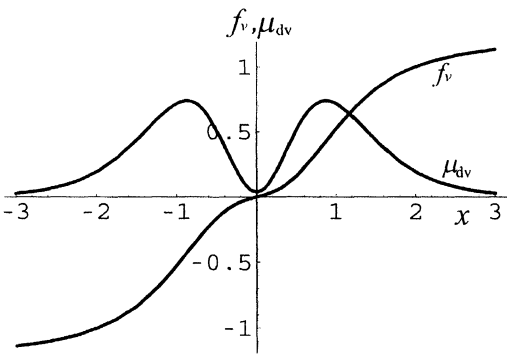

Figure 7.9: The virgin magnetization curve and the corresponding differential permeability for $A_0 = 0.04$

It is often important to know the differential permeability of the hysteresis loop where it intersects the vertical axis. This is represented by the first derivative of the hysteresis curve, i.e. $\frac{df_+}{dx}$ in the second or $\frac{df_-}{dx}$ in the forth quadrant. By differentiating (3.3a) we can see that the slopes of the hysteresis loops at $x = 0$ are independent of the value of the maximum magnetization and only depend on the coercivity value of a_0 as shown in (7.23),

$$\frac{df_+}{dx} = (\text{sech } a_0)^2 . \tag{7.23}$$

This slope or differential permeability is always the same as the slope of the initial anhysteretic curve at the point of origin. By taking the first derivative of the expression of f_s by x we arrive the following expression:

$$\frac{df_0}{dx} = \{(\text{sech } a_0)^2 + [\text{sech}(-a_0)]^2\}/2 \tag{7.24}$$

which leads to the same expression as in (7.23).

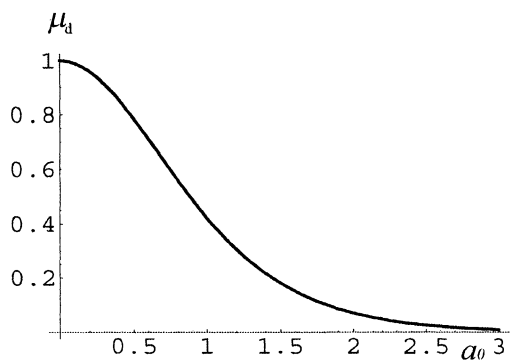

Figure 7.10: The differential permeability of the hysteresis loop at the point of intersection and the initial permeability of the anhysteretic magnetization curve as the function of coercivity

The differential permeability at the point of intersection is plotted in Figure 7.10 as a function of a_0.

References

[1] D. Jiles, *Magnetism and Magnetic Materials* (Chapman and Hall, N.Y., 1991).
[2] I.D. Mayergoyz, Dynamic Preisach model of hysteresis. IEEE Trans. on Magn. **24**, 2925–2927 (1988).
[3] I.D. Mayergoyz, *Mathematical Models of Hysteresis* (Springer-Verlag, N.Y., 1991).

8. Magnetic Energy

8.1 Stored Magnetic Energy

For a practical magnet designer there is an important parameter that governs the shape and the size of the design. This is the energy per unit volume that the magnet can store. This is vitally important for permanent magnets and it deserves special consideration. For a permanent magnet the integral of the field – induction product for the whole space must be zero as there is no external energy is added to the closed system [1]. The system is in an equilibrium state. This total energy can be divided to the energy inside the volume of the magnet v and the energy outside the boundaries of the magnet. It is self–explanatory from (8.1) that the two energies inside and outside of the magnet must be equal,

$$\int^{\text{space}} HB \; \mathrm{d}v = \int^{\text{inside}} HB \; \mathrm{d}v + \int^{\text{outside}} HB \; \mathrm{d}v = 0 \,. \tag{8.1}$$

Since outside of the magnet $B = \mu_0 H$ we can write the following equation

$$\int^{\text{inside}} \mu_0 H^2 \; \mathrm{d}v = \int^{\text{outside}} HB \; \mathrm{d}v \,. \tag{8.2}$$

That is to say that the total energy of the field H outside the magnet is equal to the HB product inside the magnet integrated over the whole volume of the magnet. The physical boundaries of the magnet are normally well defined, therefore, it is enough to calculate the energy stored in a unity volume of the magnet. This energy density w stored in a medium permeated by a magnetic field can be expressed as

$$w = \int_0^B H \; \mathrm{d}B = HB - \int_0^H B \; \mathrm{d}H \,. \tag{8.3}$$

Let us differentiate the expression of the induction f_- in (3.3b) and substitute it into (8.3) and then replace H with the normalized excitation x. The stored energy per unit volume can be expressed in the following mathematical form

$$w = \int x \; [\mathrm{sech}(x + a_0)]^2 \; \mathrm{d}x \,. \tag{8.4}$$

A simple but representative quantity for this energy, often used in practice, is the product of the magnetic induction and the magnetic field per unity volume. The larger the $(HB)_{\max}$

Mathematics of Hysteretic Phenomena. Jeno Takács

ISBN: 3-527-40401-5

product for a magnetic material the better are its magnetic properties. By taking f_+ from (3.3b) and expressing x from it, the energy product HB (the equivalent of the f_+x product) can be described as

$$HB = f_+ x = f_+[\text{arctanh}\,(f_+ + b_1) - a_0] \tag{8.5}$$

as a function of the magnetic induction f_+.

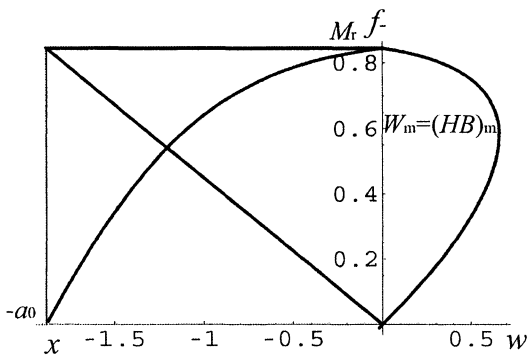

Figure 8.1:The "demagnetization" curve and the magnetic energy versus induction

The energy density w or energy product, as it is often called, is depicted in Figure 8.1, in the first quadrant, as a function of magnetic induction f_+ as calculated from (8.5). In the second quadrant the demagnetization curve, part of the hysteresis loop is shown. This is representative of the total hysteresis loss, and it is proportional to the area enclosed under the demagnetization curve. This is the work needed to totally demagnetize the magnet. The maximum energy stored in the magnet $W_m = (HB)_{max}$ is marked by the point where the straight line, defined by the $(a_0, 0)$ and $(0, B_r)$ coordinates and the demagnetization curve intersect. This is an important quantity in the optimization of the magnetic component design, particularly for permanent magnets and represents an upper limit [2–4] in magnet design. Basically this is the maximum amount of work the magnet can do outside its own boundaries. This limit characterizes a particular ferromagnetic medium and according to Hoselitz's findings [5] it can not be altered by any physical or chemical means.

As we said before the energy maximum is marked by the intersection of the straight line with the f_- demagnetization curve as shown in Figure 8.1. The slope of the line is set by the two points defined by the intersections between the demagnetization curve and the horizontal and the vertical axes, i.e. where $x = 0$ and where $f_- = 0$. The calculation of the maximum energy requires the solution of the following equation for the normalized field x:

$$\tanh\,(x + a_0) - b_1 = \frac{\tanh\,(x + a_0) - b_1}{\text{arctanh}\, b_1 - a_0}\, x\,. \tag{8.6}$$

The solution of this equation for x normally requires graphical methods or iterative numerical calculation on a computer, however, for the solutions of this kind of transcendental equations computer routines are available as part of readily obtainable mathematical packages.

8.2 Hysteretic Loss

Energy loss occurs in magnetic components due to the phenomenon of hysteresis, which in the literature is referred to as hysteretic energy loss. In practice, various losses are present in all electromagnetic power devices and the hysteretic loss forms a major part of these core losses. The reduction of these losses including the hysteretic loss plays an important role in the design and optimization of magnetic components. Because of this, the accurate prediction of these losses forms an important part of the general theory and design procedure of magnetic devices. These losses turn into heat and this often leads to undesirable temperature changes in magnetic components. This problem in general terms is still unsolved. A solution to the problem of calculating the hysteretic loss for periodic input functions in magnetic devices is given by Steinmetz [6]. His empirical solution shows that the loss due to the hysteretic phenomenon is equal to the area of the hysteresis loop formed by the periodic input variation. As was pointed out in the Introduction, given two points within the area confined by the major hysteresis loop, there are only two curves that can pass through those points and satisfy the conditions of mimicking the major loops. One belongs to the ascending set of curves and mimics the ascending saturation curve, the other is part of the descending family of curves and follow the shape of the descending saturation curve. The model does not allow any other solutions. These two curves form a closed loop and are described basically by tangent hyperbolic functions, T(x).

As the magnetic state of the medium changes around the loop, the work required to magnetize or demagnetize the medium can be expressed mathematically as the product of the magnetizing field and the change in the magnetization. This is described in detail in Section 8.1. Equations (8.7a) and (8.7b) describe the elementary energy density obtained by the magnetic substance for an elementary change in its state of magnetization (df_+) and demagnetization (df_-),

$$dw_+ = x\, df_+ \qquad \text{for magnetization} \tag{8.7a}$$

and

$$dw_- = x\, df_- \qquad \text{for demagnetization.} \tag{8.7b}$$

After differentiating the expressions of f_+ and f_- by x in (3.12) and substituting them into (8.7) we can put the expressions for the elementary change into the following forms

$$dw_+ = x\, [\text{sech}\,(x - a_0)]^2\, dx \tag{8.8a}$$

and

$$dw_{-} = x\ [\text{sech}\ (x + a_0)]^2\ dx \tag{8.8b}$$

The integration of dw_{+} and dw in (8.8), between the limits of x_1 and x_2, the two extreme values of the magnetic field, will give us the areas under the up- and down-going parts of the loop. The area inside the loop, i.e. the difference between w_{-} and w_{+}, represents the work per unit volume needed to magnetize and demagnetize the sample in one cycle. This is the energy lost or converted into heat during the cycle. According to Steinmetz's rule [6] w_0 the total energy loss density can be calculated as

$$w_0 = w_{+} - w_{-} = [x \tanh\ (x - a_0) + \ln\ \text{ch}\ (x - a_0)]_{x1}^{x2}$$

$$- [x \tanh\ (x + a_0) - \ln\ \text{ch}\ (x + a_0)]_{x1}^{x2}. \tag{8.9}$$

It is obvious from the expression that w_0 is only dependent on the two limits between which the excitation is oscillating and totally independent of the path the excitation is moving between the two specified limits. Sinusoidal or triangular excitation waveforms produce the same energy loss.

8.3 Hysteretic Loss in a Transformer

In electrical engineering practice the transformer is one of the fundamental components used. As a current/voltage converter, it handles virtually all electrical power used in industry and households the world over. Because of its importance it was a subject of research and investigation in order to improve its performance and efficiency. The loss due to the cyclic magnetization and demagnetization, which the transformer core is subjected to, was recognized from early days and its reduction was regarded as vital in all applications. This power is not only lost, therefore the useful output from the transformer is less than its input, but it turns into unwanted heat, which may increase the temperature of the magnetic core. The increase in the temperature can alter the magnetic properties of the core, therefore the performance of the transformer. At very low magnetization the subject of transformer loss is well covered by the work of Rayleigh [7], Steimetz [6], and Hoselitz [5]. At medium fields and at fields approaching saturation, approximations worked out by Lamont [8], which led to the Frõhlich–Kennelly relation [9,10] and later modeled by Becker and Doring [11] and Bozorth [8]. So far there has been no overall analytical approach produced covering the losses in all three regions of magnetization. In the following, by using the T(x) model, calculations of hysteretic losses in transformers will be given, covering the whole range of magnetization from zero to saturation level.

When the magnetic core of a transformer is subjected to a cyclic excitation, the magnetization will follow a set of symmetrical hysteresis loops whose return points form the anhysteretic magnetization curve. In the following calculation it is assumed that there is no DC excitation applied to the magnetic core and there is no reversible magnetization either. The presence of either the DC bias or the reversible magnetization or the presence of both makes the calculations here slightly more complicated, nevertheless, the model described here still applicable to the calculation of the hysteresis loss.

Let us assume that the excitation is changing cyclically between the two extreme values of x_m and $-x_m$ then the substitution of these values for the integration limits x_1 and x_2 shown in (8.9) will give us the energy loss per unit volume per cycle. This is given in (8.10),

$$w_0 = 2\,[\ln\cosh(x_m + a_0) - \ln\cosh(x_m - a_0) - 2\,b_1 x_m]\,. \tag{8.10}$$

Taking (8.3) into consideration, the use of $dw_{1,2} = f_{+,-}dx$ for starting equations would have yielded identical result. Up to now the only way to measure the energy loss was the graphical integration of the area within the hysteresis loop. This, although applicable in some cases, often proves difficult in practice. The T(x) model offers a purely analytical approach to the solution of this problem.

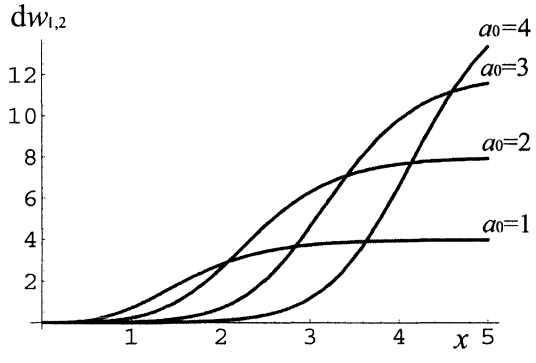

a

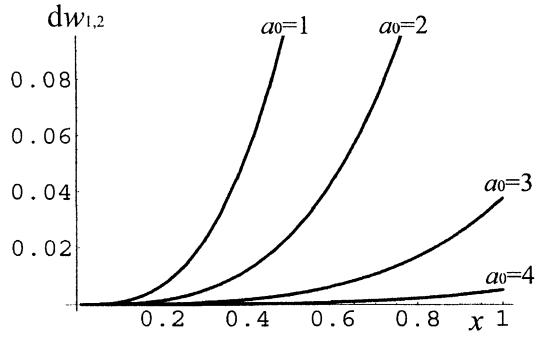

b

Figure 8.2: Hysteresis loss against (a) large peak excitation values; (b) Small peak excitation values for the coercivity values of a_0 = 1, 2, 3, and 4

In practical applications where the magnetic material is subjected to cyclic magnetization, like in a power-transformer design, one of the important factors could be the power lost in the volume of the transformer due to the hysteresis. Its measure p is the power per unity volume or power density. This is related to the energy so that the power density is the time derivative of the energy density, as shown below

$$\cdot\, p_0 = \frac{\mathrm{d}w_0}{\mathrm{d}t} \tag{8.11}$$

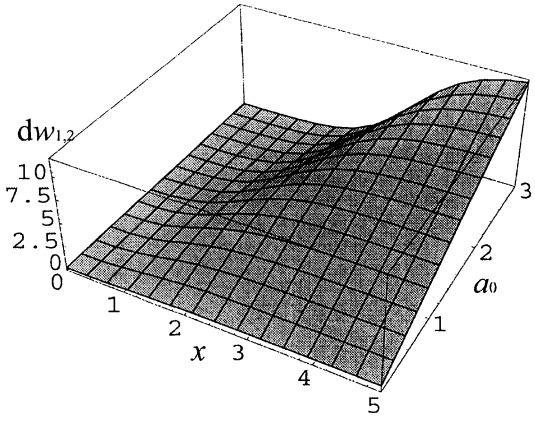

Figure 8.3: Surface map of the hysteretic losses as a function of the excitation field ($0 < x < 5$) and the coercivity ($0 < a_0 < 3$)

As we have seen, neither w_0 nor p_0 depend on the time behavior of the periodic excitation only on the positive and negative maxima. We are at liberty therefore to write p_0 in the following form

$$p_0 = \frac{w_0}{T} = f\ w_0 \tag{8.12}$$

where T is the duration of one period of the time function and f is the frequency. This expression shows the power loss to be proportional to the frequency of the periodic excitation. Steimetz [6] has formulated an expression for the hysteretic-loss density, based on observations, which is applicable for a wide range of magnetization and has been used for loss calculations,

$$p_0 = k f\ B_{\max}^{1.6}\ . \tag{8.13}$$

Here k is the Steinmetz constant, which only differs in a multiplier factor from the coercivity of the magnetic material, f is the frequency and $B_{\max}$ is the maximum magnetization in the cycle. He assumed a linear dependency of the hysteretic losses on the coercive force in a wide range of magnetization as shown in Figure 8.4, where the hysteretic-loss density is plotted for a fixed maximum magnetization for one cycle against a_0 calculated from (8.10). It shows that, particularly at large magnetization the hysteresis-loss density is linearly dependent on the coercive force value of the magnetic material when the maximum magnetization is kept constant, for a very wide range of coercivity values, providing the

following condition is satisfied $x_m >> a_0$. The curves are plotted with x_m as parameter, where x_m is ranging between 1 and 6 on the normalized scale.

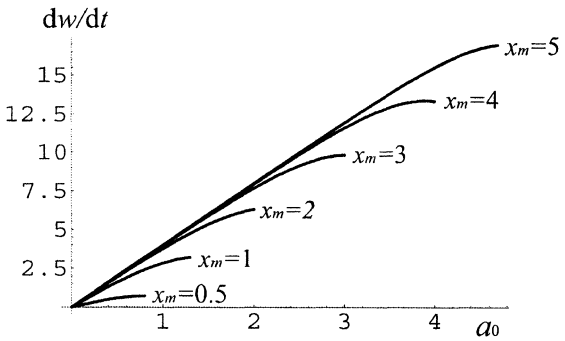

Figure 8.4: Hysteretic loss density versus coercivity in normalized units for the x_m values of 1, 2, 3, 4, 5, and 6

In Figure 8.5 two graphs are depicted, p_0 the power density for one cycle, as a function of x_m the maximum magnetization value, calculated from (8.10) and also from the Steinmetz formula, given in (8.13). In the calculation it was assumed that the relationship between maximum magnetization and excitation follows the anhysteretic magnetization curve (for definitions and other details see Chapter 4). The parameters were selected from the middle of the linear range and taken as $a_0 = 2$ for the coercivity and $k = 8$ for the normalized Steinmetz constant.

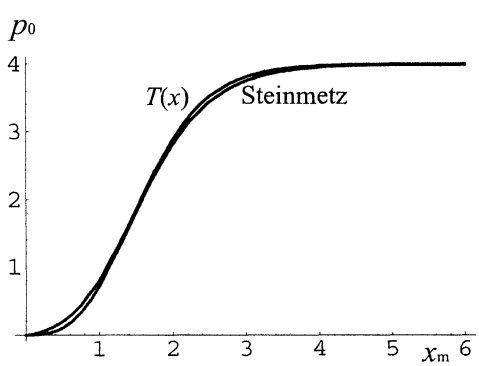

Figure 8.5: Power-loss density p_0 versus maximum magnetization x_m for $a_0 = 2$ and $k = 8$ in normalized units

The graph shows the good agreement between the Steinmetz approximation and the T(x) model in the middle of the magnetization range. Figure 8.6 shows that the deviation between the two approaches is within 2.5%. At low and high magnetization the Steimetz approximation will produce increasingly large errors in the calculation. For good agreement

the normalized coercivity range is $0.5 < a_0 < 4$ with the corresponding Steinmetz constant of $2 < k < 16$.

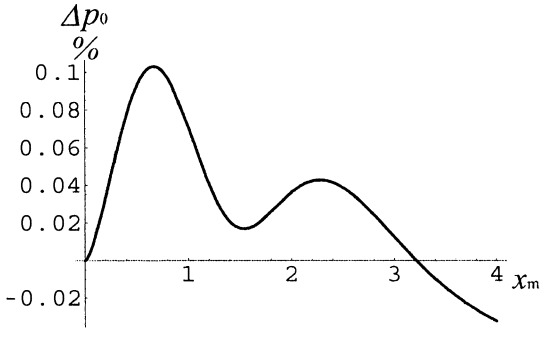

Figure 8.6: The difference between the two power-density figures calculated from the T(*x*) model and the Steinmetz approximation as the percentage of maximum magnetization

References

[1] D. Jiles, *Introduction to Magnetism and Magnetic Materials* (Chapman and Hall, N.Y., 1998).
[2] D. Hadfield, *Permanent Magnet and Magnetism* (Iliffe Books, London, 1962).
[3] M. McCaig and A.G. Clegg, *Permanent Magnets in Theory and Practice* (Pentech Press, London, 1987).
[4] R.J. Parker, *Advances in Permanent Magnets* (Wiley, N.Y., 1990).
[5] K. Hoselitz, *Ferromagnetic Properties of Metals and Alloys* (O.U.P. Oxford, 1952).
[6] C. Steinmetz, Note on the law of hysteresis. The Electrician. **No. 659, XXVI**, 261–262 (1891).
[7] J.W. Lord Rayleigh, On the behavior of iron and steel under the operation of feeble magnetic force. The Philosophical Magazine. **5, 23**, 225–245 (1887).
[8] R.M. Bozorth, *Ferromagnetism* (Van Nostrand, N.Y., 1951).
[9] O. Frõhlich, Investigation of dynamoelectric machines and electric power transmission and theoretical conclusions therefrom. Electrotechn. Z. **2**, 134–141 (1881).
10] A.E. Kennelly, Magnetic reluctance. Trans. Am. IEE. **8**, 485–517 (1891).
[11] R. Becker and W. Doring, *Ferromagnetismus* (Springer-Verlag, Berlin, 1938).

9. Time Functions and Magnetization

9.1 Introduction

Ferromagnetic materials are often subjected to periodically varying field excitation in practical applications. Power and audio transformers, magnetic storage devices for digital or analogue information, video and audio recorders, etc., are all affected by the nonlinear behavior of the ferromagnetic elements in the system. This effect is very much of a practical problem and it has been a subject of investigation since the introduction of transformers in electrical circuits [1]. In the following we are going to investigate analytically what happens when the excitation field, which the ferromagnetic medium is subjected to, varies with time, i.e. $x(t)$ is a periodic time function with ω frequency as described in (9.1). In the following we assumed that the frequency of the excitation is so slow as not to cause magnetic viscosity or any other aftereffects, phenomena that are going to be discussed in later chapters.

$$x(t) = D_0 \sin \omega t \quad . \tag{9.1}$$

Here $x(t)$ signifies the normalized magnetic excitation of D_0 amplitude to which the specimen is subjected. We have to recall (3.2) and (3.3) and substitute (9.1) for x. The new expression for the magnetization waveform as a time function driven around the hysteresis loop in one cycle between $t = 0$ and $2\pi\omega$ will be

$$f_+ = \tanh\ (D_0 \sin \omega\, t - a_0) + b_1 \qquad \text{for} \begin{cases} 0 \le \omega\, t \le \pi/2 \\ 3\pi/2 \le \omega\, t \le 2\pi \end{cases} \tag{9.2a}$$

$$f_- = \tanh\ (D_0 \sin \omega\, t + a_0) - b_1 \qquad \text{for } \pi/2 \le \omega\, t \le 3\pi/2\,. \tag{9.2b}$$

In the case of a periodic function with a constant periodicity this pattern will be repeated ad infinitum in every $2\pi\omega$ period.

When an alternating current is applied to an inductive circuit component with an iron core then the waveforms of secondary parameters will not follow that of the primary input. This is due to two factors, one being the hysteresis, and the other the nonlinear relationship between field and magnetization, as described in mathematical form in (3.3). The secondary response in general terms follows Faraday's law, therefore the shape of the response will follow the shape of the first derivative by t of the magnetic induction. After taking the first derivative of (9.2) by t we arrive at the expressions representative of the secondary response of the component (assuming $D_0 = 1$).

Mathematics of Hysteretic Phenomena. Jeno Takács

ISBN: 3-527-40401-5

$$\frac{df_+}{dt} = \omega \cos \omega t \operatorname{sech} (\sin \omega t + a_0)^2 \quad \text{for} \begin{cases} 0 \le t\ \omega \le \pi/2 \\ 3\pi/2 \le t\ \omega \le 2\pi \end{cases} \tag{9.3a}$$

$$\frac{df_-}{dt} = \omega \cos \omega t \operatorname{sech} (\sin \omega t - a_0)^2 \quad \text{for } \pi/2 \le t \le 3\pi/2\,. \tag{9.3b}$$

As we can see from (9.3) the amplitude of the first derivative will be linearly proportional to the frequency and their phase will be shifted by 90° relative to that of the input signal. The secant hyperbolic multiplier in both expressions represents the deviation from the pure simple harmonic. In Figure 9.1 a sinusoidal input $x(t)$ waveform is plotted with the waveform of the df_+, df_- induction functions and their first derivatives $\frac{df_+}{dt}$ and $\frac{df_-}{dt}$. In the calculation the following parameter values were used: $x_m = 0.75$, $a_0 = 1$, $\omega = 1$, and $D_0 = 1$.

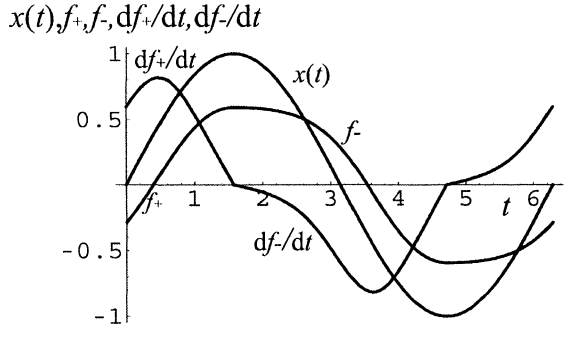

Figure 9.1: Waveforms of the input signal, the induction, and its first derivative

With increasing input signal amplitude the dominating even harmonics in the magnetization waveform will rapidly increase, as shown in Figure 9.2, with its shape approaching the square wave. The waveforms are plotted for the same numerical parameter values as before. In Figure 16.3 the first derivatives of the same waveforms are shown. They show the rapid increase of the odd harmonics as the amplitude of the input current increases.

As is often the case in practical applications the magnetic device is subjected to DC and AC fields at the same time. A typical example is a choke when DC and AC currents simultaneously pass through its winding. Further to this, the reversible magnetization is often not negligible, i.e. $A_0 \neq 0$. This case is described by (3.11). After the substitution of (9.1) into (3.11) we arrive at the time-dependent expression of the biased hysteresis in the following form, which also includes the reversible magnetization,

$$f_+ = \tanh\ (D_0 \sin \omega t - a_0) + b_u + A_0 x \quad \text{for} \begin{cases} 0 \le t\ \omega \le \pi/2 \\ 3\pi/2 \le t\ \omega \le 2\pi \end{cases} \tag{9.4a}$$

$$f_{-} = \tanh\ (D_0 \sin \omega\, t + a_0) - b_d + A_0 x \qquad \text{for } \pi/2 \le t\ \omega \le 3\pi/2, \tag{9.4b}$$

where b_u and b_d are defined in (3.10).

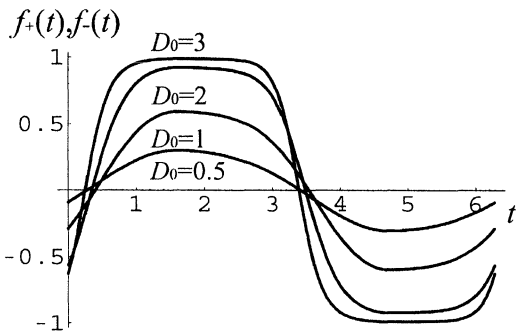

Figure 9.2: The waveform of the magnetization in normalized units for the input excitation amplitudes of $D_0 = 0.5$, 1, 2, and 3.

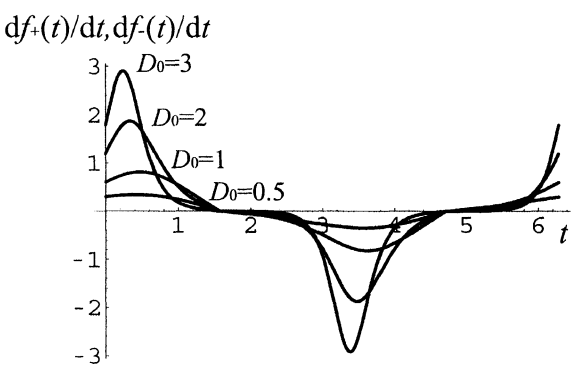

Figure 9.3: The first time derivative of the magnetization waveform for input amplitudes of $D_0 = 0.5$, 1, 2, and 3.

In Figure 9.4 three magnetization curves are shown. One is depicting the case without DC bias and reversible magnetization. The second is a biased case with the DC amplitude of 0.4 and $A_0 = 0$. The third curve shows the case of AC magnetization with DC bias of 0.4 amplitude added and with a reversible magnetization amplitude of $A_0 = 0.05$.

The curves show the changes in the waveforms of the magnetization relative to the simplest case, due to DC bias and in the presence of the reversible magnetization. In Figure 9.5 the first derivatives of the same waveforms are shown correspondingly with AC input signal combined with DC bias ($d_0 \neq 0$) and also with reversible magnetization included ($A_0 \neq 0$).

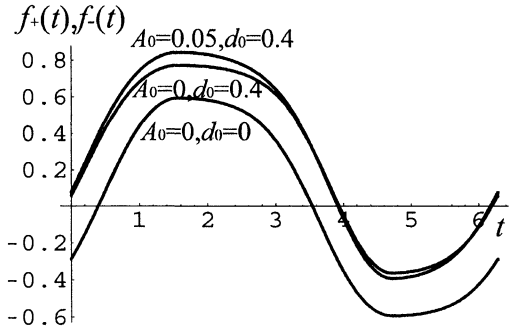

Figure 9.4: Magnetization waveforms for (a) $d_0 = 0$, $A_0 = 0$; (b) $d_0 = 0.4$, $A_0 = 0$; (c) $d_0 = 0.4$, $A_0 = 0.05$

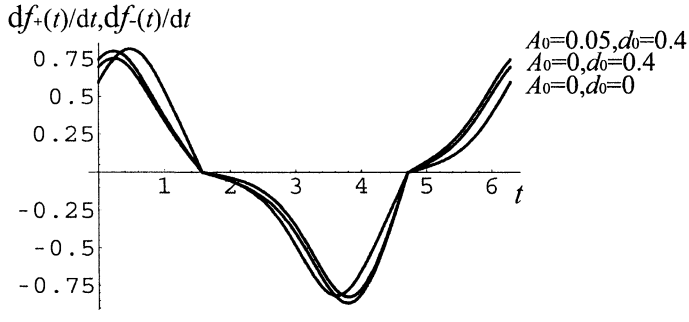

Figure 9.5: The waveform of the first derivative of the magnetization for input excitation amplitude of (a) $d_0 = 0$, $A_0 = 0$; (b) $d_0 = 0.4$, $A_0 = 0$; (c) $d_0 = 0.4$, $A_0 = 0.05$

9.2 Distortion Caused by the Magnetic Nonlinearities to Periodic Magnetization

It has been shown in Section 9.1 that the increasing amplitude of the excitation rapidly increases the distortion in the induction and in its first derivative. In practical applications it is important to limit the distortion of the signal going through the system. It is primarily important therefore to be able to calculate the effect of each circuit component on the signal including the ferromagnetic elements. The two nonlinearities, the hysteresis and the saturation effect, both change the frequency content of the output signal by introducing different higher harmonics. The distortion they cause can be separated in the mathematical treatment. One of the most important parts of the magnetization is the low-field magnetization region of the initial magnetization curve. Rayleigh [2] observed that the change in permeability at low field is a linear function of the field in very good approximation and this leads to a quadratic dependence between induction and field. He suggested that a parabola could represent the initial part of the magnetization curve. This

made the calculation of the higher harmonics relatively easy at low excitation. At higher amplitudes, however, the harmonic analysis had to be done in the past by numerical methods.

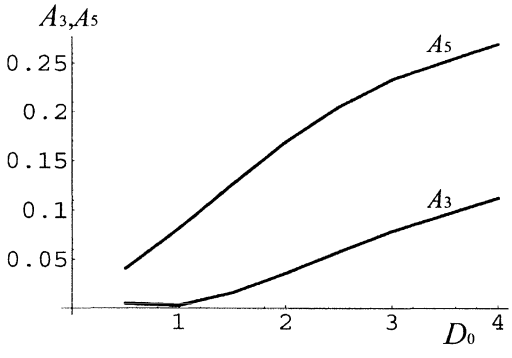

Figure 9.6: The amplitude of the 3rd and the 5th harmonics in the waveform of the magnetization versus the amplitude of the harmonic excitation for the normalized coercivity of $a_0 = 0.5$

Equations (9.2) and (9.3) describe the waveform of the induction and its first derivative. From Figures 9.1 and 9.2 one can see that both waveforms suffer amplitude as well as phase distortion relative to the input waveform. The phase distortion is strongly dependent on the value of a_0 (coercivity). For "fatter" hysteresis loops (large coercivity) the phase shift is larger, indicating an increasing presence of out-of-phase components in the Fourier spectrum. The saturation effect flattens the top and bottom of the waveform increasing the higher harmonics as the excitation drives the magnetic substance nearer to saturation. As its shape approaches the square wave its Fourier spectrum will get richer in the odd harmonics and its Fourier spectrum gets nearer to that of the square wave whose spectrum is composed entirely of odd harmonic components.

In Figures 9.6 and 9.7 A_3 and A_5, the amplitudes of the 3rd and the 5th harmonics of the first derivative, are depicted as the function of x_m the excitation amplitude for $a_0 = 0.5$ and $a_0 = 1$, respectively. The two graphs show a remarkable similarity in character, while doubling the coercivity increased the higher harmonics by approximately three-fold.

The curves in both graphs indicate the rapid increase of the higher harmonics with the magnitude of the excitation field. In applications where the distortion of the waveform is to be kept low, the amplitude of the excitation should not exceed the normalized amplitude of $x_m = 0.5$. This is normally a vital consideration in the design of audio and other analogue applications of magnetic components.

In Figure 9.8 the effect of a_0 the coercive force is shown on the distortion of the magnetization waveform. It can be seen that the waveform of the magnetization is seriously affected by a_0 over the normalized value of 1. Between the value of $a_0 = 1$ and 2 the amplitude of the third harmonics can double.

Time-dependent excitation functions applied to systems with hysteretic properties form an important part of the investigations of hysteretic phenomena. Models, like for instance the one developed by Chua [3,4], are based on time-dependent properties of the hysteretic media and are known as dynamic models. One of the parameters that are closely related to the hysteresis coefficient of the dynamic characteristic of a hysteretic medium is the first

time derivative of the magnetization as shown before. This is normally represented as the function of the excitation field as shown in Figure 9.9 calculated for sinusoidal excitation for a_0 varying between 0 and 2.

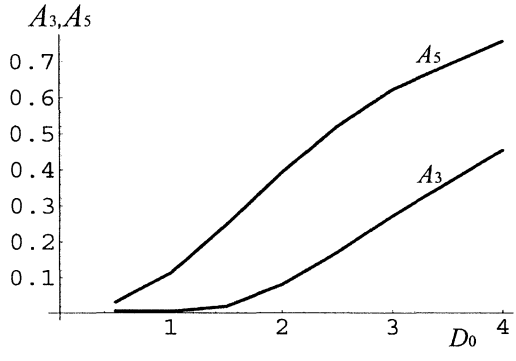

Figure 9.7: The amplitude of the 3rd and the 5th harmonics in the waveform of the first derivative of the magnetization versus the amplitude of the harmonic excitation for the normalized coercivity of $a_0 = 1$

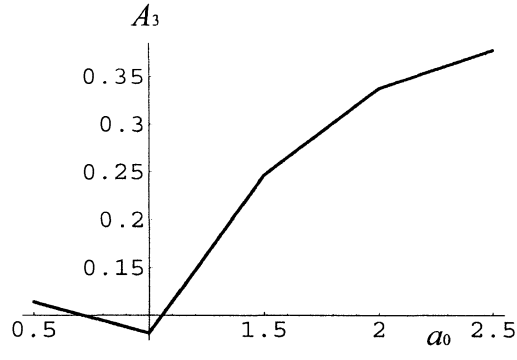

Figure 9.8: The amplitude of the third harmonics in the waveform of the magnetization as a function of a_0 coercivity.

A great deal of effort has been spent on research correlating the hysteretic properties of magnetic components, like transformers, and to the Fourier spectrum of their output when they are subjected to harmonic excitation. It is in the general practical interest to be able to calculate the distortion caused by the double nonlinearity of the magnetic components in a circuit [5]. In 1983 Willcock and Tanner [6] worked out a method for the harmonic expansion of the hysteresis loop. Other people suggested the reconstruction of the hysteresis loop from the distortion suffered by the magnetization waveform due to the magnetic distortions [7].

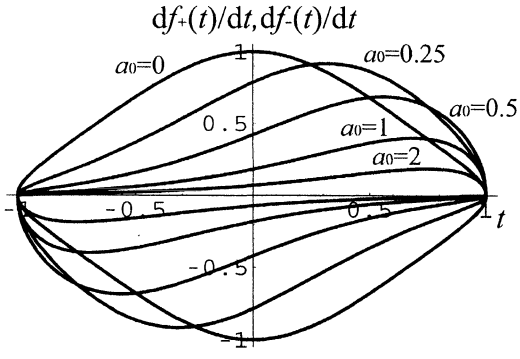

Figure 9.9: The first time derivative of magnetization versus exciting field for the coercive force values of $a_0 = 0$, 0.25, 0.5, 1, and 2, at sinusoidal excitation when $\omega = 1$

9.3 Fourier Analysis of Hysteretic Distortions

9.3.1 The Exponential Model for Fourier Analysis

When a waveform is described by the function of $f(\xi) = f(\xi + 2L)$ with the periodicity of $2L$ the Fourier series corresponding to $f(\xi)$ periodic function is defined to be

$$f(\xi) = \frac{\alpha_0}{2} + \sum_{n=1}^{\infty} (a_n \cos \frac{n\pi\xi}{L} + b_n \sin \frac{n\pi\xi}{L}) \tag{9.5}$$

where the Fourier coefficients α_0, a_n and b_n are defined as

$$\alpha_0 = \frac{1}{L} \int_{-L}^{L} f(\xi)\, d\xi \tag{9.6a}$$

$$a_n = \frac{1}{L} \int_{-L}^{L} f(\xi) \cos \frac{n\pi\xi}{L}\, d\xi \tag{9.6b}$$

$$b_n = \frac{1}{L} \int_{-L}^{L} f(\xi) \sin \frac{n\pi\xi}{L}\, d\xi \quad n = 1, 2, \ldots . \tag{9.6c}$$

It is obvious that these coefficients can only be calculated in a closed form when the integrals in (9.6) can be evaluated without expanding $f(\xi)$ into infinite sequence.

There are a number of models presently in use to deal with effects associated with the double nonlinearity of the hysteresis, none of the functions, however, describing these models, including the T(x) model, fulfil the criteria for closed integration in (9.6). In 1973 Macfadyen et al. [8] suggested the use of exponential functions for modeling the hysteresis loop. This idea was used by Teape et al. [9] and later by Hwang [10] and also by Hodgdon

[11] for solving practical problems. Although this approach looked promising at the time, soon it was taken over in popularity by other models. Nowadays, the exponential model is hardly used although its potential to use it, for instance, for Fourier analysis has never been fully explored.

There is an important group of periodic functions that allows us to carry out the Fourier analysis in closed form by using the exponential model [12]. This group contains all the periodic functions that can be constructed by using straight lines, such as the various triangular waveforms, the trapezoid and the square wave.

Let us review briefly the exponential model of the hysteresis loop. For the modeling of the loop, it should be divided into four regions between the positive x_m and negative maxima $-x_m$ and zero magnetization represented by the coercivity on the horizontal axis a_0 and $-a_0$, respectively.

$$f_e(x) = \begin{cases} 1-\exp\left[-q\left(x-a_0\right)\right]+b_{12} & \text{for} \quad a_0 \le x \le x_m \\ 1-\exp\left[-q\left(x+a_0\right)\right]-b_{12} & \text{for} \quad x_m \ge x \ge -a_0 \\ -\{1-\exp\left[q\left(x+a_0\right)\right]\}-b_{12} & \text{for} \quad -a_0 \ge x \ge -x_m \\ -\{1-\exp\left[q\left(x-a_0\right)\right]\}+b_{12} & \text{for} \quad -x_m \le x \le a_0 \end{cases} \tag{9.7}$$

where q is an exponent governing the shape of the magnetization functions $f_e(x)$ and b_{12} is defined as

$$b_{12} = \{\exp\left[-q\left(x-a_0\right)\right]-\exp\left[-q\left(x+a_0\right)\right]\}/2\,. \tag{9.8}$$

A major hysteresis loop as described by the exponential model is shown in Figure 9.10 and the four expressions describing function $f_e(x)$ running between the limits above are given in (9.7).

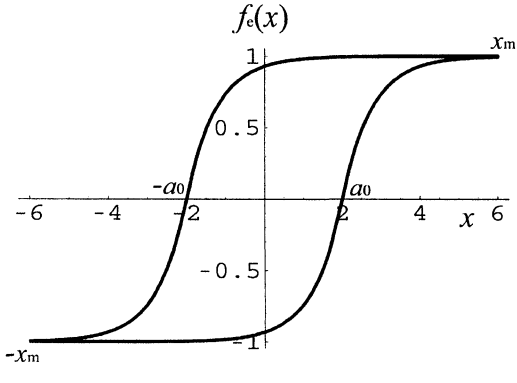

Figure 9.10: The hysteresis loop modeled with exponential functions showing the four regions

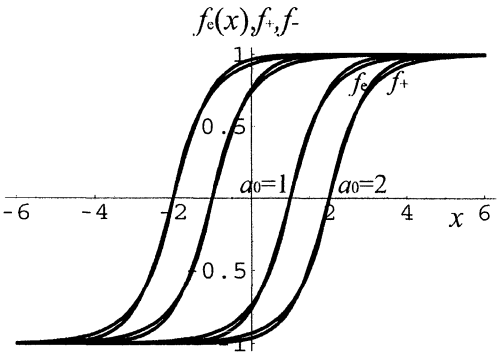

Figure 9.11: Typical hysteresis loops modeled by (1) T(x) model; (2) exponential model

Two typical hysteresis loops are depicted in Figure 9.11 modeled by using the exponential and the T(x) model. It shows that the deviation in the shape of the loops modeled by the two different models is small and in some practical applications this difference is small enough to use the exponential model for the Fourier analysis. For higher accuracy additional exponential terms can be used with different exponents. The process may take more steps but it is not going to be more complicated. Depending on the number of exponential terms used the error can be reduced beyond a specified limit.

So far we assumed no reversible magnetization in the process (A = 0). When the reversible magnetization is not negligible the expressions in (9.7) will have an extra term A_0x linearly dependent on the excitation time function $x(t)$ (for detailed explanation the reader is referred to Chapter 3). The integration of this term, however, for the waveforms listed above (all linear functions of time) is trivial, therefore in the following the reversible magnetization will be assumed to be negligible.

9.3.2 Triangular Excitation

A single period of $x(t)$ triangular waveform of unity amplitude, symmetrical around the horizontal axis with periodicity of $2T$ is shown in Figure 9.12. This waveform is formulated in the expressions in (9.9). The corresponding magnetization waveform $f_e(t)$ calculated from (9.7) is also shown.

The starting points of the waves are shown at the positive maximum for the sake of simplicity and to ease the calculation. In the analysis, triangular waves stretching between negative and positive infinity are assumed, therefore we are at liberty to choose the starting point arbitrarily anywhere without affecting the validity of the following calculations. Two corresponding points are equally well defined for all hysteretic loops. These are the two magnetization values at the positive and negative maxima of the excitation

$$x(t) = \begin{cases} -\dfrac{2A}{T}t + A & \text{for} \quad 0 \le t \le T \\ \dfrac{2A}{T}(t - \dfrac{3T}{2}) & \text{for} \quad T \le t \le 2T \end{cases} \tag{9.9}$$

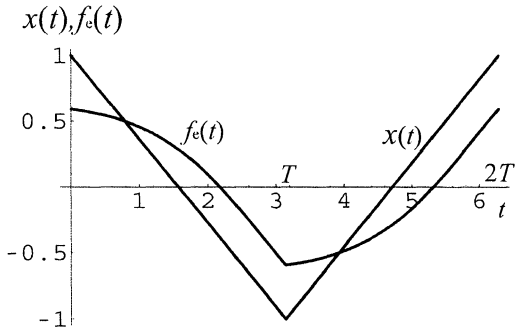

Figure 9.12: Triangular excitation function $x(t)$ and the corresponding magnetization function $f_e(t)$ calculated by using the exponential model

The substitution of the expressions of $x(t)$ from (9.9) into (9.7) results in the formulation of the magnetization time function, which is now a piecewise-continuous waveform distorted by the hysteretic process. The integration, leading to the Fourier components of the frequency spectrum of the distorted waveform can be carried out according to (9.6). The calculation will lead to the following expressions for the Fourier coefficients:

$$\alpha_0 = 0 \tag{9.10a}$$

$$a_n = \frac{2}{nT}(\sin\ n\frac{a_0 T}{2A}\ \sin n\frac{T}{2} - \cos\ n\frac{a_0 T}{2A}\ \cos n\frac{T}{2})(1-\cos\ nT)$$

$$+\frac{2\,q\frac{2A}{T}\exp(-qA)\cosh qa_0}{T\,[n^2+(q\frac{2A}{T})^2]}(1-\cos\ nT)$$

$$-\frac{2\,n}{T\,[n^2+(q\frac{2A}{T})^2]}(\sin\ n\frac{a_0 T}{2A}\ \sin n\frac{T}{2} - \cos\ n\frac{a_0 T}{2A}\ \cos n\frac{T}{2})(1-\cos\ nT) \tag{9.10b}$$

$$b_n = \frac{2}{nT}[\sin\ n\frac{a_0 T}{2A}\ \sin n\frac{T}{2} - \cos\ n\frac{a_0 T}{2A}\ \cos n\frac{T}{2} - \exp\ (-qa_0)](1-\cos\ nT)$$

$$-\frac{2\,n}{T\,[n^2+(q\frac{2A}{T})^2]}[\sin\ n\frac{a_0 T}{2A}\ \sin n\frac{T}{2} - \cos\ n\frac{a_0 T}{2A}\ \cos n\frac{T}{2}$$

$$-\exp\ (-qa_0)](1-\cos\ nT). \tag{9.10c}$$

9.3.3 Triangular Excitation and the Anhysteretic Process

Periodic magnetization often follows the anhysteretic process. It is appropriate therefore to apply the triangular excitation to the anhysteretic curve and calculate the Fourier components of the magnetization waveform. Since the shape of the curve is different from the normal hysteresis loop the Fourier components introduced by the process will also be different from the general case described in Section 9.3.1.

The anhysteretic magnetization process is defined in Chapter 4 and its characteristic curve is formulated in (4.7). With the combination of (4.7) and (9.7) the three regions of the anhysteretic magnetization curve f_s can be formulated in the following expressions.

$$f_s = \begin{cases} (f_{e1} + f_{e2})/2 = 1 - \cosh\ qa_0\ \exp\,(-qx) & \text{for} \quad x_m \geq x \geq a_0 \\ (f_{e2} + f_{e4})/2 = \{\exp(-qa_0)[\exp\ qx - \exp\ (-qx)]\}/2 & \text{for} \quad a_0 \geq x \geq -a_0 \\ (f_{e3} + f_{e4})/2 = -1 + \cosh\ qa_0\ \exp\ qx & \text{for} \quad -a_0 \geq x \geq x_m \end{cases} \tag{9.11}$$

where the indexes of the f_n functions refer to the line numbers in (9.7).

After the substitution of the expressions of the triangular-wave excitation in (9.9) into (9.11) and the subsequent integration of the resulting time function as described in (9.6), α_0, a_n, and b_n, the Fourier coefficients of the magnetization waveform will come to the following expressions,

$$\alpha_0 = 0 \tag{9.12a}$$

$$a_n = \frac{2}{nT}\ \sin n\frac{T}{2}\ \cos n\frac{a_0 T}{2A}\ (1 - \cos\ nT)$$

$$+ \frac{2\,q\,\frac{2A}{T}\exp\,(-qA)\cosh qa_0}{T\,[n^2 + (q\frac{2A}{T})^2]}(1 - \cos\ nT) \tag{9.12b}$$

$$b_n = -\frac{2}{nT}\cos\ n\frac{a_0 T}{2A}\ \cos n\frac{T}{2}(1 - \cos\ nT)\,. \tag{9.12c}$$

9.3.4 The Rayleigh Region

In 1887 Rayleigh [2] approximated the low-field region of the hysteresis loop with quadratic parabolic curves. This approximation holds well in the region where the hysteresis loop has low distortion in the vicinity of its crossover point with the horizontal axis. It has been used for calculating the Fourier components of the magnetization waveform with good results. Rayleigh's model, however, breaks down at medium- and high-level excitation. To overcome this shortcoming of his model, Lamont [13] followed by Becker and Doring [14]

and later Bozorth [13] have suggested another approximation near to saturation. This is, however, in the form of infinite series that requires a large amount of inconvenient calculations.

Rayleigh parabolic approximation of the hysteresis loop can be expressed, by using the original notations, in the form shown in (9.13). The choice of symbols seems unconventional and they are only used for historical authenticity. Here B is the magnetization as a function of H, the exciting field μ_0 represents the reversible permeability (not the permeability of free space) and H_m is the amplitude of the field applied. The positive and negative signs relate to the ascending and the descending part of the hysteresis loop, respectively,

$$B = (\mu_0 + 2aH_m)\, H \pm a\,(H_m^2 - H^2) \tag{9.13}$$

The constant multiplier a in the second term governs the shape of the parabolic curve.

The exponential model as formulated in (9.7) describes the hysteresis loop in the Rayleigh region and in the medium and saturation field region as well. The expressions in (9.7), however, in the low-field region can be simplified further. When the Rayleigh criterion, $A \leq a_0$ i.e. the amplitude of the excitation is below the value of the coercivity, is satisfied, then two regions of the hysteresis loop will shrink to zero and the number of expressions in the characteristic equation will be reduced to two. This new set of expressions for the low field Rayleigh region is given in (9.14),

$$f_{e1} = 1 - \exp\,[-q\,(x + a_0)] - b_{12} \qquad \text{for the descending part} \tag{9.14a}$$

$$f_{e2} = -\,[1 - \exp\,q\,(x - a_0)] + b_{12} \qquad \text{for the ascending part,} \tag{9.14b}$$

where

$$b_{12} = 1 - \exp\,(-qa_0)\cosh qx_m\,. \tag{9.15}$$

The Rayleigh model works reasonably well but only in a confined region of the hysteresis loop, for low excitation. The exponential model at the same time is applicable in the full excitation range, including the saturation region. By using the T(x) model as a reference the possible error was calculated between the reference T(x) and the two hysteresis loops modeled by using the Rayleigh parabolic approximation and the exponential model by using the same parameters in all cases. The point-by-point difference between the Rayleigh and the T(x) model was formed and plotted in Figure 9.13, using (9.13) and (3.3). This shows a 5% deviation from the reference within the specified limits of Rayleigh range ($A \leq a_0$). Outside this range the Rayleigh model deviates from the reference very rapidly leading to large errors and to the loss of applicability for calculations. Against this, the difference between the exponential model and T(x) shows an error of 4% within the Rayleigh region as depicted in Figure 9.14. This is a maximum error and this will not be exceeded outside the Rayleigh region up to the maximum limit into the deep saturation excitation. This possible error can be further reduced and minimized below a specified limit by adding further exponential terms as discussed before.

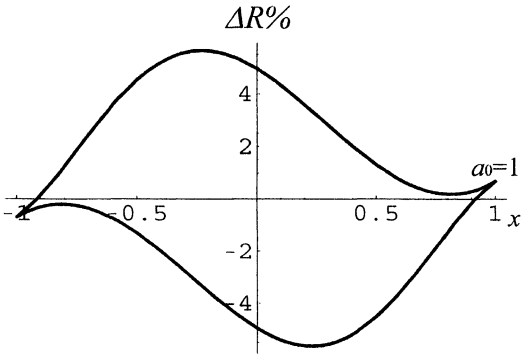

Figure 9.13: The error (ΔR) of the Rayleigh model (R) relative to the T(x) model as a function excitation

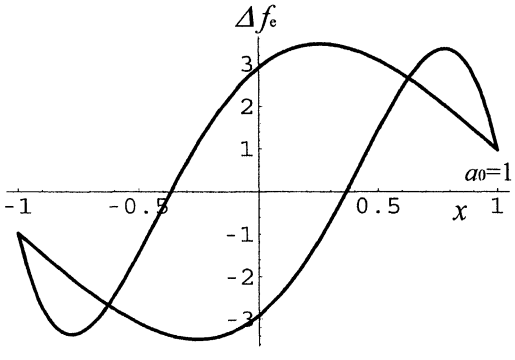

Figure 9.14: The error (Δf_e) of the exponential model relative to the T(x) model in the Rayleigh region as a function of excitation

9.3.4.1 Hysteretic process

Let us assume that triangular excitation is applied in a hysteretic process and the input fulfills the Rayleigh criterion. The magnetization in this condition can be calculated by substituting $x(t)$ expression from (9.9) into (9.14) choosing again $2T$ for the periodicity in time. This will lead us to the following expression for the magnetization function as a time function $f_h(t)$ with the hysteretic distortion.

$$f_h(t) = \begin{cases} 1 - \exp\left[-q\left(\frac{2A}{T}t + A + a_0\right)\right] - b_{12} & \text{for } 0 \le t \le T \\ -\left\{1 - \exp\, q\left[\frac{2A}{T}\left(t - \frac{3T}{2}\right) - a_0\right]\right\} + b_{12} & \text{for } T \le t \le 2T \end{cases} \tag{9.15}$$

For the calculation of the Fourier coefficients $f_h(t)$ has to be substituted into (9.6) and the integration to be carried out. This will yield the expressions shown in (9.16) for α_0, a_n, and b_n coefficients,

$$\alpha_0 = 0 \tag{9.16a}$$

$$a_n = \frac{4\, q\frac{2A}{T}\, \exp(-qa_0)\cosh qA}{T\,[n^2 + (q\frac{2A}{\pi})^2]}\,(1-\cos nT) \tag{9.16b}$$

$$b_n = \frac{2}{nT}[1-\exp(-qa_0)\cosh qA]\,(1-\cos nT) \tag{9.16c}$$

9.3.4.2 Anhysteretic Process

In the case of the anhysteretic process the regions of the loop again reduced to two, therefore we only need two characteristic equations to describe the process. Assuming the same triangular excitation, the magnetization as a time function will come in the following form,

$$f_a(t) = \begin{cases} \dfrac{\exp(-qa_0)}{2}\exp\{q[-\dfrac{2A}{T}(t-\dfrac{T}{2})]\} \\ \\ -\dfrac{\exp(-qa_0)}{2}\exp\{-q[-\dfrac{2A}{T}(t-\dfrac{T}{2})]\} & 0<t<T \\ \\ \dfrac{\exp(-qa_0)}{2}\exp\{q[-\dfrac{2A}{T}(t-\dfrac{3T}{2})]\} \\ \\ -\dfrac{\exp(-qa_0)}{2}\exp\{-q[-\dfrac{2A}{T}(t-\dfrac{3T}{2})]\} & T<t<2T \end{cases} \tag{9.17}$$

After the substitution of (9.17) into (9.6) the integration can be carried out, which will produce the following expressions for the Fourier coefficients,

$$\alpha_0 = 0 \tag{9.18a}$$

$$a_n = \frac{q\frac{2A}{T}\exp(-qa_0)\cosh qA}{T\,[n^2 + (q\frac{2A}{\pi})^2]}\,(1-\cos nT) \tag{9.18b}$$

$$b_n = 0 \tag{9.18c}$$

In ferromagnetic component design and also in circuit calculations the waveform of prime interest is not that of the magnetization but usually the secondary output parameters such as the current or the voltage developed across the circuit element. These quantities are generally proportional to the first derivative by time of the magnetization function. By applying this law to the Fourier components, the frequency spectrum of the required output waveform of a ferromagnetic component (transformer, choke, etc.) can be calculated by taking the first time derivative of the Fourier components of the magnetization waveform.

9.4 Laplace Transform of Waveforms with Hysteretic Distortion

9.4.1 General Remarks

Ferromagnetic components are normally used in conjunction with other components forming a circuit. Circuits or systems are designed to perform a task specified by the designer. It is an indispensable part of the design process to study and understand the dynamic behavior of the system. Although most of the time we will talk about electrical quantities such as voltages and currents, the principles described here are also applicable to other fields where a variety of other quantities are involved in the design process such as forces, displacements, flow rates, temperatures and so forth. Although the techniques for system design by use of a limited number of components, which performs in a prescribed manner, might be quite different in different fields, the analytical tool used in the design is based on the same general principles.

A system or a circuit is a collection of interconnected components with one set of dynamic variables called inputs or excitations and another one called outputs or responses. The objective of the system analysis is to predict how the collection of components responds, when a specified input excitation is applied. The analysis starts with the known characters of the individual components described by their mathematical models. These are combined in order to characterize the system by which its response to certain excitation might be calculated.

In the early part of the 20th century Laplace transformation or operational calculus as it often called became an indispensable tool for the system designers. The first step in an analogue system design is to transform the components and combine them into a system in the Laplace domain. Most circuit components have their standard transforms, which makes it an easy task to build them into a circuit. When the excitation is applied to the circuit input in a transformed form, the response in the Laplace domain might be calculated by using only the four basic arithmetic operations.

One group of circuit components, however, does not fit into these neat categories. A simple model in the circuit cannot replace magnetic components such as chokes and transformers characterized by the double nonlinearity. So far they have been represented by their so-called equivalent circuits composed of linear elements. These equivalent circuits give relatively good approximations in the region of low signal level and when the effect of the hysteresis is negligible. When the coercivity of the ferromagnetic core is large or when the excitation level takes the substance nearer to saturation in the nonlinear region, these

equivalents become unworkable. The time response of the system to the input cannot be calculated in the described fashion.

The Laplace transform of an $f(t)$ time function is defined by the following integral in (9.19)

$$\mathcal{L}\{f(t)\} = F(s) = \int_0^\infty f(t) \exp(st)\, dt\,. \tag{9.19}$$

Here $F(s)$ is the Laplace transform of the $f(t)$ time function and s is the Laplace operator. The difficulty to describe mathematically the time response of these components due to two reasons; the first is the lack of a suitable model to describe the double nonlinearity and the second is the difficulty to carry out the integration in (9.19) in closed form. Out of the presently known models so far, only the exponential model fulfills the criterion for closed-form integration and only for a limited number of waveforms [15], as for the Fourier series (see Section 9.3.1).

9.4.2 Triangular Waveform with Hysteretic Distortion

The triangular waveform of the excitation function is shown in Figure 9.12 and formulated in the expressions in (9.9). The substitution of this periodic time function in (9.9) into the mathematical expression of the model in (9.7) will yield the expression of the magnetization as a piecewise-continuous time function in the following form

$$f_h(t) = \begin{cases} 1 - \exp\{-q[-\frac{2A}{T}(t-\frac{T}{2}) + a_0]\} - b_{12} & 0 \le t \le \frac{T}{2} + t_0 \\ -1 + \exp\{q[-\frac{2A}{T}(t-\frac{T}{2}) + a_0]\} - b_{12} & \frac{T}{2} + t_0 \le t \le T \\ -1 + \exp\{q[\frac{2A}{T}(t-\frac{3T}{2}) - a_0]\} + b_{12} & T \le t \le \frac{3T}{2} + t_0 \\ 1 - \exp\{-q[\frac{2A}{T}(t-\frac{3T}{2}) - a_0]\} + b_{12} & \frac{3T}{2} + t_0 \le t \le 2T \end{cases} \tag{9.20}$$

where

$$t_0 = \frac{a_0 T}{2A}$$

and

$$b_{12} = \exp(-qA) \sinh qa_0\,. \tag{9.21}$$

When $f_h(t)$ is substituted into (9.19) the transforming integral can be executed in a closed form and $F_h(s)$ the Laplace transform of the waveform distorted by the hysteretic process can be calculated.

$$F_h(s) = \frac{1}{s}[1 - \frac{\exp\ (-s\frac{a_0 T}{2A})}{\cosh\ s\frac{T}{2}} - \exp\ (-qA)\sinh qa_0\ \tanh s\frac{T}{2}]$$

$$+\frac{\exp\ (-qA)}{(q\frac{2A}{T})^2 - s^2}[q\frac{2A}{T}\frac{\sinh\ (s\frac{T}{2} - qa_0)}{\cosh\ s\frac{T}{2}} + s\frac{\cosh\ (s\frac{T}{2} - qa_0)}{\cosh\ s\frac{T}{2}}]$$

$$-\frac{s\exp\ (-s\frac{a_0 T}{2A})}{(q\frac{2A}{T})^2 - s^2}\frac{1}{\cosh\ s\frac{T}{2}} \tag{9.22}$$

9.4.3 Triangular Waveform with Anhysteretic Distortion

When the process in hand is anhysteretic then $x(t)$ in (9.9) should be substituted into the characteristic equation of the anhysteretic process in expression (9.11). This will yield the magnetization as a function of time of the anhysteretic process produced by a triangular excitation

$$f_s(t) = \begin{cases} 1 - \cosh\ qa_0\ \exp\{-q[-\frac{2A}{T}(t - \frac{T}{2})]\} & 0 \le t \le \frac{T}{2} - t_0 \\ \frac{\exp\ (-qa_0)}{2}\{\exp\ q[-\frac{2A}{T}(t - \frac{T}{2})] & \\ \quad - \exp - q[-\frac{2A}{T}(t - \frac{3T}{2})]\} & \frac{T}{2} - t_0 \le t \le \frac{T}{2} + t_0 \\ -1 + \cosh\ qa_0\ \exp\{-q[-\frac{2A}{T}(t - \frac{T}{2})]\} & \frac{T}{2} + t_0 \le t \le T \\ -1 + \cosh\ qa_0\ \exp\{-q[-\frac{2A}{T}(t - \frac{3T}{2})]\} & T \le t \le \frac{3T}{2} - t_0 \\ \frac{\exp\ (-qa_0)}{2}\{\exp\ q[\frac{2A}{T}(t - \frac{3T}{2})] & \\ \quad - \exp - q[-\frac{2A}{T}(t - \frac{3T}{2})]\} & \frac{3T}{2} - t_0 \le t \le \frac{3T}{2} + t_0 \\ 1 - \cosh\ qa_0\ \exp\{-q[-\frac{2A}{T}(t - \frac{3T}{2})]\} & \frac{3T}{2} + t_0 \le t \le 2T \end{cases} \tag{9.23}$$

The substitution of $f_s(t)$ function into (9.19) and the subsequent integration will lead to the $F_s(s)$ Laplace transform of the magnetization waveform.

$$F_s(s) = \frac{1}{s}\left(1 - \frac{\cosh s\frac{a_0 T}{2A}}{\cosh \frac{T}{2}s}\right) + \frac{\cosh qa_0 \exp(-qA)}{(q\frac{2A}{T})^2 - s^2}\left[q\frac{2A}{T}\tanh\left(\frac{T}{2}s\right) + s\right]$$

$$-\frac{\exp(-qA)(\cosh qa_0 + \sinh qa_0)}{[(q\frac{2A}{T})^2 - s^2]}\, s\frac{\cosh s\frac{a_0 T}{2A}}{\cosh \frac{T}{2}s}. \tag{9.24}$$

9.4.4 The Rayleigh Region

9.4.4.1 Hysteretic Process

It has been shown in Section 9.3.4.1 that the small-signal region the number of characteristic equations is reduced to two as shown in (9.14) and by substituting the triangular time function from (9.9) into (9.14) the magnetization function resulted from hysteretic magnetization can be derived in the following form

$$f_h(t) = \begin{cases} 1 - \exp\{-q[-\frac{2A}{T}(t - \frac{T}{2}) + a_0]\} - b_{12} & 0 \le t \le T \\ -\{1 - \exp q[\frac{2A}{T}(t - \frac{3T}{2}) - a_0]\} + b_{12} & T \le t \le 2T \end{cases} \tag{9.25}$$

and

$$b_{12} = 1 - \exp(-qa_0)\cosh qA.$$

The substitution of $f_h(t)$ into (9.19) and the execution of the integration will yield the Laplace transform of hysteretic magnetization waveform due to triangular field excitation.

$$F_h(s) = q\frac{2A}{T}\exp(-qa_0)\cosh qA\,\frac{\tanh s\frac{T}{2}}{s(q\frac{2A}{T} - s)}$$

$$-\frac{\exp(-qa_0)\sinh qA}{(q\frac{2A}{T} - s)} \tag{9.26}$$

9.4.4.2 Anhysteretic Process

When the process of magnetization is anhysteretic, then the magnetization becomes a single-valued function of the excitation. By assuming a triangular excitation again $f_s(t)$ the magnetization as a function of time can be described by the following mathematical expressions

$$f_s(t) = \begin{cases} \exp(-q\,a_0)\sinh\left[-q\dfrac{2A}{T}\left(t-\dfrac{T}{2}\right)\right] & 0 \le t \le T \\ \exp(-q\,a_0)\sinh\left[q\dfrac{2A}{T}\left(t-\dfrac{3T}{2}\right)\right] & T \le t \le 2T \end{cases} \tag{9.27}$$

The substitution of these expressions into (9.19) and the subsequent integration will result in the Laplace transform of the distorted magnetization waveform in the Rayleigh region.

$$F_s(s) = \frac{\exp(-q\,a_0)}{\left(q\dfrac{2A}{\pi}\right)^2 + s^2}\left(q\frac{2A}{T}\cosh qA \tanh s\frac{T}{2} - s\sinh qA\right). \tag{9.28}$$

The formulation of the Laplace transforms of these waveforms enables the designer to regard circuit elements with ferromagnetic properties as same as other components for the waveforms specified here. From the circuit response, the higher harmonics generated by the hysteretic process can be calculated directly by using the mathematical relationship between the Laplace and the Fourier transformation [16,17].

When the required quantity is the output voltage or the output current, a multiplication of the calculated Laplace transforms with the Laplace operator s in each case will lead to the required results. This is equivalent of differentiation by t in the time domain.

9.4.4.3 Application

The picture would not be complete without the demonstration of the power of the method described in the previous section.

Let us see what happens when a magnetic field changes slowly between two values linearly in a periodic manner and the field is monitored with a search coil. In order to increase sensitivity a high permeability ferrous material is used in its core. The e.m.f. developed across the search coil can be calculated in the following form by applying Faraday's law of electromagnetic induction,

$$\mathbf{V}(t) = -NA_1\frac{\mathrm{d}\mathbf{B}}{\mathrm{d}t} \tag{9.29}$$

where $\mathbf{V}$ is the voltage developed on the coil, N is the number of turns on the coil and $\mathbf{B}$ is the induction. $\mathbf{B}$ has the following relationship to the $\mathbf{\Phi}$ flux linking the coil,

$$\mathbf{\Phi} = \mathbf{B}A_1, \tag{9.30}$$

where A_1 represents the cross-sectional area of the coil. Assuming that the coil is operating in the Rayleigh region (maximum value of the field is smaller than the coercivity) then the

Laplace transform of the induction will be proportional to the expression in (9.26). Assuming also that we are only interested in the waveform of the monitored signal long after it started, we can lump all constants into K_1 and say that the Laplace transform of the induced e.m.f. $V(s)$ due to the periodically changing field, is proportional to the term representing the periodic part of the process in (9.26)

$$V_1(s) = K_1\, s\, [\frac{1}{(s - q\frac{2A}{T})} - \frac{\tanh s\frac{T}{2}}{s\,(s - q\frac{2A}{T})}]. \qquad (9.31)$$

The expression inside the square bracket represents the Laplace transform of the induction and the s operator outside the bracket implies the first derivative of the bracketed expression by time. The expression in (9.31) can be rewritten in the following form:

$$V_1(s) = K_1\, s\, [\frac{1}{s} - \frac{\tanh s\frac{T}{2}}{s^2}](1 + q\frac{2A}{sT}). \qquad (9.32)$$

It is now obvious that the first term is the Laplace transform of a triangular waveform with $2T$ periodicity, having the value of +1 at $t = 0$. The second term is the integral of the same expression by t. The voltage developed on the coil will be the first derivative of the sum of these two expressions as shown. The predicted waveforms of the voltage and the induction are plotted in Figure 9.15.

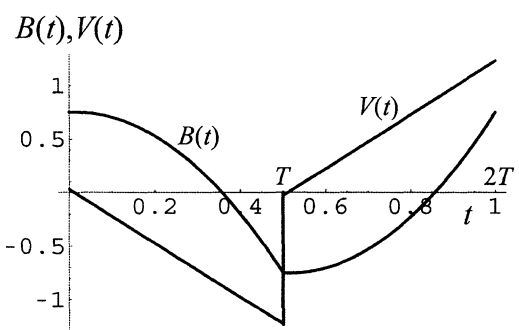

Figure 9.15: The waveforms of the induction and the voltage developed on the search coil at the hysteretic process

Due the difficulties in calculations, caused by the double nonlinearity people often assume anhysteretic magnetization in place of the hysteretic process. When this is the case the voltage developed across the coil will be proportional to the expression given in (9.28) as given in (9.33) following the steps outlined before,

$$V_2(s) = K_2\, s\, \{\frac{1}{s} - \frac{\tanh s\frac{T}{2}}{s^2}[1+(q\frac{2A}{s\,T})^2]\}\,. \tag{9.33}$$

Now the first term in the bracket represents a triangular wave and the second term is the second integral of the same expression. The sum of the two terms represents the induction time function and its first derivative as before gives the voltage on the search coil. The waveform calculated from (9.33) is depicted in Figure 9.16.

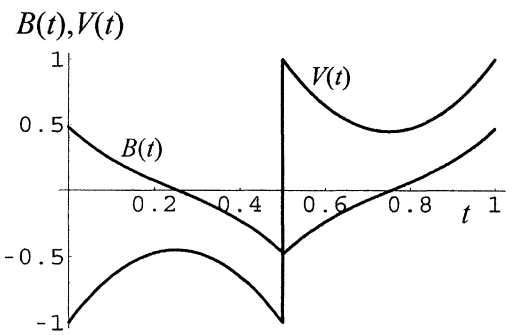

Figure 9.16: The waveforms of the induction and the voltage developed on the search coil at the anhysteretic process

It is obvious from the two graphs that the two processes produce two vastly different results even in the low-amplitude excitation (Rayleigh) region. It should be a fair warning to be very circumspect when equivalents are used in design or calculations.

The transformation of these Laplace transforms back to the time domain has some similarity to the Laplace operations to lossy systems. However, there are subtle differences between the two cases and caution is needed in carrying out the transformation to the time domain. In most cases the time function is recognizable for the user experienced in transformations from its standard form. The transform that has no standard form in the time domain, can be transformed into an infinite series of periodic trigonometric time functions by a method, known since 1953 [16], based on Cauchy's theorem. Some of these infinite series are listed in the handbooks for Laplace transforms. The ways of finding the time functions from the Laplace transforms will cover most if not all the functions resulting from the transformations associated with magnetic phenomena.

It is worth noting that due to the close relationship between the two transformations, Laplace and the Fourier, the method described here is also suitable for the calculation of the Fourier components of signals waveforms, distorted by hysteretic processes, in exponential as well as in trigonometric form [16,17].

References

[1] S. Evershed, The magnetic circuit of transformers: closed versus open. The Electrician **XXVI** 477, 508, 534, 597, 634, 662, 690, 724, 755, 784 (1891).

[2] J.W. Lord Rayleigh, On the behavior of iron and steel under the operation of feeble magnetic force. The Philosophical Magazine **5**, 23, 225 (1887).
[3] L.O. Chua and K.A. Stromsmoe, Lumped–circuit models for non-linear inductors exhibiting hysteresis loops. IEEE Trans. on Circuit Theory **17**, 564–574 (1970).
[4] L.O. Chua and S.C. Basso, A generalised hysteresis model. IEEE Trans. On Circuit Theory, **19**, 36–48 (1972).
[5] Y. Saito, Three-dimensional analysis of magnetodynamic fields in electromagnetic devices taken into account the dynamic hysteresis loops. IEEE Trans. Magn. **18, No. 3**, 546–551 (1982).
[6] S.N.M. Willcock and B.K. Tanner, Harmonic analysis of B-H loops. IEEE Trans. Magn. **19, No. 5**, 2265–2270 (1983).
[7] P. Del Vecchio, A. Salvini, L. Carraniri and G.M. Veca, Ferromagnetic materials excited by a distorted periodic field source. COMPEL Int. J. Comp. Math. E and E. Eng. **17, No. 3**, 398–401 (1998).
[8] W.K. Macfadyen, R.R.S. Simpson and W.S. Wood, Representation of magnetisation curves by exponential series. Proc. IEE. **120, No. 8**, 902–904 (1973).
[9] W.J. Teape, R.R.S. Simpson, R.D. Slater and W.S. Wood, Representation of magnetic characteristic, including hysteresis, by exponential series. Proc. IEE. **121, No. 9**, 119–120 (1974).
[10] J.H. Hwang, Exponential series for B/H curve modelling. Proc. IEE. **123, No.6**, 559–560 (1976).
[11] M.J. Hodgdon, Mathematical theory and calculations of magnetic hysteresis curves IEEE. Trans. Magn. **24, No. 6**, 3120–3122 (1988).
[12] J. Takács, Fourier analysis of hysteretic distortion. COMPEL Int. J. Comp. Math. E and E. Eng. **22, No. 2**, 398–401 (2003).
[13] R.M. Bozorth, *Ferromagnetism* (Van Nostrand, N.Y., 1951).
[14] R. Becker and W. Doring, *Ferromsgnetismus* (Springer, Berlin, 1938).
[15] J. Takács, Laplace transforms of waveforms with hysteretic distortion.(To be published)
[16] J. Takács, A Fourier amplitúdók meghatározása operátorszámitással. Mag. Hir. Techn. **4, No.7–8**, 93–96 (1953).
[17] J. Takács, Notes on "Fourier Series Derivation" Proc. IEEE. **49, No.9**, 1446 (1961).

10. Magnetic Transient or Accommodation

10.1 General Remarks

Observations, supported by experiments, show that when a ferromagnetic substance is subjected to repetitive minor loops, starting from another state of magnetization the new final state will not take effect instantaneously. It will change around for a while converging to a steady equilibrium loop. This process is normally referred to as an applied field accommodation process and this associated phenomenon is a stabilization process, which is in fact a transient, called accommodation or reptation in the literature. This transient often takes some time to settle at steady state and may take a number of cycles to reach the stable minor loop. Similarly to other transient phenomena, it is important to describe it with a mathematical model to provide an analytical tool for the investigation of the behavioral pattern of the substance, which reflects on its internal structure. The magnetic transient has been the subject of intensive research [1–5]. It has to be emphasized again that the processes described here are independent of the rate of change and are not to be confused with other rate-dependent changes or aftereffects, like for instance, the effect of viscosity (see Chapter 12), where change can occur at constant field or even after the field has been removed. This phenomenon is viewed here separately without the combination with other effects.

10.2 Transient Starting from Remanence

When a sample is magnetized to the point of x_{m0} on the hysteresis loop and then the magnetizing field is removed, the magnetic state of the sample declines to the point of remanence where the hysteresis loop crosses the vertical axis of magnetization. This state of the sample will stay until it is subjected to a magnetizing field again. The change in the magnetic state now will be dependent on two factors, firstly on the remanence of the sample and secondly on the applied magnetic field. Let us assume that a linearly changing field is applied to the sample, which is periodically reversed, changing symmetrically between its positive and negative maxima. Although here we consider this simple triangular waveform the end result will be applicable to any waveform of the applied field. Now the field will cycle between the two reversal points x_r and $-x_r$. Let us also assume that at the beginning the cyclic magnetization will start moving in the positive direction. This choice is completely arbitrary and does not affect the end result of this analysis. By recalling the rule of return-point-memory the sample will remember the maximum field of the loop where magnetization was interrupted and the magnetization at the first instance will move on a line leading to x_{m0}. The line of approach will be the same as that described in Chapter 5 and the

Mathematics of Hysteretic Phenomena. Jeno Takács

ISBN: 3-527-40401-5

curve will follow the path of the first order minor reversal loop. In mathematical terms the function of magnetization in the first step will be as described in (10.1).

$$f_{+1} = \tanh\ (x - a_0)\ b_1 + c_1 \tag{10.1}$$

where

$$b_1 = [\tanh\ (x_{m0} + a_0) - \tanh\ (x_{m0} - a_0)]/2 \tag{10.2}$$

and c_1 can be calculated from the condition that at $x = 0$, at the starting point, $f_{+1}(0)$ will be equal to the value of the initial hysteresis loop $f_{-}(0)$, where f_{-} is defined in (3.3a) as

$$f_{-} = \tanh\ (x + a_0) - b_1 . \tag{3.3a}$$

On the approach to x_{m0}, however, the magnetizing path is going to be interrupted and reversed at x_r, the peak value of the cyclic magnetization. This point belongs to one and only one hysteresis loop, which is characterized by its maximum x_{m1}. For the descending branch of the hysteresis loop the numerical value of this maximum can be calculated as

$$x_{m1} = \operatorname{arctanh} \sqrt{\frac{f_{+1}(x_r) - \tanh\ (x_r + a_0) + \tanh\ a_0}{[f_{+1}(x_r) - \tanh\ (x_r + a_0)](\tanh\ a_0)^2 + \tanh\ a_0}} . \tag{10.3}$$

For the calculation of this formula see (10.13) and (10.14). When the interruption is at $x_r = 0$ the formula in (10.3) goes into expression (3.5).

When the magnetizing field is reversed at a positive x_r in the second leg of the process, the magnetizing path will follow another minor loop, which this time will approach $-x_{m0}$ in the manner described in Chapter 5. The process will be interrupted again and reversed at the negative maximum of the magnetizing field $-x_r$. The repeated reversals of the field at $x = x_r$ will produce open loops f_{-n-1} and f_{+n}, where n represents the number of reversals. This transient process converges to a stable closed loop characterized by the value of x_r. The final loop forms part of the same family of loops as the initial loop and its maxima f_{+n} $(-x_r)$ and $f_n(x_r)$ will be located on the loci of all maxima of the same family, the anhysteretic magnetization curve. The ascending paths of the process can be described in mathematical terms in the following way

$$f_{+n} = \tanh\ (x - a_0) - b_n + c_n \tag{10.4}$$

where n is the number of reversals

$$b_n = [\tanh\ (x_{m(n-1)} + a_0) - \tanh\ (x_{m(n-1)} - a_0)]/2 \tag{10.5}$$

$$c_n = c_{n0} \frac{\tanh\ (x_{m(n-2)} - a_0) - \tanh\ (x - a_0)}{\tanh\ (x_{m(n-2)} - a_0) - \tanh\ (-x_r - a_0)} \tag{10.6}$$

and f_{+n-2} equals f_{-n-1} at $x = x_r$.

A process calculated from the equations above is depicted in Figure 10.1. In the calculations the following parameters were used: $a_0 = 3$, $x_{m0} = 1.5$, and $x_r = \pm 1$.

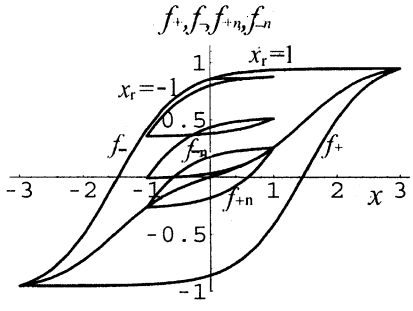

Figure 10.1: Magnetic transient loops starting from a state of remanent magnetization, leading to a steady-state loop

When the amplitude of the cycling magnetizing field is large (as in the example) a small number of reversals are enough to bring the process into a state of equilibrium. With smaller amplitude the number of reversals will rapidly increase and, as is often the case in practice, the sample going through such a magnetization process, needs an appreciable time to reach a steady-state condition. In Figure 10.2 transient loops are depicted when the cycling amplitude is reduced to and $x_r = \pm 1/2$.

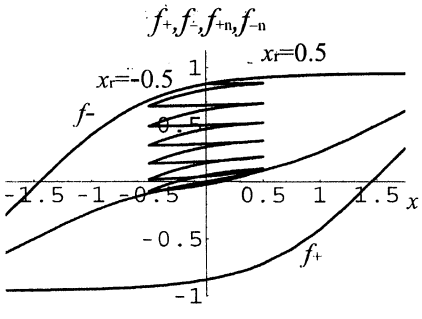

Figure 10.2: Magnetic transient minor loops with smaller amplitude starting from the point of remanent magnetization

10.3 Transient Starting from a Point of Magnetization with DC Field

10.3.1 Inside the Hysteresis Loop

Small-amplitude cycling magnetization can occur on either the ascending or the descending part of the hysteresis loop. Since the two processes require different mathematical formulation they are going to be treated here separately.

10.3.1.1 Ascending Side

Let us consider the case when starting from a constant DC magnetized state the sample is subjected to a small cycling magnetic field of a constant magnitude superimposed on the DC field. We assume that the magnetic state of the sample was previously moved slowly around a hysteresis loop (magnetized) and stopped at a field of interruption marked by x_r on the ascending part of the hysteresis loop as shown in Figure 10.3. The choice of the interruption again is arbitrary and it does not affect the end result. The mathematical expressions describing the hysteresis loop at the start are given in Chapter 3 in (3.2) and (3.3) and b_1 is specified above in (10.2).

For the sake of simplification we assumed again that the linear term is negligible therefore $A_0 = 0$. Let us consider the state of the sample before the cyclic magnetization starts. By recalling the rule of return-point-memory we can say that the sample remembers only two reference points. First is the point of interruption x_r, the second point is x_{m0} the extremum of the hysteresis loop described in (3.2). The subscript 0 signifies again the beginning of the process and describes the positive field maximum of the loop, which is the locus of the point of interruption x_r before the cyclic variation started. All other values of maxima have been wiped out from the memory. By recalling the geometric axiom No. 4 one can say that through these points – the point of interruption and the negative maximum x_{m0} – there are only two lines allowed to be drawn. Out of the two, the descending curve is the only one that can describe the path that the first descending leg of the cyclic magnetization will follow. Similarly to the reversal loops discussed in Chapter 5, the path will copy the descending part of the major loop and follow the path of a first-order minor reversal loop. It will pass through the two fixed points, namely the point of interruption x_r and the negative extremum $-x_{m0}$.

$$f_{+1} = \tanh\ (x - a_0) - b_n + b_{d1} \tag{10.10}$$

where b_1 is defined in (10.2) and b_{d1} in (5.4).

This path of the magnetization will, however, never reach the maximum but it is going to be interrupted, stopped, and reversed at a field value of $x = x_r - \Delta x$, where Δx is the peak-to-peak amplitude of the periodic AC field excitation. At this point the induction can be calculated from (10.11) by substituting $x_r - \Delta x$ for x. thus $f_{+1}(x_r - \Delta x)$. This induction value, however, belongs to one and only one minor loop (see Axiom 5 in Introduction), which is characterized by its maximum excitation field value x_{m1}. At this point the descending part of the minor loop is equal to the ascending path, therefore x_{m1} can be calculated from this equality. In mathematical terms

at $x = x_r - \Delta x$

$$f_{-1}(x_r - \Delta x) = \tanh\ (x_r - \Delta x - a_0) + b_2 \tag{10.11}$$

where

$$b_2 = [\tanh\ (x_{m1} + a_0) - \tanh\ (x_{m1} - a_0)]/2\,. \tag{10.12}$$

By using the following identities

$$\tanh\ (x_{m1} + a_0) = \frac{\tanh\ x_{m1} + \tanh\ a_0}{1 + \tanh\ x_{m1}\ \tanh\ a_0} \tag{10.13a}$$

$$\tanh\ (x_{m1} - a_0) = \frac{\tanh\ x_{m1} - \tanh\ a_0}{1 - \tanh\ x_{m1}\ \tanh\ a_0} \tag{10.13b}$$

(10.13) can be solved for x_{m1}, with the following result

$$x_{m1} = \operatorname{arctanh} \sqrt{\frac{f_{+1}(x - \Delta x) - \tanh\,(x - \Delta x - a_0) - \tanh a_0}{[f_{+1}(x - \Delta x) - \tanh\,(x - \Delta x - a_0)](\tanh a_0)^2 - \tanh a_0}}\,. \tag{10.14}$$

This maximum will overwrite all negative values of maxima in the memory of the magnetic substance and all other values will be wiped out, in accordance with the "wiping-out" property.

The following path f_{+2} will start from the point defined by the $(x_r - \Delta x, f_{-1}(x_r - \Delta x))$ coordinates and end up at the point defined by $(x_r, f_{-1}(x_r))$. On the grounds of Axiom 5, only one ascending path can be drawn through these two fixed points. These two points already determine the descending path of the AC magnetization. The return leg will mimic the ascending part of the hysteresis loop and will be shifted to meet the conditions above. The function f_{-2} (second step) describing the ascending half of the first minor AC loop will take the following form

$$f_{-2} = \tanh\,(x - a_0) + b_2 + c_0\,. \tag{10.15}$$

Here c_0 is the shifting constant that will change between $x = x_r$ and at $x = x_r - \Delta x$ following Axiom 7 and needs to be calculated in (10.15). There are two conditions to be satisfied, therefore at the first instance two constants have to be determined. First, the descending and the ascending paths will cross over at $x = x_r$ therefore the two functions will be equal at this point thus

$$c_6 = f_{-1} - \tanh\,(x - a_0) - b_2 \qquad \text{for} \quad x = x_r\,. \tag{10.16}$$

Secondly, the two paths will cross over again when $x = x_m - \Delta x$ therefore another constant can be calculated from this condition.

$$c_5 = f_{-1} - \tanh(x - a_0) - b_2 \qquad \text{for} \quad x = x_m - \Delta x \,. \tag{10.17}$$

Finally, the transition between c_5 and c_6 will be, according to Axiom 7, which yields the following expression for c_0,

$$c_0 = c_6 \frac{\tanh(x_r - \Delta x - a_0) - \tanh(x - a_0)}{\tanh(x_r - \Delta x - a_0) - \tanh(x_r - a_0)} + c_5 \frac{\tanh(x_r - a_0) - \tanh(x - a_0)}{\tanh(x_r - a_0) - \tanh(x_r - \Delta x - a_0)} \,. \tag{10.18}$$

With the substitution of (10.28) into (10.15) we will satisfy the necessary conditions to close the loop at $x = x_r$ representing the positive peak and at $x = x_m - \Delta x$ representing the negative peak of the cyclic excitation and covering a full excursion of a cycle.

The calculation of the following cycles will follow a similar pattern. In the next step, however, x_{m0} will be replaced by x_{m1} and x_{m1} by x_{m2}, and so on in succession held in the sample memory. In the successive loop calculations each sequence will have its own maximum, indexed by the sequence number (n for the nth loop) and calculated as shown, from (10.14). The loops in every step change their size and after a number of cycles approach an equilibrium state till they finally settle down to a steady state. From then on the shape of the loop will not change and the process will follow the same up and down path. As an illustration, Figure 10.3 depicts a set of converging transient loops with the steady-state loop at the end of it, for the following parameters: $x_{m0} = 2.5$, $a_0 = 1.5$, $x_r = 1.5$, and $\Delta x = 0.5$.

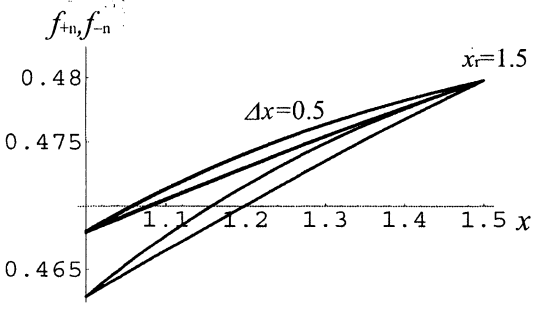

Figure 10.3: Transient minor loops starting from a DC magnetic state. No part of the major hysteresis loop is depicted

After the first large step the transient state approaches equilibrium in small steps and the state of magnetization reaches the steady equilibrium after seven completed cycles. Figure 10.3 does not show the part of the major loop where the process started from and where x_r the starting point is.

10.3.1.2 Descending Side

In this section we consider a case similar to that of Section 10.3.1.1 except this time the slow magnetizing process is stopped at one point on the descending part of the hysteresis loop and the superimposed cyclic small variation will start in the direction opposite to the main field of magnetization. The small-field magnetization will traverse in some fashion between the point of interruption and that set by the maximum amplitude of the cycling field Δx. By using the logic and the rules explained in Chapter 5 the first leg of the process will follow the path of the first-order reversal loop towards the positive maximum x_{m0}. This can be formulated in the following expression

$$f_{-1} = \tanh(x - a_0) + b_1 + b_{u1} \tag{10.29}$$

where f_{-1} signifies the first leg mimicking the ascending part of the hysteresis loop and b_1 and b_{u1} are specified in expressions (10.2) and (5.6), respectively. This process will stop and reverse at the point of $x = x_r + \Delta x$ where the traversing magnetization field reaches its maximum value. The corresponding induction f_{-1} ($x_r + \Delta x$) at this point will mark a maximum x_{m1} value corresponding to a loop to which this point belongs on the hysteretic plane. With the use of the expressions in (10.13), x_{m1} can be calculated as before

$$x_{m1} = \operatorname{arctanh} \sqrt{\frac{f_{+1}(x + \Delta x) - \tanh(x + \Delta x + a_0) - \tanh a_0}{[f_{+1}(x - \Delta x) - \tanh(x + \Delta x + a_0)](\tanh a_0)^2 + \tanh a_0}} . \tag{10.20}$$

This is the maximum, which the next leg is going to approach after having all positive maxima wiped out from its memory. The return path has to go through the two points specified by (x_r, f_{-1}) and $(x_r + \Delta x, f_{-1}(x_r + \Delta x))$ coordinates. The equation describing the only descending line that satisfies the conditions will be

$$f_{-2} = \tanh(x + a_0) - b_2 + c_0 . \tag{10.21}$$

Here b_2 is the constant that will change between b_1 at $x = x_r$ and b_{11} at $x = x_r + \Delta x$ following Axiom 7 and specified in (10.12). Similarly to the shifting constant before, c_0 can be calculated from the two conditions above coming to the following expression

$$c_0 = c_6 \frac{\tanh(x_r + \Delta x + a_0) - \tanh(x + a_0)}{\tanh(x_r + \Delta x + a_0) - \tanh(x_r + a_0)} + c_5 \frac{\tanh(x_r + a_0) - \tanh(x + a_0)}{\tanh(x_r + a_0) - \tanh(x_r + \Delta x + a_0)} \tag{10.22}$$

where c_5 and c_6 constants satisfy the above criteria.

The process follows a pattern similar to that described in Section 10.3.1.1. After a number of cycles the process arrives at an equilibrium state. From then on the induction will cycle around the same small loop while the exciting field traverses between x_r and $x_r - \Delta x$. A change in the dynamic state of this equilibrium will only be triggered by a change in the ongoing conditions of the field excitation.

Loops calculated from these equations, starting on the descending leg of the hysteresis loop, are depicted in Figure 10.4. The numerical values of the parameters used in the calculation were as follows: $x_{m0} = 3$, $x_r = -0.75$, $\Delta x = 0.5$, and $a_0 = 1$. The transient reached the equilibrium state after six cycles.

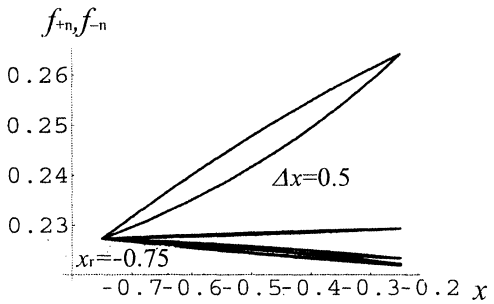

Figure 10.4a: Transient loops starting from a DC magnetic state on the descending leg of the hysteresis loop. No part of the major hysteresis loop is shown

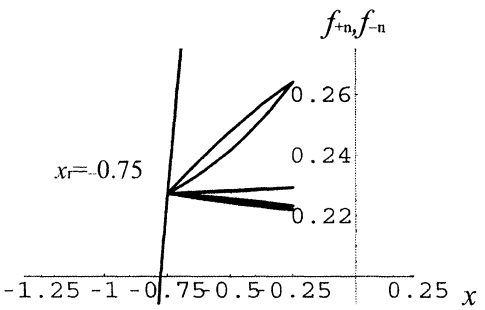

Figure 10.4b: The same transient loops starting from a DC magnetic state on the descending leg of the hysteresis loop also showing a part of the major loop

10.3.2 Transient outside the Hysteresis Loop

In the previous sections the cycling magnetization started going up in the opposite direction to that of the main magnetizing field. On the ascending part of the hysteresis loop the first leg of the cycle reduced the induction whilst on the descending part it increased the induction before returning to its original state. As a result of this the transient loops all fell inside of the major loop where the small loops have started. This, however, is not necessarily the case. The cycling magnetization in practice can start in either direction and the choice is not always up to the experimenter to decide. When the magnetizing process stops on the ascending side of the hysteresis loop and the cyclic exciting field starts up in

the same direction then the initial conditions will differ from that described in Section 10.3.1.1. At the start of the cycling process, since it is outside of the hysteresis loop, the sample has no memory of any return maximum. Due to this lack of first direction it can only select the second possible choice, the saturation point, from which any further increase in the exciting field will not produce any change in the magnetic state of the sample. This field value is not usually excessively large and on the normalized scale it falls between 3 and 5.

The first leg of the cycle must go over two fixed points set by the coordinates of the point of interruption x_r and the saturation point x_{m1}. The process moves from a loop characterized by x_{m0}. With

$$b_1 = [\tanh(x_{m0} + a_0) - \tanh(x_{m0} - a_0)]/2 \tag{10.22}$$

at $x = x_r$ and zero at the saturation point the function describing the first leg can be put in the following mathematical form:

$$f_{-1} = \tanh(x - a_0) + b_2 \tag{10.23}$$

where b_2 can be calculated from the conditions set above as

$$b_2 = b_{-1}\frac{\tanh(x_{m1} - a_0) - \tanh(x - a_0)}{\tanh(x_{m1} - a_0) - \tanh(x_r - a_0)}. \tag{10.24}$$

The return path will follow the tangent hyperbolic line through two points. The two crossovers at x_r and $x_r + \Delta x$ will set the conditions for calculating the two shifting constants

$$c_3 = f_{-1} - \tanh(x + a_0) + b_3 \text{ for } x = x_r + \Delta x \tag{10.25}$$

where

$$b_3 = [\tanh(x_{m1} + a_0) - \tanh(x_{m1} - a_0)]/2 \tag{10.26}$$

and

$$c_6 = f_{-1} - \tanh(x + a_0) + b_3 \text{ for } x = x_r. \tag{10.27}$$

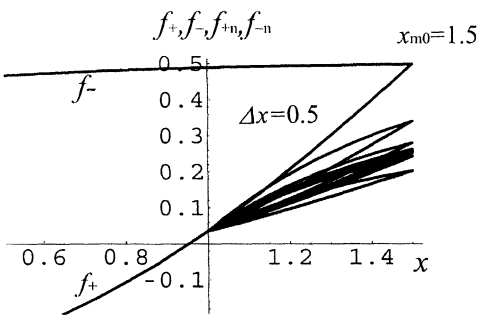

Figure 10.5: Small loops outside of the host hysteresis loop. The graph shows part of the hysteresis loop to which the starting point belongs

With the final shift of c_0, whose expression formally is identical to (10.22), the mathematical formulation of the return path will be as follows

$$f_{+2} = \tanh(x + a_0) - b_2 + c_0 \tag{10.28}$$

By using the formulation above for the successive cycles and upgrading the index of x_m by one, the model will describe the iterative process that approaches the steady-state condition beyond which there will be no further change to the shape and size of the small cycle.

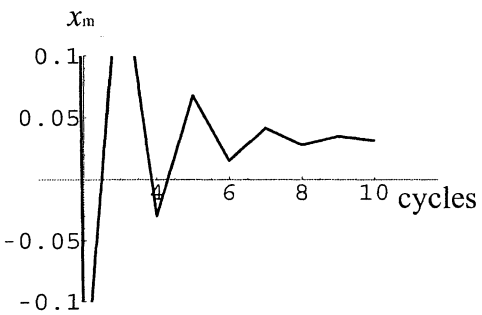

Figure 10.6: The characteristic x_m values as function of number of cycles

Calculated from (10.23) and (10.28) a set of small loops are plotted in Figure 10.5. The numerical parameter values used in the calculation were as follows: $a_0 = 1.5$, $x_{m0} = 1.5$, $x_r = 1$, and $\Delta x = 0.5$. The saturation excitation value was 5 but the actual numerical value does not influence the result of the calculation. The equilibrium state was reached after ten cycles and the intermediate states oscillate around the final loop. The characteristic x_m values for each step are plotted in Figure 10.6.

The process shows a perfect analogy to the damped oscillatory conditions of electronic circuits.

References

[1] E. Della Torre and G. Kádár, Hysteresis modeling II: Accommodation. IEEE Trans. Magn. Magn. **27**, 3811–3814 (1987).
[2] I.D. Mayergoyz, *Mathematical Models of Hysteresis* (Springer Verlag, N.Y., 1991).
[3] E. Della Torre, *Magnetic Hysteresis* (IEEE Press, N.Y., 1999).
[4] E. Della Torre and F. Vajda, Parameter identification of the complete-moving hysteresis model using major loop data. IEEE Trans. Magn. Magn. **30**, 4987–5000 (1994).
[5] F. Vajda, E. Della Torre, M. Pardávi-Horváth and G. Vértesy, A variable variance Preisach model. IEEE Trans. Magn. **MAG-29**, 3793–3795 (1993).

11. Magnetic Recording

11.1 Analogue Recording with AC Bias

11.1.1 Historical Background

Poulsen demonstrated successful recording of acoustic information on magnetic media for the first time in 1898 [1] by recording human voice on ferromagnetic wire on a device called the "telegraphone". Magnetic tapes have been used as storing media for analogue information successfully since Carlson's patent in 1927 [2] long after the AC bias was devised. Although the benefit of the currently exclusively used AC bias in the analogue recording process has been recognized, in the early days of magnetic tape-recording, its full and satisfactory explanation eluded scientists. To describe this rather seemingly simple process in words is not easy, but putting this into mathematical terms until now has proven far too difficult. Various theories and models have been offered to explain the role of the AC bias in the last half century. Those that survived the scientific scrutiny provide explanations for some or most of the associated problems, but the full coherent picture is still unresolved. These models, due to their limitations, often produce contradicting results. Although now the underlying phenomena are reasonably well understood and the various models help us to understand the process, some of those involved in magnetic recording still approach the problem with an open mind looking for a theoretical explanation.

It would be very difficult, if not impossible, to list all contributions published on this subject during those years, because every decade produced its own model with its unique explanation. Toomin and Wildfeuer [3], Holmes and Clarke [4], Wetzel [5], Camras [6] and others put forward their ideas in the 1940s. The 1950s were marked by the contributions of Bedford [7], Westmijze [8], Greiner [9], Axon [10], Woodward and Della Torre [11]. The 1960s and 1970s brought new approaches and new models like those of Mee [12,13], Eldridge and Daniel [14], Herbert and Patterson [15] and Bertram [16], some of which are accepted now in text books as standard models. One idea, however, put forward by Sebestyén and Takács in 1961 [17] failed to attract much attention. This model was based on the assumption that the analogue information is recorded on the tape as a modulation on the "carrier" in the changing shape of the bias waveform. The shape of the recorded wave might change due to the nonlinear nature of the medium but the information is still contained in the Fourier spectrum of the recorded signal. Not surprisingly, that was one of those models, which, due to the lack of computing facilities at the time, was impossible to prove let alone put it into a computable mathematical form.

In the following analytical approach, ideal conditions are assumed and for the sake of presenting the mathematical model everything associated with the recording and reproducing process will be taken as ideal. Naturally the various limitations and losses such as gap loss, separation, losses due to the finite thickness of the medium and mistracking

Mathematics of Hysteretic Phenomena. Jeno Takács

ISBN: 3-527-40401-5

would apply in practical cases. These, however, are well-understood phenomena and well documented in the literature. No particular orientation of recording, horizontal, vertical or both, will be assumed in the analysis, but at playback it will be assumed that all recordings are played back faithfully irrespective of their orientation.

11.1.2 The Recording Process

Nowadays, as a general practice, all linear analogue recording systems, sound and instrumentation likewise, apply AC biasing at recording. In this form of recording the low-frequency information is combined with, in fact linearly added to, a high-frequency signal and the sum of the two current applied to the winding of the recording head. The magnetic tape, moving at a speed in the field created in the gap of the recording head, is exposed to the field. During the passage of the medium in the rapidly changing field, the field cycles the magnetic particles round the hysteresis loop a number of times. As we have seen in Chapter 4 when the field is the combination of an AC and a DC then the medium is exposed to an anhysteretic magnetization process and we know from experience that the replayed information is a single-valued function of the recorded signal [18,19]. This process is characterized by the anhysteretic magnetization curve shown in Figures 4.1 and 4.2 and also described by the expression in (4.7). By the substitution of

$$x = A \cos \Omega t + B \sin \omega t \tag{11.1}$$

into (4.7), the induction in the magnetic media due to the alternating field can be calculated. Here A and B represent the normalized dimensionless amplitudes of the low-frequency information and the AC bias, respectively, while

$$\Omega = \frac{2\pi}{\mathrm{T}}$$

is the frequency of the recorded information and

$$\omega = \frac{2\pi}{\tau}$$

is the frequency of the bias. The combined field (11.1) projected on the anhysteretic curve (4.2) will result in an expression for the magnetization shown in (11.2),

$$f_s = [\tanh\ (A \cos \frac{2\pi}{T}\ t + B \sin \frac{2\pi}{\tau} t + a_0)$$

$$+ \tanh\ (A \cos \frac{2\pi}{T}\ t + B \sin \frac{2\pi}{\tau} t - a_0)]/2\,. \tag{11.2}$$

The waveforms of the combined low-frequency information and the bias field as described in (11.1) and the resulting induction are depicted in Figure 11.1 between 0 and 4π for the ω to Ω ratio of 40. The same induction waveform for $T = 40\tau$ is shown in Figure 11.2.

The tape moves in the front of the recording head with constant linear velocity **v**. When the tape leaves the field created in the gap of the recording head, the state of the magnetic particles will decay from the state of anhysteretic induction to a state remanence, determined by the anhysteretic remanent magnetization curve of the magnetic substance on tape. The process is described in Chapter 6. The combined bias and signal, resulted from the high- and low-frequency field, will stay remanent on the magnetic tape, reference to (6.20), described by (11.3). We shall see that due to the anhysteretic recording process the recorded signal on the tape, and consequently the reproduced information, will also be a single-valued function of the recording signal as supported by experimental results,

$$f_{r+} = \tanh\ a_0 - [\tanh\ (A\cos\frac{2\pi}{\Lambda}\xi + B\sin\frac{2\pi}{\lambda}\xi + a_0)$$

$$+\tanh\ (A\cos\frac{2\pi}{\Lambda}\xi + B\sin\frac{2\pi}{\lambda}\xi - a_0)]/2 \quad \text{for} \quad \begin{cases} 0 \le \xi \le \lambda/4 \\ 3\lambda/4 \le \xi \le \lambda \end{cases} \tag{11.3a}$$

$$f_{r-} = \tanh\ (-a_0) + [\tanh\ (A\cos\frac{2\pi}{\Lambda}\xi + B\sin\frac{2\pi}{\lambda}\xi + a_0)$$

$$-\tanh\ (A\cos\frac{2\pi}{\Lambda}\xi + B\sin\frac{2\pi}{\lambda}\xi - a_0)]/2 \quad \text{for} \quad \lambda/4 \le x \le 3\lambda/4 \tag{11.3b}$$

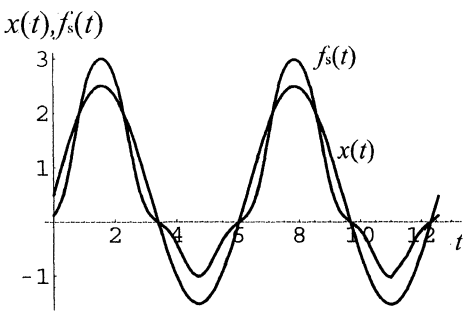

Figure 11.1: The combined field (x) and induction (f_s) waveforms shown for two bias wavelengths

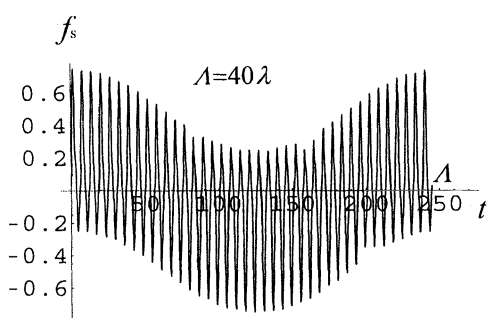

Figure 11.2: The waveform of the induction for 40 bias wavelengths (one signal wavelength)

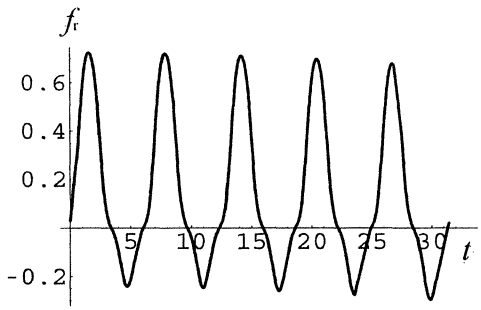

Figure 11.3: The waveform of the remanent magnetization recorded in the magnetic medium for five bias wavelengths in normalized units

The combined remanent waveform, recorded in the magnetic medium, calculated from (11.3) is shown in Figure 11.3. for a period of 5λ (five bias wavelengths). As we can see, the movement of the tape converted the magnetization time function into a linear space remanence function, where ξ, the new independent variable, is the linear position in the length of the tape. The recording frequency in this new space domain becomes the recorded wavelength. In this transformation Λ and λ represent the recorded wavelengths of the information and the bias, respectively, related to the recording frequencies in the following way:

$$\Lambda = \frac{2\pi}{\Omega} v \text{ and } \lambda = \frac{2\pi}{\omega} v \tag{11.4}$$

where **v** the velocity vector points in the direction of ξ and $v = |\mathbf{v}|$.

11.1.3 The Process of Replay

To read the information recorded in the magnetic medium, the recording process has to be reversed. The recording medium is moved in front of the reproducing head normally, with the same constant linear velocity and the information is read back from the tape by the reading head. Let us see the mathematics of this process. In order to find E the replayed voltage, developed across the winding of the reproducing head, one has to apply Faraday's law in this form

$$E = -N\frac{\mathrm{d}\Phi}{\mathrm{d}t} = -NA\frac{\mathrm{d}M_r}{\mathrm{d}t} \tag{11.5}$$

where N is the number of turns on the reading head, Φ is the flux engaged with the head during replay. M_r the remanent magnetism is linked to the flux Φ by the following relation

$$M_r = \frac{\Phi}{A}. \tag{11.6}$$

and A is the engagement area between head and tape. Its magnitude is determined by the physical attributes, design, and geometry of the head.

Under ideal conditions, with an infinitely narrow replay gap, it would not be difficult to replay the whole recorded information in its entirety as shown in Figure 11.3 or rather its derivative as can be seen from (11.5). In practice, however, primarily due to the gap loss (this is due to the finite width of the gap in the replay head) the bias signal will not be or will only partially be replayed. One has to create special conditions to satisfy the criteria of $\lambda > g$ (where g is the width of the replay gap) to be able to detect the bias wavelength λ on the tape. The presence of the bias at replay, however, is a well-known phenomenon especially in wide-band recording, and is classified as bias noise. The recording of the bias forms no part of the presently accepted standard models of magnetic recording, therefore this "phenomena" is regarded as a troublesome side effect in the process of magnetic recording. People have long worked on the reduction or the total elimination of the "noise" caused by the "leakage" (as it is often referred to) of the bias without perhaps realizing that this forms the foundation of AC bias recording.

During the process of replaying the signal, recorded in the form formulated in (11.3), will be reverted into a time function in the way opposite to the process at recording by running the linearly stored information in front of a head, which is basically the same as the head at recording. After transforming the information into the time domain, in the following calculations Ω and ω will replace Λ and λ, respectively, and t will take the place of ξ the independent variable in (11.3) as described in (11.4).

We have seen that the information is coded into the shape of the "carrier" (bias) at recording in the manner, which in fact is unique and not even similar to the well-known amplitude modulation. By applying Faraday's law to the remanent signal, reverted into a time function by the moving tape and taking the first derivative of f_r by t, we can calculate the replayed signal as a function of time. The output voltage from the replay head will then be proportional to the first derivative of f_r by t as shown below in (11.7)

$$f_{r+}' = \frac{df_{r+}}{dt} = \frac{1}{2}\{[\text{sech}\,(a_0 + A\cos\Omega t + B\sin\omega t)]^2\,(B\omega\cos\omega t + A\Omega\sin\Omega t)$$

$$- [\text{sech}\,(a_0 - A\cos\Omega t - B\sin\omega t)]^2\,(-B\omega\cos\omega t$$

$$+ A\Omega\sin\Omega t)\}\ \text{for}\ \begin{cases} 0 < t < \pi/2 \\ 3\pi/2 < t < 2\pi \end{cases} \tag{11.7a}$$

$$f_{r-}' = \frac{df_{r-}}{dt} = -\frac{1}{2}\{[\text{sech}\,(a_0 + A\cos\Omega t + B\sin\omega t)]^2\,(B\omega\cos\omega t - A\Omega\sin\Omega t)$$

$$- [\text{sech}\,(a_0 - A\cos\Omega t - B\sin\omega t)]^2\,(-B\omega\cos\omega t$$

$$+ A\Omega\sin\Omega t)\}\ \text{for}\ \pi/2 < t < 3\pi/2. \tag{11.7b}$$

Figure 11.4 shows the plot of the expression f_r' as a function of time. The effect of the low-frequency "modulation" is clearly visible on the replayed "carrier" waveform.

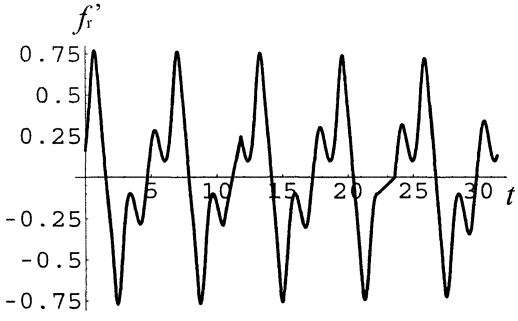

Figure 11.4: The ideal replayed signal including the low frequency and the bias for five bias wavelengths

It is obvious to the reader that the expression in (11.7) can be split into bias and signal components represented by the cos Ωt and the sinωt multiplying terms, respectively. The coefficient of the low-frequency information C_Ω, which is the replayed amplitude of the recorded information (sin Ωt) from expression (11.7) is as follows:

$$C_{\Omega+} = \frac{-A\Omega}{2}\{-[\text{sech}\,(a_0 + A\cos\Omega t + B\sin\omega t)]^2 + [\text{sech}\,(a_0 - A\cos\Omega t - B\sin\omega t)]^2\} \quad (11.8a)$$

$$C_{\Omega-} = \frac{A\Omega}{2}\{[\text{sech}\,(a_0 + A\cos\Omega t + B\sin\omega t)]^2 - [\text{sech}\,(a_0 - A\cos\Omega t - B\sin\omega t)]^2\}. \quad (11.8b)$$

As one can see from (11.8) the two coefficients $C_{\Omega+}$ and $C_{\Omega-}$ above are identical and they are the functions of the recorded signal and bias amplitudes A, B, the low and the bias frequencies Ω and ω, respectively, and also a_0 the coercivity of the recording substance. In Figure 11.5 the full retrieved low-frequency information is shown, on its own, under ideal conditions, without the bias spectrum.

In an ideal world and with an infinitely narrow replay head gap, all frequencies forming part of the "low" frequency term recorded on the tape, shown in Figure 11.5 would be replayed. Due to the frequency limitation, however, imposed by the finite gap, acting as a low-pass filter or integrator, only the long wavelength, the low-frequency content will be reproduced as an output. In a wide-band system the bias is partially replayed, particularly when gap wavelength ratio approaches the second peak on the gap-loss curve. This phenomenon is well documented and fully explained in the literature [18–21].

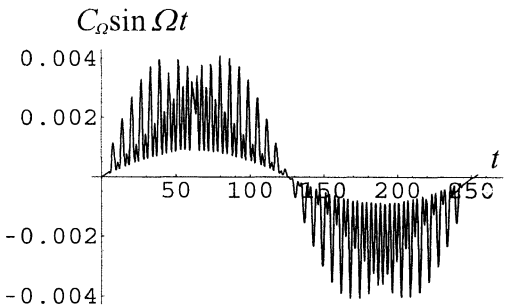

Figure 11.5: The low-frequency component of the spectrum includes high-frequency components from the bias

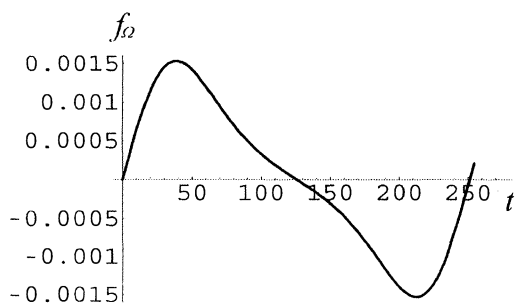

Figure 11.6: The replayed monochromatic information recorded on a magnetic tape (bias amplitude is not optimized) in normalized units

The final waveform of the replayed information f_Ω after a perfect integrating effect of the head has been taken into consideration, is formulated in (11.9) and plotted in Figure 11.6,

$$f_\Omega = \frac{-A\Omega \cos \Omega t}{2}[\text{sech}\,(a_0 - A \cos \Omega t - B)]^2$$

$$- [\text{sech}\,(a_0 + A \cos \Omega t + B)]^2 . \qquad (11.9)$$

11.1.4 Record, Replay Characteristics

Expressions (11.7a) and (11.7b) show that the amplitude of the reproduced information is dependent on the coercivity of the recording material, both amplitudes of the bias and recording signal as well as on bias and signal frequencies at recording. In this section the interdependence of the various parameters will be calculated with their effect on the reproduced information. First, C_Ω is plotted as a function of the bias amplitude B for various monochromatic recordings. Figure 11.7 shows the normalized amplitudes of three replayed frequencies of Ω = 1/80, 1/40, 1/20, and 1/10 with Ω values normalized to the bias

frequency ω and for the recorded relative amplitude value of $A = 0.5$. One can see the linear increase in amplitude with the recorded frequency. In practice the rate of change is limited by the gap loss for recorded wavelengths comparable with g the width of the gap of the replay head. The peak represents the bias amplitude for the maximum output. Below this is the underbiased and above it is the overbiased region.

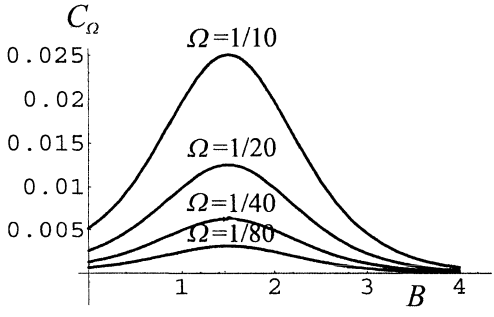

Figure 11.7: Replayed signal amplitude versus bias amplitude, signal frequency as parameter

In order to show the replayed amplitude dependence on the bias frequency, in Figure 11.8 the amplitude of a single frequency is plotted against B the bias amplitude, with the bias frequency as parameter for $\omega = 0.75$, 1, 1.5, and 1.75 values. The plot shows that around the unity ω value the curves run near to each other and the optimum only shifts for large changes in the bias frequency. In this calculation the parameter values were the same as before.

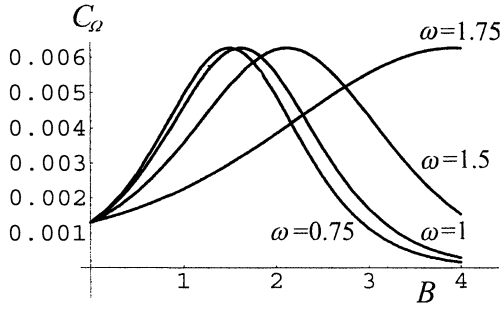

Figure 11.8: Replayed signal amplitude versus bias amplitude, bias frequency as parameter

For most practical cases the selected bias frequency falls into the region where a small frequency change will not cause a noticeable change in the optimum bias conditions (i.e. curves between $\omega = 0.7$–1).

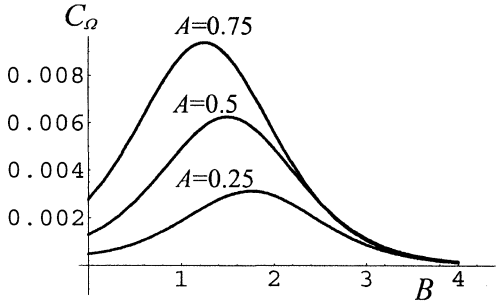

Figure 11.9: Replayed signal amplitude versus bias amplitude recording, signal amplitude as parameter

Figure 11.9 depicts the dependence of the output on A, the low-frequency amplitude. It shows that while the output grows linearly with A, the optimum bias conditions will shift towards the lower bias amplitude with increasing A.

In Figure 11.10 the output amplitude is plotted against B the bias amplitude with the coercivity a_0 as the parameter. The curves show a very strong dependence of the bias on the coercivity. The higher the coercivity the higher the AC bias amplitude required for the same low-frequency output.

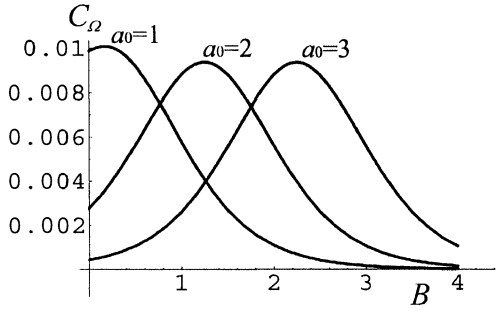

Figure 11.10: Replayed signal amplitude versus bias amplitude, the coercivity as parameter

11.1.5 Distortion

The fidelity of the replayed information from the recorded medium is the measure of the quality of the recording media and the recording process. The deviation from the original signal, called distortion, is the result of the nonlinear nature of the recording process. In the signal output the distortion manifests itself in the frequency spectrum, which is different from that of the input signal. The difference between the two spectra is the measure of the distortion. For a faithful reproduction this difference between the two spectra should be minimized. In the case of the AC recording the correct bias setting plays a vital part in the fidelity of the recording process. At recording there is only one bias setting that will produce minimum distortion to the output. Assuming monochromatic harmonic information is recorded on the magnetic medium Figure 19.11 depicts three output signals recorded with

low-level bias (underbiased), high-level bias (overbiased) and the correct biasing. The two signals recorded with nonoptimized bias visibly differ from the monochromatic sinusoidal waveform recorded with the optimum bias amplitude.

The distortion d of a monochromatic signal is defined as

$$d = \frac{\sqrt{\sum_n a_n^2}}{a_0} \tag{11.10}$$

where a_n is the amplitude of the nth harmonics in the Fourier spectrum of the signal replayed from the magnetic medium and a_0 is the amplitude of the fundamental frequency or the first harmonic. The distortion suffered by the signal during recording can be studied by Fourier analysis of the waveform of the replayed signal under varying conditions. By varying B the bias amplitude the Fourier analysis shows a strong minimum in the distortion as a function of B. Due to under- or overbiasing the distortion of the signal rapidly increases with the dominant second harmonics (2Ω) in the spectrum. The 3rd and 4th harmonics can be significant but the other higher harmonics make insignificant contribution to the distortion of the recorded signal at playback. The distortion as a function of the bias amplitude B is plotted in Figure 11.12. The noted numerical parameters were used in the calculation. In calculating the distortion, up to the 4th harmonics were taken into consideration.

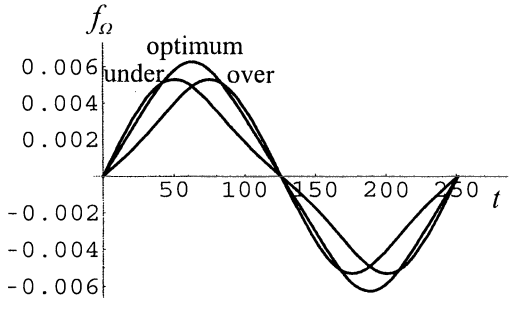

Figure 11.11: Replayed monochromatic signal waveforms recorded with the following recording conditions, underbiased, overbiased, and optimum biased

For general reading on the subject of magnetic recording the reader is referred to the literature [21–23].

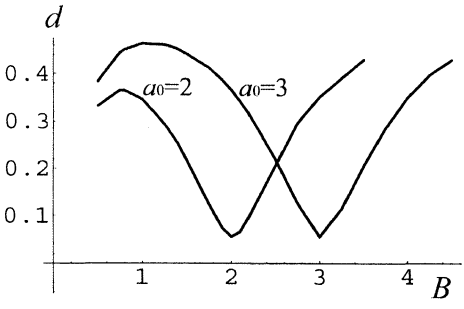

Figure 11.12: Distortion versus recording bias amplitude for $a_0 = 2$ and 3

11.2 Analogue Recording with DC Bias

Although the use of DC bias, for recording information on magnetic tape, is only of historical interest, I felt that for the sake of completeness the model has to be applied to this problem as well, in order to investigate and prove its general applicability. Fundamentally by the application of DC bias at recording the signal to be recorded is shifted to the more linear section of the curve of remanent magnetization, thus avoiding the highly nonlinear part of the remanent magnetization curve around zero and the saturation region. The bias B now becomes a constant and the expression for the field excitation will be as follows

$$x = A \cos \Omega t + B . \tag{11.11}$$

The substitution of x in (11.11) into the expression of the anhysteretic remanent magnetization (see (6.20)) will yield the following expression for the magnetic information on the recording medium:

$$f_{r+} = \tanh\ (-a_0) + [\tanh\ (A \cos \Omega t + B + a_0) - \tanh\ (A \cos \Omega t + B - a_0)]/2 \quad \text{positive going} \tag{11.12a}$$

$$f_{r-} = \tanh\ a_0 - [\tanh\ (A \cos \Omega t + B + a_0) - \tanh\ (A \cos \Omega t + B - a_0)]/2 \quad \text{negative going.} \tag{11.12b}$$

Although these expressions are similar to (11.3) they are left in the form of time functions in order to simplify the procedure. In fact, at recording they are converted to a function of ξ on the tape and reverted again at replay in the same way as in the case of the AC bias. The significant difference is, however, that the bias here is no longer a sinusoidal time function as in the AC case, but represented by a time-independent "constant". The field and the magnetization of a single frequency produced with DC bias are shown in Figure 11.13 over two periods of the recorded waveform.

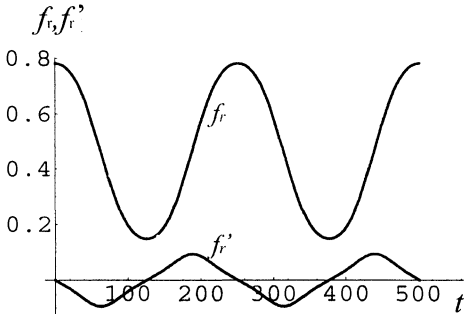

Figure 11.13: The excitation $x(t)$ and the magnetization $f_r(t)$ waveforms with DC bias as functions of time.

After the application of Faraday's law (described in (11.5) to (11.11)) the recorded information can be reproduced. After differentiating f_{r+} and f_{r-} in (11.12) by t as in the case of AC bias, the output can be formulated as in (11.13) below,

$$f_{r+}' = -\frac{df_{r+}}{dt} = \frac{A\,\Omega \sin \Omega\, t}{2}\{[\text{sech}\,(A\cos\Omega\, t + B + a_0)]^2$$

$$- [\text{sech}\,(-A\cos\Omega\, t - B + a_0)]^2\} \quad \text{for the positive part} \tag{11.13a}$$

$$f_{r-}' = -\frac{df_{r-}}{dt} = \frac{-A\,\Omega \sin \Omega\, t}{2}\{[\text{sech}\,(A\cos\Omega\, t + B + a_0)]^2$$

$$+ [\text{sech}\,(-A\cos\Omega\, t - B + a_0)]^2\} \quad \text{for the negative part.} \tag{11.13b}$$

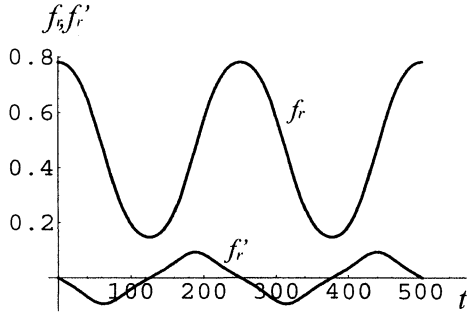

Figure 11.14: The remanent and the replayed signal waveforms with the recorded signal reverted into a time function for simplicity

In the DC biased case, assuming positive bias, all actions are going to take place in the first quadrant, therefore only the positive remanence curve f_{r+} and its replay function f_{r+}' are

going to play a part in the recording process. The waveform of the signal reproduced from a monochromatic recording is plotted in Figure 11.4 with remanent recorded waveform.

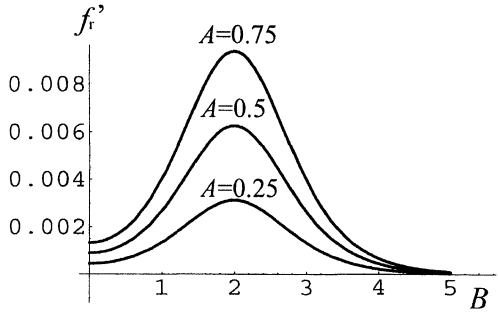

Figure 11.15: Replayed signal amplitude versus bias amplitude, recording signal amplitude as parameter A = 0.25, 0.5, and 0.75

The amplitude of the replayed signal $C_{\Omega+}$ as can be see from (11.13) is the function of B the magnitude of the DC bias, the coercivity a_0, the frequency Ω and the amplitude A of the recorded signal. Its dependence on B is plotted in Figure 11.15 with A as the parameter for the values of A = 0.25, 0.5, and 0.75.

$$f_\Omega = C_\Omega \cos\ \Omega t = \frac{-A\Omega}{2}\{[\text{sech}\ (A \cos \Omega t + B + a_0)]^2$$

$$+ [\text{sech}\ (-A \cos \Omega t - B + a_0)]^2\} \cos\ \Omega t\ . \qquad (11.14)$$

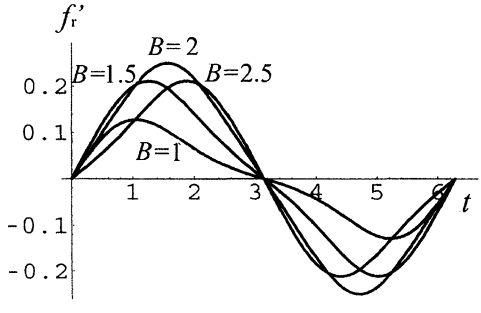

Figure 11.16: Replayed signal waveforms for bias amplitudes B = 1, 1.5, 2, and 2.5 (B=2 is optimum)

The optimum bias where the signal replayed with the minimum distortion is at the inflection point where the concave and convex sections of the remanent magnetism curve meet. In Figure 11.16 four outputs of monochromatic sinusoidal recorded signals are plotted, with under biased (B = 1, 1.5), optimum biased (B = 2) and over biased (B = 2.5) biasing conditions. The waveforms recorded with non optimum bias show visible distortion. In

Figure 11.17 $C_{\Omega+}$ is plotted against B and a_0 is being used as parameter for a_0 = 1.5, 2, and 2.5, which also marks the horizontal coordinate of the inflection point on the anhysteretic remanance curve. With increasing coercivity of the recording material the bias increases for the same signal output but the magnitude of the peak intensity remains the same. By selecting recording material with different coercivity it will not change the magnitude of the replayed information.

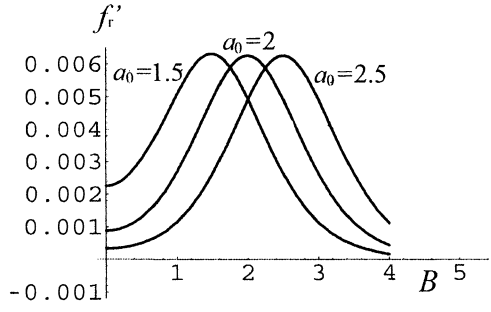

Figure 11 17: Replayed signal amplitude versus bias amplitude coercivity as parameter a_0 = 1.5, 2, and 2.5

Figures 11.15, 11.16, and 11.17 are analogous to Figures 11.7, 11.11, and 11.10 and have similar characters.

11.3 Saturation Pulse Recording in Magnetic Media

As is often the case the information in the magnetic media is recorded not in the analogue form like the AC and DC recording described in Sections 11.1 and 11.2, but coded in a train of pulses. Although there are cases when the information is carried in the form of modulation for instance in pulse position, phase or pulse length, most cases nowadays fall into the category of digital recording. In all cases of pulse recordings, however, the medium is completely saturated during the pulse duration into one or the other direction. This is the so-called nonreturn-to-zero recording or NRZ for short. The problems associated with this kind of recording are quite distinct from that of the nonsaturating recording. There is no need, for instance, to erase previously recorded information from the tape prior to recording. Saturation recording will wipe out any recordings left in the medium. Normally the medium for digital recording is saturated in one direction for "1" and in the other direction for "0". At replay, following Faraday's law (see (11.5)) the coded information is recovered from the first derivative of the recorded signal. In an ideal case the presence or absence of these pulses would be enough to extract the original information from the recording. The faithful reproduction of the information from the medium is, however, a function of a number of factors, like the design of the recording and the reading head, the properties of the magnetic recording medium, etc. In the following we concentrate on the mathematical description of the process taking place in the medium and will regard all other factors like heads, recording, and replay conditions as ideal. The shape of the replayed signal has a limiting

effect on vital factors like recording density defined as the number of pulses deposited on the tape per unit length.

Under ideal conditions the pulses to be recorded are perfect with infinitely short rise time at the beginning and infinitely fast changeover at the changeover point. In practice, however, it is impossible to achieve pulses of such short rise time, therefore the pulses to be recorded here will have finite rise and changeover periods like practical pulses. Figure 11.18 depicts pulses changing from positive-going to negative-going half, representing a "1" and a "0" on the binary scale.

Let us take a single period of a train of pulses to be recorded that has a duration of $2T$ and its rise time from 0 to maximum value is τ as shown in Figure 11.18. The function f_p formulating the pulse for $2T$ period is shown in (11.14).

$$f_p = \begin{cases} \dfrac{x_m}{\tau} & \text{for} \quad 0 < t < \tau \\ x_m & \text{for} \quad \tau < t < T - \tau \\ -\dfrac{x_m}{\tau}(t - T) & \text{for} \quad T - \tau < t < T + \tau \\ -x_m & \text{for} \quad T + \tau < t < 2T - \tau \\ \dfrac{x_m}{\tau}(t - 2T) & \text{for} \quad 2T - \tau < t < 2T \end{cases} . \tag{11.14}$$

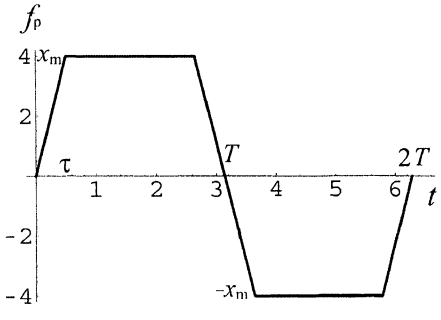

Figure 11.18: The shape of pulse to be recorded on magnetic media

The maximum field excitation is $x_m = 4$ on an arbitrary scale.

The induction produced by the above excitation is

$$f_i = \begin{cases} \tanh\left(\frac{t\,x_m}{\tau} + a_0\right) - b_1 & 0 < t < \tau \\ \tanh\left(x_m + a_0\right) - b_1 & \tau < t < T - \tau \\ \tanh\left[-\frac{(t-T)\,x_m}{\tau} - a_0\right] + b_1 & T - \tau < t < T + \tau \\ \tanh\left(-x_m - a_0\right) + b_1 & T + \tau < t < 2T - \tau \\ \tanh\left[\frac{(t-2T)\,x_m}{\tau} + a_0\right] - b_1 & 2T - \tau < t < 2T \end{cases} \tag{11.15}$$

where b_1 is specified in (3.2).

The waveform of the induction function is plotted in Figure 11.19 for x_m values of 3, 4, 5, 6, and $a_0 = 3$. During calculation the slope of the pulse, i.e. the ratio between τ and x_m was kept constant. The waveform of the pulses recorded in the magnetic medium as remanent magnetism can be calculated by projecting the original input waveform to the recording head onto the loop of remanent magnetism as described (6.6) and (6.8) and depicted in Figure 6.2. The mathematical formulation of the recorded remanent pulse is shown in (11.17) and its waveform is shown in Figure 11.20. The reader has to be warned that in reality the recorded information on the tape is no longer a time function. Due to the motion of the tape it is converted to a function of ξ as before. At replay, however, it reverts again to a time function as we have seen in section 11.2. Leaving these two linear conversions out of the calculations does not affect the final results.

$$f_r = \begin{cases} \tanh\left(-a_0\right) + \tanh\left(\frac{t\,x_m}{\tau} + a_0\right) & \\ \qquad - \tanh\left(\frac{t\,x_m}{\tau} - a_0\right) - b_1 & \text{for} \quad 0 < t < \tau \\ \tanh a_0 - b_1 & \text{for} \quad \tau < t < T - \tau \\ \tanh a_0 + \tanh\left[-\frac{(t-T)\,x_m}{\tau} - a_0\right] & \\ \qquad - \tanh\left[-\frac{(t-T)\,x_m}{\tau} + a_0\right] + b_1 & \text{for} \quad T - \tau < t < T + \tau \\ \tanh\left(-a_0\right) + b_1 & \text{for} \quad T + \tau < t < 2T - \tau \\ \tanh\left(-a_0\right) + \tanh\left[-\frac{(t-2T)\,x_m}{\tau} + a_0\right] & \\ \qquad - \tanh\left[\frac{(t-T)\,x_m}{\tau} - a_0\right] - b_1 & \text{for} \quad 2T - \tau < t < 2T \end{cases} \tag{11.16}$$

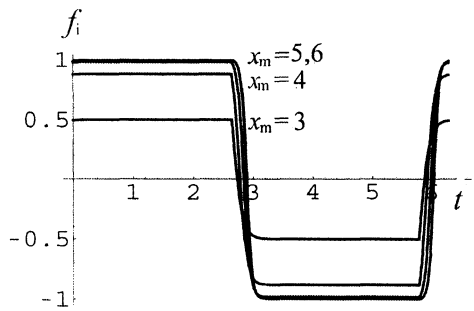

Figure 11.19: The induction waveform of a recorded pulse for $x_m = 3$, 4, 5, and 6

At replay we apply Faraday's law as described in expression (11.5) and in doing so we produce the first derivative by time of f_r the remanent magnetism described in (11.16). This first derivative is shown in (11.17). This expression carries all the information about the recorded input signal and it is proportional to the total replayed information. It contains all the time-dependent elements necessary to recreate the original recorded information.

The remanent waveform of the pulse recorded on the tape is shown in Figure 11.20 with the waveform of the replayed information, i.e. its first derivative.

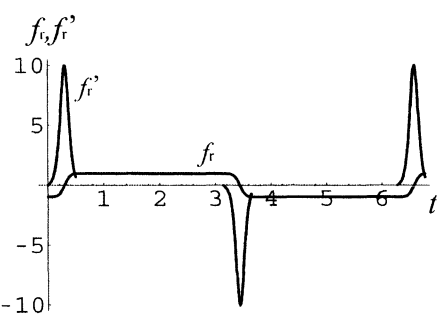

Figure 11.20: The waveform of the pulse remanent in the recording medium and the first derivative representing the replayed signal

References

[1] V. Poulsen, Danish Patent No. 2653 (1899). US Patent No. 789,336 (1905).
[2] W.L. Carlson et al., US Patent 1,640,881 (August 1927).
[3] H. Toomin and D. Wildfeuer, The mechanism of supersonic frequencies as applied to magnetic recording, Proc. Inst. Radio Engs **32**, 664–668 (1944).
[4] L.C. Holmes and D.L. Clark, Supersonic bias for magnetic recording. Electronics, **18**, 126–136 (1945).

[5] W.W. Wetzel, Review of the present status of magnetic recording theory. Audio Eng., Nov. 3, 14–17, Dec. 31, 12–16(1947). Jan. 32, 26–30 (1948).
[6] M. Camras, Graphical analysis of linear magnetic recording using high frequency excitation. Proc. Inst. Radio Engrs. **37**, 569–573 (1949).
[7] L.H. Bedford, Magnetic tape recording, Electronic Radio Engrs., **36, No.9**, 320–322 (1959).
[8] W.K. Westmijze, Studies on magnetic recording. Philips Res. Rep. **8** (1953).
[9] F. Greiner, Das feld im sprechckopf mit und ohne band, Nachrichten Technik, **5**, 295–298 and 351–354 (1955).
[10] P.E. Axon, An investigation into the mechanism of magnetic tape recording. J. Inst. Elect Engrs. **Pt.III**, 99, 106–126 (1952).
[11] J.G. Woodward and E. Della Tore, Magnetic characteristics of recording tapes and the mechanism of the recording process. J. Audio Eng. Soc., **7, No.4**, 189–195 (1959).
[12] C.D. Mee, Applications and limitations of the new magnetic recording model. IRE Trans. Audio, **10, No.6**, 16–163 (1962).
[13] C.D. Mee, *The Physics of Magnetic Recording* (North-Holland Publ. Co., N.Y.,1984).
[14] D.F. Eldridge and E.D. Daniel, New approach to AC biased magnetic recording. IRE Natl. Conv. Record, **Pt.7**, 33–41 (1962).
[15] J.R. Herbert and D.W. Patterson, A computer simulation of the magnetic recording process. IEEE Trans. Magn.**1, No. 4**, 352–357 (1965).
[16] H.N. Bertham, Long wavelength AC bias recording theory. IEEE Trans. Magn. **Mag-10, No. 4**, 1039–1048 (1974).
[17] L.G. Sebestyén and J. Takács, Magnetic recording; Theory of tape magnetisation. Electronic Technology Aug. 274–278 (1961).
[18] D.E. Speliotis, On remanence loops and recording performance. J. Appl. Phys. **67, No. 9**, 5358–5360 (1990).
[19] A.L. Priberio, AC bias recording and Preisach diagrams. J. Appl. Phys. **67, No. 9**, 5382–5384 (1990).
[20] C.D. Mee and E D. Daniel, *Magnetic Recording* (McGraw-Hill Co. N.Y. 1988).
[21] C.B. Pea, *Magnetic Recording in Science and Industry* (Reinhold Publ. Co, 1967).
[22] C.D. Mee, *The Physics of Magnetic Recording* (North Holland Publ. Co., N.Y., 1986).
[23] C.E. Lowman, *Magnetic Recording* (McGraw-Hill Book Co., N.Y., 1972).

12. Other Hysteretic Phenomena

12.1 Magnetic Viscosity or Creep

So far all the magnetic phenomena described here were regarded as independent of the rate of change. This does not mean that all phenomena associated with magnetism are independent of time. Some of the effects will not stop with the removal of the exciting field and the magnetic state of the material will continue to change some time after the excitation has ceased. Others will not have an instantaneous effect on the material and the new equilibrium state is only reached after a certain delay. These time-dependent phenomena have been categorized in the literature as aftereffects [1,2]. There are a number of aftereffects recognized and observed experimentally, however, not all of them are fully explained to date by using physical principles. Some are irreversible, like aging but unlike those above, aging does not fall into the category of aftereffects that are restricted to those that permit the return to the original state by magnetic means. People have studied a number of aftereffects [3–5]. One of these we are going to consider here is the phenomenon called "viscosity" in the literature [6–10]. Ewing [11] observed as long ago as 1885 that when a magnetic excitation was applied to a magnetic specimen, often a long time is needed for the magnetic state to reach its final value. The duration of the change observed was longer than it was expected from known causes like eddy current and in many cases the eddy current explanation for the lag was not applicable anyway. Jordan [12] suggested in 1924 that this form of lag is due to something analogous to viscosity and often referred to as Jordan lag. An analogous lag was also observed during elastic mechanical deformation [13]. Ever since Ewing's observation this phenomenon has been an object of investigation [14].

Let us consider the case when in the excitation field an instant step is applied to the material. The experimental observations show that the magnetic state or magnetization of the specimen will change in two stages. There will be an instant μH_1 change at the time when the step function steps in and that will be followed by a gradual change that eventually will reach an H_2 value added to the first step. In a simple case this second stage can be described by an exponential function in time, so the whole magnetization process can be described mathematically by expression (12.1) below,

$$M = \mu\left[H_1 + H_2\left(1 - \exp\frac{t}{\tau}\right)\right] \tag{12.1}$$

where M is the magnetization, μ is the permeability and τ is the time constant of the change. By denoting the ratio of $H_2/H_1 = \beta$ (12.1) can be rewritten in the following form

Mathematics of Hysteretic Phenomena. Jeno Takács

ISBN: 3-527-40401-5

$$M = \mu H_1 \left[1 + \beta \left(1 - \exp \frac{t}{\tau} \right) \right]. \tag{12.2}$$

This equation is well known in electronics as the step response of an equivalent electrical circuit, made up from a resistor R_1 and a lossy capacitor C in series, with a parallel loss resistance of R_2 as shown in Figure 12.1. Its impedance Z is given in (12.3)

$$Z = R_1 \left(1 + \frac{\beta}{\tau} \frac{1}{\frac{1}{\tau} + p} \right) \tag{12.3}$$

where $\beta = R_2/R_1$ and $\tau = R_2C$ is the time constant of the circuit.

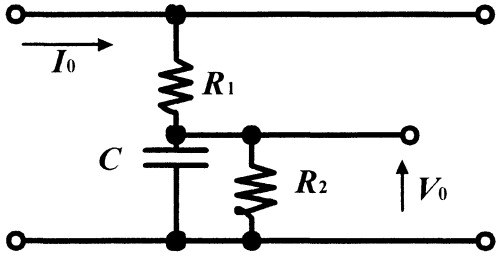

Figure 12.1: Equivalent electrical circuit to explain the time dependency in (12.2)

Magnetic materials are often subjected to AC magnetization therefore it is appropriate to investigate this delay effect when harmonic excitation is applied. Let us assume sinusoidal current excitation stepping in at $t = 0$ in the form of $i(t) = I_0 \sin \omega t$ and use Laplace transformation to solve the problem. The Laplace transform of a sinusoidally changing time function of ω frequency is shown in (12.5),

$$\mathcal{L}\, I_0[\sin \omega t] = I_0 \frac{\omega}{\omega^2 + s^2}. \tag{12.5}$$

After using (12.4) and (12.5), $V_0(s)$ the transformed voltage developing across the output terminals due to the sinusoidal current of I_0 amplitude, as shown in Figure 12.1, can be calculated in the following form

$$V_0 = I_0 \omega R_1 \left[\frac{1}{\omega^2 + s^2} + \frac{\beta}{\tau} \frac{1}{(s + \frac{1}{\tau})(\omega^2 + s^2)} \right]. \tag{12.6}$$

After the transformation of (12.6) from the Laplace to the time domain the time response of the system to a sinusoidal input will be as follows

$$\mathcal{L}^{-1}[V_0(s)] = v_0(t) = R_1 I_0\{\sin\ \omega t + \frac{\beta\omega\tau}{1+\omega^2\tau^2}[\exp(-\frac{t}{\tau})$$

$$-\cos\ \omega t + \frac{1}{\omega\tau}\sin\ \omega t]\}\,. \tag{12.7}$$

The exponential term represents the transient due to the fact that the harmonic function steps in at $t = 0$ and the function is zero for $t < 0$. The application of the above calculation to (12.2), after having neglected the transient term, will give us the time response of the magnetic specimen for AC excitation. It shows that its response is the same as to the response of a harmonic field excitation shown in (12.8),

$$\frac{M}{\mu} = H_0(t) = H_1\{\sin\ \omega t + \frac{\beta\omega\tau}{1+\omega^2\tau^2}[-\cos\ \omega t + \frac{1}{\omega\tau}\sin\ \omega t]\} \tag{12.8}$$

For convenience we used the same symbol β for the resistor and the field ratio, the same symbol τ was used also for the electrical and magnetic time constant.

It is customary to define the loss angle δ as the ratio between the amplitude of the out-of-phase and the in-phase components which, by using (12.8) leads us to the expression of

$$\tan\ \delta = \frac{-\beta\omega\tau}{(1+\beta)+\omega^2\tau^2} \tag{12.9}$$

$\tan\ \delta$ is often referred to as the loss factor [8].

So far we have neglected the saturation effect and the hysteresis when AC excitation is applied to the magnetic substance. In order to determine the hysteretic time behavior of the magnetic substance the above results has to be applied to the mathematical expressions describing the phenomena of saturation and hysteresis as described in Chapter 3. By substituting expression (12.8) for x, the normalized excitation field, into (3.3), replacing H_1 by the amplitude x_m and neglecting the transient term, we arrive at the expressions describing both the time-dependent aftereffect and the hysteretic phenomenon in the following form

$$f_+ = \tanh\ \{x_m[\sin\ \omega t + \frac{\beta\omega\tau}{1+\omega^2\tau^2}(-\cos\ \omega t + \frac{1}{\omega\tau}\sin\ \omega t)] - a_0\} + b_1$$

for increasing t values (12.10a)

$$f_- = \tanh\ \{x_m[\sin\ \omega t + \frac{\beta\omega\tau}{1+\omega^2\tau^2}(-\cos\ \omega t + \frac{1}{\omega\tau}\sin\ \omega t)] + a_0\} - b_1$$

for decreasing t values, (12.10b)

where b_1 as per definition

$$b_1 = \{\tanh\ [x_m(1+\frac{\beta}{1+\omega^2\tau^2}) + a_0] - \tanh\ [x_m(1+\frac{\beta}{1+\omega^2\tau^2}) - a_0]\}/2\,. \tag{12.11}$$

The effect of this magnetic viscosity on the hysteresis loop has also been observed [15]. The shape of the measured hysteresis loop depends on the speed of taking the measurement and when harmonic excitation is being used the hysteresis loop measured becomes dependent on the frequency used. In order to show the effect on the hysteresis loop let us substitute $y = \sin\ \omega t$ in (12.10) and then by using the trigonometric identity of $\cos\ \omega t = \sqrt{1-\sin^2 \omega t}$ the expressions of f_+ and f_- can be transformed into the following form

$$f_+ = \tanh\ [x_m \frac{1+\omega^2\tau^2+\beta}{1+\omega^2\tau^2} y - (a_0 + x_m \frac{\beta\omega\tau}{1+\omega^2\tau^2}\sqrt{1-y^2}\}] + b_1 \qquad \text{for increasing } y \tag{12.12a}$$

$$f_- = \tanh\ [x_m \frac{1+\omega^2\tau^2+\beta}{1+\omega^2\tau^2} y + (a_0 - x_m \frac{\beta\omega\tau}{1+\omega^2\tau^2}\sqrt{1-y^2}\}] - b_1 \qquad \text{for decreasing } y, \tag{12.12b}$$

while t is running between $\pi/2$ and $3\pi/2y$ will change from -1 to 1, and the excitation between x_m to $-x_m$, therefore the rate dependence can be investigated by plotting f_+ and f as a function of y.

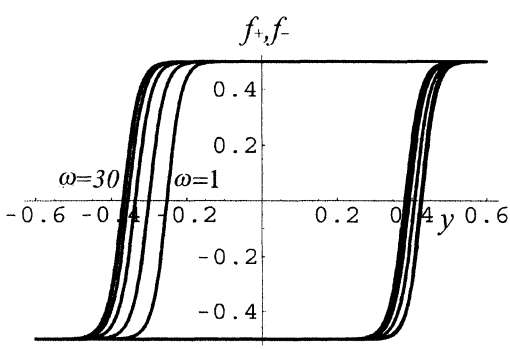

Figure 12.2: Hysteresis loops showing the dependency on the cycling frequency for the normalized frequency values of ω = 1, 2.5, 5, 10, 20, and 30

A set of hysteresis loops calculated from (12.13) are depicted in Figure 12.2 showing the general effect of the rate of change in the field excitation on the induction. The presence of the "viscosity" shifts the hysteresis loop towards the first quadrant as the cycling frequency, or as sweep rate increases. This effect, however, is more pronounced on the descending part

of the loop, as can be seen on the loops in Figure 12.3. The experimental results are presented here with the permission of O'Grady et al. [15].

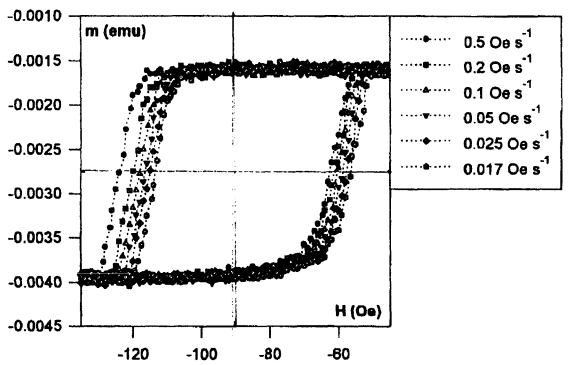

Figure 12.3: Experimental results showing the effect of the change of rate in the sweeping excitation field on the hysteresis loop (courtesy of O'Grady et al.)

For the calculations the following normalized parameters were used: $x_m = 4$, $a_0 = 1.5$, $\tau = 1$, $\beta = 0.2$, $C_0 = 6$, and $\omega = 1$, 2.5, 5, 10, 20, and 30. This effect and the behavior of the loop against the rate of change has been verified experimentally as shown in Figure 12.3.

12.2 Hysteresis Loop of Coupled Systems

Although the hysteresis manifests itself most of the time in a sigmoid shape there are instances when the shape differs from the "classical" character. One of the differing shapes has been reported by Williams and Goertz in 1952 and Taniguchi in 1956 [16,17]. The alloy of Fe-Co-Ni called Pernivar showed a wasp-waisted hysteresis loop. Since then this shape has been referred to in the literature as "wasp-waisted" or "Pernivar-like" hysteresis loops for obvious reasons. This is not the only alloy that shows this deviation from the normal hysteresis but other alloys have also been found showing similar character. These constricted loops, as recently has been found, also occur when a soft ferromagnetic layer is coupled to an antiferromagnet [18]. The same constricted hysteresis loop can also occur when Permalloy is baked at 425° C for 24 h [19]. While alloys have symmetrical wasp-waisted hysteresis loops the coupled layers can display displacement of the loop along the field axis. First this phenomenon was regarded as a scientific curiosity [20] but later, in a different form, it was used in the fast-developing thin-film and multilayer technology. It seems that the modeling and the characterization of the phenomenon with practical parameters is forming a vital part of the multilayer research. The physical explanation behind this phenomenon can and certainly does differ, from case to case, and there is no intention here to go into the various explanations and theories of this effect. For this, the reader is referred to the literature [19,21].

In all this seemingly different characters created by this effect, there is one common factor, that is the effect of the hysteresis. This book is devoted to the various hysteresis loops and the geometrical descriptions of hysteretic phenomena. In the following a mathematical model, based on the T(x) function, will be given with parameters controlling the shape of the loop that can be linked to the physical parameters of the multilayer devices. This in turn will facilitate the control the character of the device at will.

Let us assume that we start with two magnetic substances, one ferromagnetic and the other antiferromagnetic. For simplicity we make them differ only in their coercive force and by recalling (3.2) and (3.3) we can characterize them in normalized form as shown in (12.13), (12.14), (12.15), and (12.16).

The first ferromagnetic substance characteristic equations are

$$f_{1+} = \tanh\ [x-(1+d)\ a_0]+b_1 \qquad \text{for increasing } x \tag{12.13a}$$

$$f_{1+} = \tanh\ [x+(1+d)\ a_0]-b_1 \qquad \text{for decreasing } x \tag{12.13b}$$

$$A_0 x - b_3$$

where

$$b_{11} = \{\tanh\ [x_m+(1+d)\ a_0]-\tanh\ [x_m-(1+d)\ a_0]\}/2 \tag{12.14}$$

The antiferrromagnetic character of the second substance can be formulated in the following mathematical expressions

$$f_{2+} = \tanh\ [x+(1-d)\ a_0]-b_1 \qquad \text{for increasing } x \tag{12.15.a}$$

$$f_{2+} = \tanh\ [x-(1-d)\ a_0]+b_1 \qquad \text{for decreasing } x \tag{12.15b}$$

and

$$b_{21} = \{\tanh\ [x_m+(1-d)\ a_0]-\tanh\ [x_m-(1-d)\ a_0]\}/2\,. \tag{12.16}$$

Here d is a dummy variable and for d = 0 (12.15) and (12.16) convert to (3.3) and (3.4), respectively. The constants b_{11} and b_{21} follow the definition in Chapter 3.

Let us assume that the ensemble is a simple linear combination of the two magnetic substances and the interaction in between them can be mathematically described as the summation of the two characteristic equations as shown in (12.17) where f_w represents a cross-coupled wasp-waisted characteristic function.

$$f_{w+} = \{\tanh\ [x-(1+d)\ a_0]+\tanh\ [x+(1-d)\ a_0]\}/2+b_3 \tag{12.17a}$$

$$f_{w-} = \{\tanh\ [x+(1+d)\ a_0]+\tanh\ [x-(1-d)\ a_0]\}/2+b_3 \tag{12.17b}$$

where

$$b_3 = \{\tanh\ [x_m - (1+d)\ a_0] + \tanh\ [x_m + (1-d)\ a_0]\}/4$$

$$+ \{\tanh\ [x_m + (1+d)\ a_0] + \tanh\ [x_m - (1-d)\ a_0]\}/4\,. \qquad (12.18)$$

Here, as before, the + and – subscripts signify the ascending and the descending legs of the hysteresis loop, respectively.

The function f_w is plotted for the parameter values of $x_m = 5$, $a_0 = 2$, and $d = 0.1$, 0.5, and 0.75 in Figure 12.4 showing a wasp-waisted character calculated from (12.17) and (12.18) in the simplest case under the control of a single parameter.

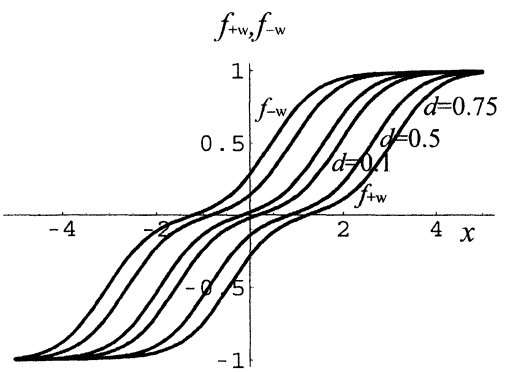

Figure 12.4: Typical wasp-waisted hysteresis loops for the normalized values of $d = 0.1$, 0.5, and 0.75

For more complicated ensembles the number of free parameters can be increased to cover various shapes of hysteresis curves. By extending the variability to all parameters we come to the following characteristic equations in canonical form.

$$f_{w+} = \{\tanh\ [\alpha x - \gamma - (1+d)\ a_0] + \tanh\ [\alpha x - \gamma + (1-d)\ a_0]\}/2 + b_3 \qquad (12.19a)$$

$$f_{w-} = \{\tanh\ [\alpha x + \gamma + (1+d)\ a_0] + \tanh\ [\alpha x + \gamma - (1-d)\ a_0]\}/2 - b_3 \qquad (12.19b)$$

$$b_3 = \{\tanh\ [\alpha x_m + \gamma + (1+d)\ a_0] + \tanh\ [\alpha x_m + \gamma - (1-d)\ a_0]\}/4$$

$$- \{\tanh\ [\alpha x_m - \gamma - (1+d)\ a_0] + \tanh\ [\alpha x_m - \gamma + (1-d)\ a_0]\}/4 \qquad (12.20)$$

The number of free parameters has been increased from one, from the simplest case, to four. These free parameters are not to be mistaken for the free parameters of the hysteresis loop discussed in Chapter 3. To demonstrate the effects of the newly introduced parameters on the character of the hysteresis loop a few hysteresis loops of various shapes are plotted in Figures 12.5, 12.6, and 12.7 using α, β, and γ as parameters, respectively.

So far all wasp-waisted hysteresis loops analyzed here had point symmetry. In other words a 180° rotation of the positive part of the loop in the first quadrant will take it to the negative part of the loop in the third quadrants shown in Figures 12.4, 12.5, and 12.6. Experience shows, however, that this kind of symmetry is not a prerequisite for a wasp-waisted character although "Perminvar-like" alloys tend to follow this rule.

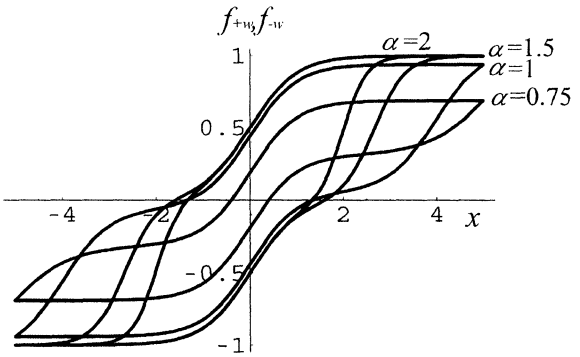

Figure 12.5: Wasp-waisted hysteresis loops with α as parameter for $\alpha = 0.75$, 1, 1.5, and 2

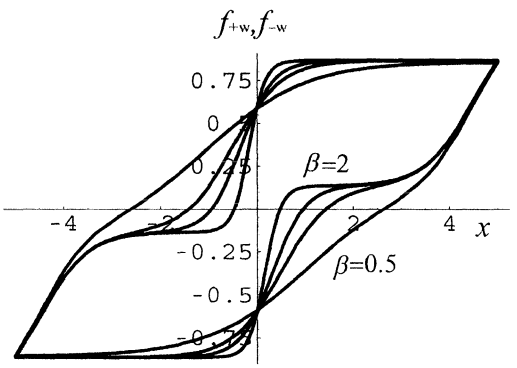

Figure 12.6: Wasp-waisted hysteresis loops with β as parameter for the normalized values of $\beta = 0.5$, 1, 1.5, and 2

In a thin-film ensemble when a soft ferromagnetic layer is coupled to an antiferromagnet the magnetization process will not follow the same process, therefore the character of the magnetization loop will be different. These materials are of critical importance as they form the basis of the spin-valve sensors and in their development the characterization of the material parameters and their effects play vital roles. In order to break away from symmetry and introduce more freedom we have to introduce more independent parameters by separating the characteristic hysteresis loops of the two layers by splitting the existing parameters. By splitting up α, β, d, b, and c to α_1, α_2, β_1, β_2, d_1, d_2, b_1, b_2, and c_1, c_2 with the maximum number of free parameters we can write the generalized characteristic equations in the following form.

$$f_{w+} = \{B_1 \tanh\ [\alpha_1 x - c_1 - (1+d_1)\ a_0]$$

$$+ B_2 \tanh\ [\beta_1 x - c_2 + (1-d_2)\ a_0]\}/2 + b_3 \qquad (12.21a)$$

$$f_{w-} = \{B_1 \tanh\ [\alpha_1 x - c_1 - (1+d_1)\ a_0]$$

$$+ B_2 \tanh\ [\beta_1 x + c_2 - (1-d_2)\ a_0]\}/2 - b_3 \qquad (12.21b)$$

$$b_3 = \{B_1 \tanh\ [\alpha_2 x_m + c_1 + (1+d_1)\ a_0]$$

$$+ B_2 \tanh\ [\beta_1 x_m + c_2 - (1-d_2)\ a_0]\}/4 - \{B_1 \tanh\ [\alpha_1 x_m - c_1 - (1+d_1)\ a_0]$$

$$+ B_2 \tanh\ [\beta_1 x_m - c_2 + (1-d_2)\ a_0]\}/4 . \qquad (12.22)$$

Figure 12.7 depicts a hysteresis loop for a typical spin-valve structure [15] calculated from (12.21) and (12.22) for the normalized parameter values tabulated below:

$x_m = 5$, $d_1 = 0.8$, $c_1 = 2$, $\alpha_1 = 15$, $\beta_1 = 2.5$, $B_1 = 1$

$a_0 = 2$, $d_2 = 0.2$, $c_2 = -1$, $\alpha_2 = 2.5$, $\beta_2 = 15$, $B_2 = 1$.

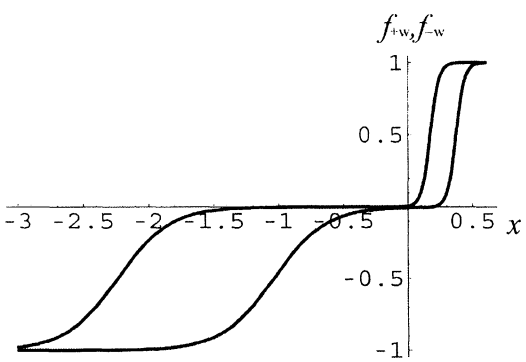

Figure 12.7: Hysteresis loop of a spin-valve structure

With the number of free parameters in hand a large variety of shapes can be produced to describe even exotic hysteresis loops. In other field of sciences hysteretic loops will not copy necessarily the sigmoid shape well known in magnetism. The freedom, however, given by these formulae will enable people to describe hysteresis loops manifesting themselves in shapes other than the sigmoid.

The model formulated here is also applicable to the case when the reversible magnetization is not negligible and A_0 has a finite value. The characteristic equations shown

in (12.23) can be derived from (12.19) and (12.20) by adding the linear term A_0x representing the reversible magnetization to it.

$$f_{w+} = \{\tanh\ [\alpha x - \gamma - (1+d)\ a_0] + \tanh\ [\alpha x - \gamma + (1-d)\ a_0]\}/2$$

$$+ A_0 x + b_3 \tag{12.23a}$$

$$f_{w-} = \{\tanh\ [\alpha x + \gamma + (1+d)\ a_0] + \tanh\ [\alpha x + \gamma - (1-d)\ a_0]\}/2$$

$$+ A_0 x - b_3 \tag{12.23b}$$

The constant b_3 is defined in (12.29).

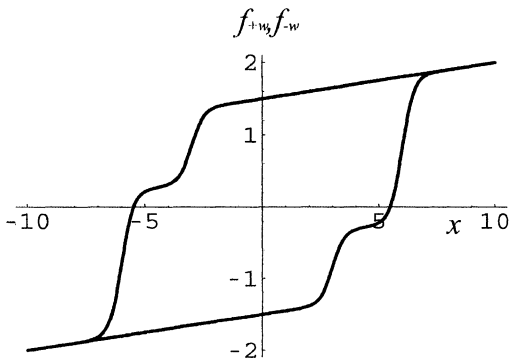

Figure 12.8: Wasp-waisted hysteresis loops with reversible magnetization.

A typical hysteresis loop representing a melt-spun specimen of $Sm_{20}Fe_{70}Ti_{10}$ after heat treatment [22] is depicted in Figure 12.8 calculated from (12.23) for the following numerical parameter values: $x_m = 10$, $a_0 = 3$, $\beta = 2$, $d = 0.3$, $A_0 = 0.05$, $\gamma = 1$, $\alpha = 1$.

References

[1] J.L Snoek, Time effects in magnetization. Physica **5**, 663–688 (1938).
[2] A. Aharoni, *Introduction to the Theory of Ferromagnetism* (Clarendon Press, Oxford, 1996).
[3] C. Korman and I.D. Mayergoyz, Preisach model driven by stochastic inputs as a model for aftereffects. IEEE Trans. Magn. **MAG-32**, 4204–4209 (1996).
[4] G. Bottoni, D. Candolfo and A. Cecchetti, Interaction effects of the time dependence of the magnetization in recording particles. J. Appl. Phys. **81**, 3809–3811 (1997).
[5] E. Della Torre and H. Bennett, A Preisach model for aftereffect. IEEE Trans. Magn. **MAG-34**, 1276–1278 (1998).
[6] R. Street and J.C. Woolley, A study of magnetic viscosity. Proc. Phys. Soc. A **62**, 562–572 (1949).
[7] E.P. Wohlfarth, The coefficient of magnetic viscosity. J. Phys. F: Met. Phys. **14, I**, 155–159 (1984).

[8] S. Chikazumi *Physics of Magnetism* (Robert Kriegler, Malabar, Florida, 1986)
[9] D.V. Berkov, On the concept of the magnetic viscosity, analytic expression for the time dependent magnetization. J. M. M. M. **111**. 327–329 (1992).
[10] A. Aharoni, Susceptibility, resonance and magnetic viscosity. Phys Rev. B. **46**, 5434–5441 (1992).
[11] J.A. Ewing, Time lag in the magnetization of iron. Proc. Roy. Soc. **46**, 260–286 (1889).
[12] H. Jordan, Ferromagnetic constants for weak fields. Elek. Nachr. Tech. **1**, 7–29 (1924).
[13] C. Zener, Anelasticity in metals. Trans. Am. Soc. Mining. Met. Eng. **167**, 155–189 (1946).
[14] E.W. Singleton and G.C. Handjipanayis, Magnetic viscosity studies in hard magnetic materials. J. Appl. Phys. **67, No. 9**, 4759–4761 (1990).
[15] A.M. Goodman, K. O'Grady, H. Laidler, N.W. Owen, X. Portier, A.K Petford-Long and F. Cebollada, Magnetization reversal process in exchange-biassed spin– valve structures. IEEE Trans. Magn. **37, No. 1**, 565–570 (2001).
[16] H.J. Williams and M. Goertz, Domain Structure of Perminvar having a rectangular hysteresis loop. J. Appl. Phys. **23, No.3**, 316–323. (1952).
[17] S. Taniguchi, Sci. Rept. Res. Inst. Tokohu Univ. **A8**, 173 (1956).
[18] D. Paceard, C. Schlenker, O. Massenet, R. Montmory and A. Yelon, A new property of ferromagnetic–antiferromagnetic coupling. Phys. Stat. Sol. **16**, 301 (1966).
[19] R.M. Bozorth, *Ferromagnetism* (Van Nostrand, Princeton, N.Y., US, 1951).
[20] G.W. Elmen, Magnetic properties of perminvar. J. Franklin Inst. **206**, 317–338 (1928).
[21] A.H. Morrish, *The Physical Principles of Magnetism* (Wiley, N.Y., US, 1965).
[22] J. Wecker, M. Katter, K. Schnitzke and L. Schultz, Magnetic hardening of Sm–Fe–Ti alloys. J. Appl. Phys. **67, No. 9**, 4951–4953 (1990).

13. Unidirectional Hysteretic Effects

13.1 Magnetostriction and Magnetoresistance

Experience shows that the magnetization of a ferromagnetic material specimen in all cases is accompanied by dimensional changes. The dimension increases in the direction of magnetization and contracts at right angles to it. The existence of this effect, called magnetostriction, was first discovered and reported by Joule in 1842 [1,2]. When the material cools and passes through the Curie point it becomes ferromagnetic and goes through a realigning process called the spontaneous magnetostriction. The randomly aligned magnetic moments at this temperature go through a process of alignment and form large clusters or domains. Whilst the moments form an order inside the domains the material still retains its magnetically neutral state. It is called the "ordered but unaligned" state. When a magnetic field is applied, the domains become ordered and aligned and turn parallel to the field causing dimensional changes and stress in the magnetic material. The field-induced magnetostriction arises when the magnetic domains are reoriented and lined up under the influence of the applied magnetic field by rotating into the direction of the field. This rotation is opposed by the binder holding the material together. This dimensional change or magnetostriction is defined as the fractional change in the length of the specimen and symbolised as $\lambda = \Delta l/l$, where λ is the fractional change, l is the length of the specimen and Δl is the change in length. The effect at right angles to the magnetic field is called the transverse magnetostriction. This particular hysteretic process is not direction sensitive and is only affected by the magnitude of the applied field. It is often called strain hysteresis in the literature. In an isotropic material the expected changes in the dimension of the specimen are the same as in a magnetic field whose vector points to the right or to the left. The material reaches its maximum or saturation magnetostriction state when all domains turned parallel to the magnetic field vector. Magnetostrictive materials exhibit hysteresis both for magnetization and for stress as functions of the applied magnetic field [3,4]. Similarly to magnetization we can distinguish between reversible and irreversible magnetostriction. A typical magnetostrictive material investigated in the recent past is Terfenol-D [5–7], its stress versus magnetic field character is similar to that depicted in Figure 13.1. For further explanation on the subject of magnetostriction the reader may go to the literature [8].

Magnetostriction is not the only hysteretic phenomena that manifests itself in this manner. The electrical resistivity of magnetic materials also changes when subjected to a magnetic field (MR). Normally there is an increase in the resistivity when the electric current is parallel or antiparallel to the field vector and a decrease when the current and the field are orthogonal [9]. This phenomenon forms an important part in the magnetic multilayer technology directed towards sensor developments.

Mathematics of Hysteretic Phenomena. Jeno Takács

ISBN: 3-527-40401-5

Let us recall the general characteristic equations of the hysteresis loop from Chapter 3 and make them independent of the field direction by taking the absolute value of the magnetization. After taking the absolute value of f_+ and f_- in (3.3) we arrive at a new set of characteristic expressions shown in (13.1) formulating a new type of hysteresis loop,

$$|f_+| = |\tanh\ (x - a_0) + b_1| \tag{13.1a}$$

$$|f_-| = |\tanh\ (x + a_0) - b_1| \tag{13.1b}$$

and

$$b_1 = |\tanh\ (x + a_0) - \tanh\ (x - a_0)|/2\,. \tag{13.2}$$

Figure 13.1 depicts a typical magnetostrictive hysteresis loop plotted by using (13.1) and (13.2) for the values of $a_0 = 0.1$ and $x_m = 3$.

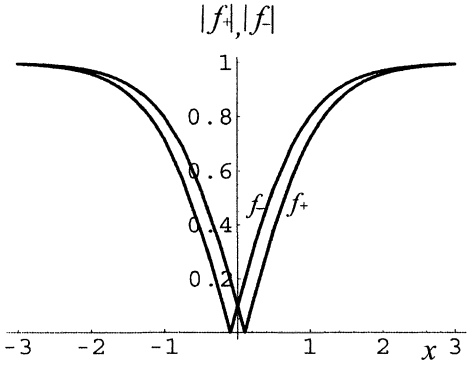

Figure 13.1: Typical magnetostrictive hysteresis loop

Here, the change in physical dimension in the case of magnetostriction and the change in electrical resistance are plotted against magnetic field. As shown in Figure 13.1 this type of hysteresis shows properties different from the "normal" magnetic hysteresis loop in two ways. One is that the strain is always positive (unidirectional) and symmetrical to the vertical axis. The other is that the transition curves in this hysteresis group, unlike in a magnetic hysteresis loop are not necessarily enclosed by the major hysteresis loop (see Chapter 5).

In Figure 13.2 a plot is shown of the magnetostriction as a function of magnetic field under compressive mechanical stress in Terfenol-D. The model also includes the effect of the irreversible magnetostriction as shown in the plot. Plot a depicts the high-stress shape of the $\lambda(H)$ function and plot b shows the zero-stress case [10,11].

Figure 13.3 depicts a typical magnetoresistive hysteresis loop showed by Au/Co ultrathin multilayers at antiparallel magnetization.

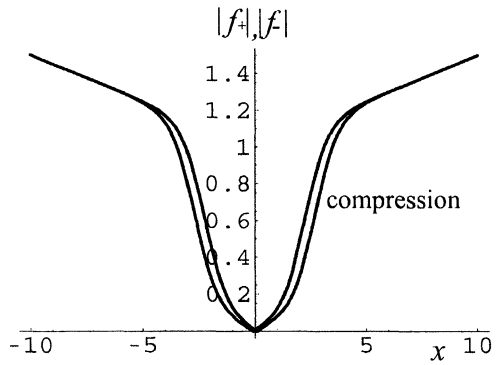

a

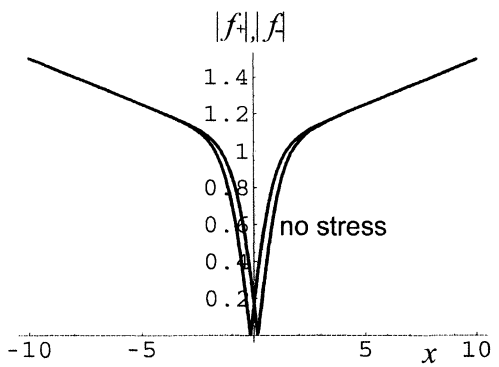

b

Figure 13.2: Calculated magnetostriction versus magnetic field curves for Terfenol-D (a) under mechanical compressive stress; (b) no mechanical stress.

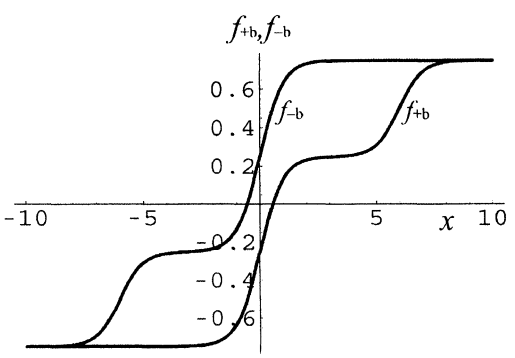

Figure 13.3: Typical magnetoresistive hysteresis loop of ultra thin multilayers of Au/Co at antiparallel magnetization in normalized units

13.2 Butterfly Hysteresis Loops

All these magnetic effects have something in common and that is the hysteretic nature of the process. These hysteretic processes combined with their insensitivity to the field direction form a sub group in the family of hysteretic processes with their own character of hysteresis, different from the "normal" hysteresis loop. This loop, because of its shape, is called the "butterfly" hysteresis loop. As we have seen in the previous section, taking the absolute value of the function of the magnetization led us to the mathematical formulation of the simple magnetostriction. This will take us a step closer to developing the general formulation of the "butterfly" hysteresis loop.

Butterfly hysteresis loops do not necessary fall into the subgroup of the hysteretic phenomena described by (13.1) and look like that shown in Figure 13.1. Shapes reported in the literature vary from a round-bottomed part above the zero line to sharp-pointed bottom parts and narrow "wings", etc. Since all the variants are possible in practice it appears that there is a need for a general model, incorporating not all but at least most of the possible shapes. The way to reach this solution is to apply Axiom 5, which says that through two fixed points only two lines can be drawn inside a major hysteresis loop. It is known that the $|f_+|$ and $|f_-|$ functions must go through the points marked by the (x_m, f_{+m}) and $(-x_m, f_{+m})$ coordinates where

$$f_{+m} = \tanh\,(x_m - a_0) + b_1 \tag{13.3a}$$

$$f_{-m} = \tanh\,(x_m + a_0) - b_1\,. \tag{13.3b}$$

By applying the tangent hyperbolic rule the equations for the two lines between the two points above can be written in the following form.

$$f_{+b} = |f_+|\frac{\tanh\,(-x_m - a_0) - \tanh\,(x - a_0)}{\tanh\,(-x_m - a_0) - \tanh\,(x_m - a_0)}$$

$$+|f_-|\frac{\tanh\,(x_m - a_0) - \tanh\,(x - a_0)}{\tanh\,(x_m - a_0) - \tanh\,(-x_m - a_0)} \quad \text{for the ascending part} \tag{13.4a}$$

$$f_{-b} = |f_+|\frac{\tanh\,(-x_m + a_0) - \tanh\,(x + a_0)}{\tanh\,(-x_m + a_0) - \tanh\,(x_m + a_0)}$$

$$+|f_-|\frac{\tanh\,(x_m + a_0) - \tanh\,(x + a_0)}{\tanh\,(x_m + a_0) - \tanh\,(-x_m + a_0)} \quad \text{for the descending part.} \tag{13.4b}$$

The two functions f_{+b} and f_{-b} are plotted in Figure 13.2 showing the characteristic behavior of magnetostrictive material with (a) and without mechanical stress (b) for the normalised

values of $a_0 = 0.1$ and $x_m = 3$. Figure 13.3 depicts a typical magnetostrictive hysteresis loop of ultra thin multilayers of Au/Co at antiparallel magnetization.

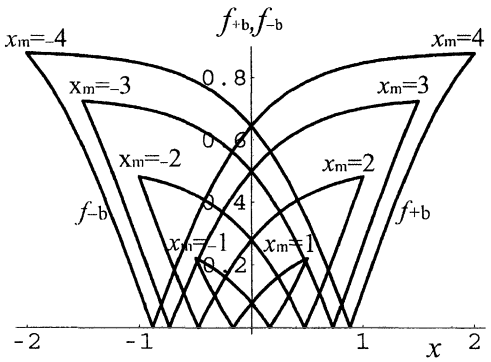

Figure 13.4: Butterfly hysteresis loops for the normalized x_m values of 1, 2, 3 and 4.

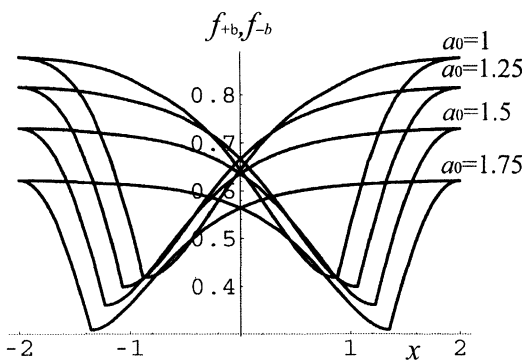

Figure 13.5: Butterfly hysteresis loop dependence on coercivity in normalized units of $a_0 = 1$, 1.25, 1.5 and 1.75, $x_m = 2$.

As we can see (13.4) gives the characteristic butterfly hysteresis of a general mathematical formulation in a normalized form. In order to make a fit to a specific case one has to use the available parameters such as the coercivity a_0 and the maximum magnetization value x_m. In Figure 13.4 the depicted loops show the dependence of the shapes on the value of maximum magnetization for $x_m = 1$, 2, 3 and 4 at $a_0 = 1$. The loops shown in Figure 13.5 show the same dependence on the value of the coercivity a_0 for the normalized values of 1, 1.25, 1.5 and 1.75 when the maximum magnetization is kept constant at $x_m = 2$.

A similar hysteresis loop has been detected in the microwave absorption in superconductive powders [12].

References

[1] J.P. Joule, On a new class of magnetic forces. Ann. Electr. Magn. Chem. **8**, 219–224 (1842).
[2] J.P. Joule, On the effects of magnetism upon the dimensions of iron and steel bars. Phil. Mag. **XXX**, 76–87, 225–241 (1847).
[3] J.L. Snoek, A mechanical counterpart to the Rayleigh law of ferromagnetic hysteresis. Physica **8**, 745–747 (1941).
[4] J.L. Snoek, Effect of small quantities of C and N on elastic and plastic properties of Fe. Physica **8**, 711–733 (1941).
[5] M.B. Moffet, A.E. Clarke, M. Wun-Vodle, J. Linberg, J.P. Teter and E.A. McLaughlin, Characterization of Terfenol-D for magnetostriction transducers. J. Acoust. Soc. Am. **89(3)**, 1448–1455 (1991).
[6] F.T. Calkins and A.B. Flatau, Transducer based measurements of Terfenol–D material properties. SPIE Proc: Smart Structures and Integrated Systems. **2717**, 709–719 (1996).
[7] J.B. Restorff, H.P. Savage, A.E. Clarkand, M. Wun-Fogle, Preisach modeling of hysteresis in Terfenol. J. Appl. Phys. **67(9)**, 501–518 (1990).
[8] S. Chikazumi, *Physics of Ferromagnetism* (Clarendon, Oxford, 1997)
[9] C. Dupas, P. Beauvillain, C. Chapert, J.P. Renard, F. Trigui, P. Veillet and E. Velu, Very large magnetoresistance effect induced by antiparallel magnetization in two ultrathin cobalt films. J. Appl Phys. **67, No. 9**, 5680–5682 (1990).
[10] D.C. Jiles and S. Hariharan, Interpretation of the magnetization mechanism in Terfenol–D using Barkhausen pulse height analysis and irreversible magnetostriction. J. Appl. Phys. **67, No. 9**, 5013–5015 (1990).
[11] J.B. Restorff, H.T. Savage, A.E. Clark and M. Wun-Fogle, Preisach modeling of hysteresis in Terfenol. J. Appl. Phys. **67, No. 9**, 5016–5018 (1990).
[12] A. Gould, S.M. Bhagat, M.A. Manheimer and S. Tyagi, Field-induced microwave absorption in high-T_c superconductive powders: evidence for a superconducting glass phase at low T. J. Appl. Phys. **67, No. 9**, 5020–5025 (1990).

Letészem a lantot. Nyugodjék
Tõlem ne várjon senki ...
J. Arany

Epilogue

"...*difficile est saturam non scribere,.*" said Juvenal. "*sed difficilior est saturam scribere*" is my conclusion.
If it is true for satire it is even truer for magnetism. Volumes of books have been written about the subject in the last century. Some are good some are not so good. Some explore the mystical theory of the magnetic effects others concentrate on the physics and the practicalities behind the phenomena. No doubt they all contribute piecemeal to the general knowledge of this rather difficult subject.

This book is my contribution, as a single building brick, to the Library of Knowledge on Magnetism.

I feel obliged to give the translations of the two quotations used in this book at the beginning and at the end. Although a large percentage of the readership would understand and enjoy these quotations in the original language, nevertheless I could not take away the enjoyment from the rest of the scientific community, not so familiar with this strange tongue. The translated passages show, no doubt in my mind, the epitome of my poetical flair and although I might not get the full approval of *Arany* for the translations, as a modern verse monger, I feel I am not very far from the correct, *modern* interpretation of the original passages, in English.

Egy kis független nyugalmat
Melyben a dal megfoganhat,
Kértem kérve
S õ halasztá évrül-évre.

J. Arany

I've longed for independence, peace
For making book writing at ease.
That was denied for years and years
Forty odd ones to be "précis".

Letészem a lantot. Nyugodjék.
Tõlem ne várjon senki ...

J. Arany

I put my *biro* down to rest
I've stopped here! Now do *your* best.

Mathematics of Hysteretic Phenomena. Jeno Takács

ISBN: 3-527-40401-5

Bibliography

Aharoni, A. (1959) Some recent developments in micromagnetics at the Weizman Institute of Science. J. Appl. Phys. **30**, 70S–78S.

Aharoni, A. (1966) Magnetization Curling. Phys. Stat. Sol. **16**, 3–42.

Aharoni, A. (1992) Susceptibility, resonance and magnetic viscosity. Phys Rev. B. **46**, 5434–5441.

Aharoni, A. (1996) *Introduction to the Theory of Ferromagnetism* (Clarendon Press, Oxford).

Andrei, P. and Stancu, A. (2000) Identification method analysis for the scalar generalized moving Preisach model using major hysteresis loops. IEEE. Trans. Magn. **36**, **No.4**, 1982–1989.

Axon, P.E. (1952) An investigation into the mechanism of magnetic tape recording. Inst. Elect Eng., Pt.III, **99**, 109–126.

Becker, R. and Doring, W. (1938) *Ferromagnetismus* (Springer-Verlag, Berlin).

Becker, R. and Doring, W. (1939) *Ferromagnetismus* (Springer-Verlag, Berlin).

Bedford, L.H. (1959) Magnetic tape recording, Electronic Radio Eng. **36**, **No.9**, 320–322.

Berkov, D.V. (1992) On the concept of the magnetic viscosity, analytic expression for the time dependent magnetization. J. Magn. Magn. Mater. **111,** 327–329.

Bernard, Y., Mendes, E. and Ren, Z. (2000) COMPEL Int. J. Comp. Math. E. E. Eng. **19**, **No.4**, 997–1006.

Bertham, H.N. (1974) Long wavelength AC bias recording theory. IEEE Trans. Magn. **Mag-10**, **No.4**, 1039–1048.

Bertotti, G. (1996) Energetic and thermodynamic aspects of hysteresis. Phys. Rev. Lett. **76**, **No.10**, 1739–1742.

Bertotti, G. (1998) *Hysteresis in Magnetism* (Academic Press, London, UK).

Bertotti, G., Basso V. and Durin G.J. (1996) Randomfree energy model for the description of hysteresis. J. Appl. Phys. **79**, 5764–5766.

Binns, K.J., Lawrenson, P.J. and Towbridge, C.W. (1992) *The Analytical and Numerical Solution of Electric and Magnetic Fields* (J. Wiley and Sons, Chichester).

Boltzman, L. (1896–98) *Vorlesungen über Gastheorie* (J.A. Burth, Leipzig).

Boltzman, L. (1962) *Lectures* (California University Press, Berkley).

Bottoni, G., Candolfo, D. and Cecchetti, A. (1997) Interaction effects of the time dependence of the magnetization in recording particles. J. Appl. Phys. **81,** 3809–3811. Bozorth R.M. (1951). *Ferromagnetism* (Van Nostrand, N.Y.).

Brauer, J.R. (1975) Simple equations for the magnetization and reluctivity curves of steel. IEEE Trans. Magn. **MAG-11**, **No.1**, 81.

Brillouin, M.L. (1927). Les moments de rotation et le magnetisme dans la mechanique ondolatoIRE J. de Phys. Radium **VIII**, 74–84. Brown W.F. (1959) Micromagnetics domains and resonances. J. Appl. Phys. **30**, 62S–69S.

Brown, W.F. (1963) *Micromagnetics* (J. Wiley and Sons, N.Y.).

Brown, W.F. (1978) *Micromagnetics* (Robert Krieger, Malabar, Florida).

Brown, W.F. and LaBonte, A.E. (1965) Structure and energy of one-dimensional domain walls in ferromagnetic films. J. Appl. Phys. **36**, **No.4**, 1380–1386.

Calkins, F.T. and Flatau, A.B. (1996) Transducer based measurements of Terfenol-D material properties. SPIE Proc: Smart Structures and Integrated Systems **2717,** 709–719.

Calkins, F.T., Smith, R.C. and Flatau, A.B. (2000) Energy-based hysteresis model for magnetostrictive transducers. IEEE Trans. Magn. **36**, **No.2**, 429–439.

Camras, M. (1949) Graphical analysis of linear magnetic recording using high frequency excitation. Proc. Inst. Radio Eng. **37**, 569–573.

Carlson, W.L. et al. (1927) US Patent 1,640,881 August

Carpenter, K.H. (1991) A differential equation approach to minor loops in the Jiles-Atherton hysteresis model. IEEE Trans. Magn. **27**, 4404–4406.

Chikazumi, S. (1986) *Physics of Magnetism* (Robert E. Krieger Publ. Co. Malabar, Florida).

Mathematics of Hysteretic Phenomena. Jeno Takács

ISBN: 3-527-40401-5

Chikazumi, S. (1997) *Physics of Ferromagnetism* (Clarendon Press, Oxford).

Chua, L.O. and Stromsmoe, K.A. (1970) Lumped-circuit models for nonlinear inductors exhibiting hysteresis loops. IEEE Trans on Circuit Theory **17**, 564–574.

Chua, L.O. and Bass, S.C. (1972) A generalised hysteresis model. IEEE Trans. Circuit Theory **19**, 36–48.

Curie, P. (1895) Magnetic properties of bodies at various temperatures. Ann. Chim. Phys. **V**, 289–405

Dapino, M.J., Smith, R.C. and Flatau, A.B. (2000) Structural magnetic strain model for magnetostrictive transducers. IEEE Trans. Magn. **36**, **No.3**, 545–556.

Davis, N. (1971) Derivation and application of an equation to the B–H loop. J. Appl. Phys. **4**, 1034–1039.

Della Torre, E. (1999) *Magnetic Hysteresis* (IEEE Press, N.Y.).

Della Torre, E. and Vajda, F. (1994) Parameter identification of the complete-moving hysteresis model using major loop data. IEEE Trans. Magn. **MAG-30**, 4987–5000.

Della Torre, E. and Kádár, G. (1987) Hysteresis modeling II: Accommodation. IEEE Trans. Magn. **Mag-27**, 3811–3814.

Della Torre, E. and Bennett, H. (1998) A Preisach model for aftereffect. IEEE Trans. Magn. **MAG-34**, 1276–1278.

Della Torre, E. (1998) Hysteresis modelling. COMPEL Int. J. Comp. Math. E. E. Eng. **17**, **No.5/6**, 682–689.

Del Vechio, P., Salvini, A., Carrarini, I. and Veca, G. M. (1998) Ferromagnetic materials excited by a distorted periodic field source. COMPEL Int. .J. Comp. E. E. Eng. **17**, **No.3**, 398–491.

Deskur, J. (1998) Models of magnetic circuits and their equivalent electrical Diagrams. COMPEL Int. J. Comp. Math. E. E. Eng. **18**, **No.4**, 600–610.

Dugdale, J.S. (1996) *Entropy and its Physical Meaning* (Taylor and Francis, London).

Dupas, C., Beauvillain, P., Chapert, C. Renard, J.P., Trigui, F., Veillet, P. and Velu, E (1990) Very large magnetoresistance effect induced by antiparallel magnetization in two ultrathin cobalt films. J. Appl Phys. **67**, **No.9**, 5680–5682.

Eldridge, D.F. and Daniel, E.D. (1962) New Approach to ac Biased Magnetic Recording. IRE Natl. Conv. Record, **Pt.7**, 33–41.

El-Hilo, M., O'Grady, K., Chantrell, R.W. and Dickson, D.P.E. (1993) Time dependent magnetisation in systems with distributed energy barriers. J. Magn. Magn. Mater. **123**, 30–34.

El-Hilo, M., O'Grady, K. and Chantrell, R.W. (1992) The origin of non-linear ln(t) behaviour in the time dependence of magnetisation. J. Magn. Magn. Mater. **109**, L164–L168.

Elmen, G.W. (1928) Magnetic properties of perminvar. J. Franklin Inst. **206**, 317–338.

Evershed, S. (1891) The magnetic circuit of transformers: closed versus open. The Electrician **XXVI**, 477, 508, 534, 597, 634, 662, 690, 724, 755, 784.

Ewing, J.A. (1893) *Magnetic Induction in Iron and Other Metals* (The Electrician Publishing Co., London).

Ewing, J.A. (1881) Effects of stress on the thermoelectric quality of metals. Proc. Roy. Soc. **XXXII**, 399–402.

Ewing, J.A. (1882) On the production of transient currents in iron and steel conductors by twisting when magnetised or by magnetising them when twisted. Proc. Roy. Soc. **XXIII**, 21–23.

Ewing, J.A. (1882) On effects of retentiveness in the magnetisation of iron and steel. Proc. Roy. Soc. **XXXIV**, 39–45.

Ewing, J.A. (1889) Time lag in the magnetization of iron. Proc. Roy. Soc. **XLVI**, 260–286.

Faiz, J. and Sharifian, M.B.B. (2001) Hysteresis loop modeling techniques and hysteresis loss estimation of soft magnetic materials. COMPEL Int. J. Comp. Math. E. E. Eng. **20**, **No.4**, 988–1001.

Fisher, J. and Moser, H. (1956) Die Nachbildung von Magnetisierungscurven durch einfache algebraishe oder transzendente Funktionen. Archiv fur Electrotechn. **XLII**, **5**, 286–299.

Frõlich, O. (1881) Investigations of dymoelectric machines and electric power transmission and theoretical conclusions therefrom. Electrotech. Z. **2,** 134–141.

Friedman, G. (1990) New formulation of the Stoner-Wohlfart hysteresis model and the identification problem. J. Appl. Phys. **67, No.9**, 5361–5363.

Füzi, J. (1999) Computationally efficient rate dependent hysteresis model. COMPEL Int. J. Comp. Math. E. E. Eng. **18, No.3**, 445–457.

Gerlach, W. and Stern, O. (1924) Über die Richtungsquantelung im Magnetfeld. Ann. Phys. (Leipzig) **47, No.16**, 673–699.

Globus, A. (1962). Influence des dimensions des parois sur la permeabilite initiale. Comptes Rendus Acad. Seances, **255**, 1709–1711.

Globus, A and Duplex, P. (1966). Separation of susceptibility mechanisms for ferrites of low anisotropy. IEEE Trans. Magn. **2**, 441–445.

Globus, A. and Guyot, M. (1972) Wall displacement and bulging in magnetization mechanism of the hysteresis loop. Phys. Stat. Sol., **B52**, 427–431.

Goodman, A.M., O'Grady, K., Laidler, H., Owen, N.W., Portier, X., Petford-Long, A.K and Cebollada, F. (2001) Magnetization reversal process in exchange-biassed spin-valve structures. IEEE, Trans. Magn. **37, No.1**, 565–570.

Gould, A., Bhagat, S.M., Manheimer, M.A. and Tyagi, S. (1990) Field-induced microwave absorption in high-T_c superconductive powders: evidence for a superconducting glass phase at low T. J. Appl. Phys. **67, No.9,** 5020–5025.

Greiner, F. (1955) Das Feld im Sprechckopf mit und ohne Band. Nachrichten Technik **5**, 295–298 and 351–354.

Hadfield, D. (1962) *Permanent Magnet and Magnetism* (Iliffe Books, London).

Herbert, J.R. and Patterson, D.W. (1965) A computer simulation of the magnetic recording process. IEEE Trans. Magn.**1, No.4**, 352–357.

Hodgdon, M.L. (1988) Mathematical theory and calculations of magnetic hysteresis curves. IEEE Trans. Magn. **14, No.6**, 3120–3122.

Holmes, L.C. and Clark, D.L. (1945) Supersonic bias for magnetic recording. Electronics **18**, 126–136.

Hoselitz, K. (1952) *Ferromagnetic Properties of Metals and Alloys* (Oxford University Press, Oxford).

Hwang, J.H. and Lord, W. (1976) Exponential series for B/H curve modelling. Proc. IEE **123, No.6**, 559–560.

Igarashi, H., Lederer, D., Kost, A., Honma, T. and Nakata, T. (1998) A numerical investigation of Preisach and Jiles models for magnetic hysteresis. COMPEL Int. J. Comp. Math. E. E. Eng. **17, No.1/2/3**, 357–363.

Iványi, A. (1997). *Hysteresis Models in Electromagnetic Computation* (Akademiai Kiado, Budapest).

Iványi, A. (1998) *Magnetic Field Computation with R-functions* (Akademiai Kiado, Budapest).

Jiles, D.C. and Atherton, D.L. (1984) Theory of ferromagnetic hysteresis. J. Appl. Phys. **55, (6)15**, 2115–2120.

Jiles, D.C. and Atherton, D.L. (1986) Theory of ferromagnetic hysteresis. J. Magn. Magn. Mater. **61**, 48–60.

Jiles, D.C. and Hariharan, S. (1990) Interpretation of the magnetization mechanism in Terfenol-D using Barkhausen pulse height analysis and irreversible magnetostriction. J. Appl. Phys. **67, No.9**, 5013–5015.

Jiles, D.C. (1991) *Magnetism and Magnetic Materials* (Chapman and Hall, N.Y.).

Jiles, D.C. (1998). *Introduction to Magnetism and Magnetic Materials* (Chapman and Hall, N.Y.).

Jiles, D.C., Thoelke, J.B. and Devine, M.K. (1992) Numerical Determination of Hysteresis Parameters for the Modeling of Magnetic Properties Using the Theory of Ferromagnetic Hysteresis. IEEE Trans. Magn. **28, No.1**, 27–35.

Jordan, H. (1924) Ferromagnetic constants for weak fields. Elek. Nachr. Tech. **1**, 7–29.

Joule, J.P. (1842) On a new class of magnetic forces. Ann. Electr. Magn. Chem. **8**, 219–224.

Josephs, R.H., Crompton, D.S. and Kraft, C.S. (1986) Characterisation of magnetic oxide recording media using Fourier Analysis of static hysteresis loops. IEEE Trans. Magn. **22**, **No.5**, 653–655.

Joule, J.P. (1847) On the effects of magnetism upon the dimensions of iron and steel bars. Phil. Mag. **XXX**, 76–87 and 225–241.

Kádár, G. (1989) The bilinear product model of hysteresis phenomena. Phys. Scr. **T25**, 161–164.

Kahler, G.R., Della Torre, E. and Vajda, F. (1994) Parameter identification of the complete-moving-hysteresis model for HTS steel. IEEE Trans. Magn. **30**, **No.6**, 4374–4376.

Karlquist, O. (1954) Calculation of the magnetic field in the ferromagnetic layer of a magnetic drum. Trans. of Roy. Inst. of Techn. Stockholm **No.86**, 1–27.

Kawai, T., Ma, B.M., Sankar, S.G. and Wallace, W.E. (1990) Effect of crystal alignment on the remanence of sintered NdFeB magnets. J. Appl. Phys. **67**, **No.9**, 4610–4612.

Kennard, E.H. (1938) *Kinetic Theory of Gases* (McGraw-Hill, N.Y.).

Kennelly, A.E. (1891) Magnetic reluctance. Trans. Am. IEE **8**, 485–517.

Kersten, M. (1938) *Problem der Technischer Magnetisirungscurve* (Springer, Berlin).

Kersten, M. (1943) *Grundlagen Theorie der Ferromagnetischer Hysterese und der Koerzitivkraft* (Hirzel, Berlin).

Korman, C. and Mayergoyz, I.D. (1996) Preisach model driven by stochastic inputs as a model for aftereffects. IEEE Trans. Magn. **MAG-32**, 4204–4209.

Kvarnsjo, L. and Engdahl, G. (1990) Examination of eddy current influence on the behaviour of a giant magnetostrictive functional unit. J. Appl. Phys. **67**, **No.9**, 5010–5012.

Lamont, J. (1867) *Handbuch des Mgnetismus* (Voss, Leipzig).

Langevin, M.P. (1905) Magnetisme et theorie des electrons. Ann. Chim. Phys. **V**, 70–127.

Lehman, S. (1964) Elektronische Datenverarbeitungen **6**, 165–172.

Lim, Y.-K. (1995) *Problems and Solutions on Thermodynamics and Statistical Mechanics* (World Scientific, Singapore).

Liorzou, F., Phelps, B. and Atherton, D.L. (2000) Macroscopic models of magnetization. IEEE Trans. Magn. **36**, **No.2**, 418–428.

Lowman, C.E. (1972) *Magnetic Recording* (McGraw-Hill Book Co., N.Y.).

Macfadyen, W.K., Simpson, R.R.S., Slater, R.D. and Wood, W.S. (1973) Representation of magnetisation curves by exponential functions. Proc. IEE **120**, **No.8**, 902–904.

Madelung, E. (1905) Über Magnetisierung durch schnellverlaufende Strome und die Wirkungweise der Rutherford-Markoni Magnetodetektors. Ann. Phys. **17**, **No.5**, 861–863.

Mayergoyz, I.D. and Keim, T.A. (1990) Superconducting hysteresis and the Preisach model. J. Appl. Phys. **67**, **No.9**, 5466–5468.

Mayergoyz, I.D. (1991) *Mathematical Models of Hysteresis* (Springer-Verlag, N.Y.).

Mayergoyz, I.D. (1986) Mathematical models of hysteresis. Phys. Rev. Lett. **56**, 1518–1521.

Mayergoyz, I.D. and Keim T. A. (1990) Superconducting hysteresis and the Preisach model. J. Appl. Phys. **67**, **No.9**, 5466–5468.

Mayergoyz, I.D. and Friedman, G. and Salling, C. (1989) Comparison of the classical and the generalised Preisach hysteresis models with experiment. IEEE Trans. Magn. **25**, 3925–3927.

Mayergoyz, I.D., Adly, A.A. and Friedman, G. (1990) New Preisach-type models of hysteresis and their experimental testing. J. Appl. Phys. **67**, 5373–5375.

Mayergoyz, I.D. and Friedman, G. (1988) Generalised Preisach model of hysteresis. EEE Trans. Magn. **24**, 212–217.

Mayergoyz, I.D. (1988) Dynamic Preisach model of hysteresis. IEEE Trans. Magn. **24**, 2925–2927.

McCaig, M and Clegg, A.G. (1987) *Permanent Magnets in Theory and Practice* (Pentech Press, London).

Mee, C.D. (1962) Applications and limitations of the new magnetic recording model. IRE Trans. Audio. **10**, **No.6**, 161–163.

Mee, C. D. (1984) *The Physics of Magnetic Recording* (North-Holland Publishing Co., Amsterdam).

Mee, C.D. and Daniel, E.D. (1988) *Magnetic Recording* (McGraw-Hill Book Co., N.Y.).

Mee, C.D. (1986) *The Physics of Magnetic Recording* (North-Holland Publishing Co., Amsterdam).

Miyata, J.J. and Hartel, R.R. (1959) The recording and reproduction of signals on magnetic medium using saturation-type recording. IRE Trans. Electronic Computers. June, 159–169.

Morrish, A.H. (1965) *The Physical Principles of Magnetism* (J. Wiley and Sons, N.Y.).

Moffet, M.B., Clarke, A.E., Wun-Vodle, M., Linberg, J., Teter, J.P., and McLaughlin, E.A. (1991) Characterization of Terfenol-D for magnetostriction transducers. J. Acoust. Soc. Am. **89(3)**, 1448–1455.

Nogues, J. and Schuller, I.K. (1999) Exchange bias. J. Magn. Magn. Mater. **192**, 203–232.

Ossart, F. and Phung, T.A. (1990) Comparison between various hysteresis models and experimental data. J. Appl. Phys. **67**, **No.9**, 5379–5384.

Otani, Y., Sun, H., Coey, J.M.D., Davis, H.A., Manaf, A. and Buckley, R.A. (1990) Magnetic-field-induced alignment in melt-spun $Pr_2Co_{14}B$. J. Appl. Phys. **67**, 4616–4618.

Paceard, D., Schlenker, C., Massenet, O., Montmory, R. and Yelon, A. (1966) A new property of ferromagnetic-antiferromagnetic coupling. Phys. Stat. Sol. **16**, 301.

Parker, R.J. (1990) *Advances in Permanent Magnets* (John Wiley and Sons, N.Y.).

Pear, C.B. (1967) *Magnetic Recording in Science and Industry* (Reinhold Publishing Co., N.Y.)

Poulsen, V. (1899). Danish Patent No.2653 (1905). US Patent No.789,336.

Preisach, F. (1935) Uber die magnetishe Nachwirkung. Zeit. Physik. **94**, 277–302.

Priberio, A.L. (1990) AC bias recording and Preisach diagrams. J. Appl. Phys. **67**, **No.9**, 5382–5384.

Rayleigh, J.W. Lord (1887) On the behaviour of iron and steel under the operation of feeble magnetic force. The Philosophical Magazine **5**, **XXIII**, 225–245.

Rees, D.G. (1987) *Foundation of Statistics* (Chapman and Hall, London).

Restorff, J.B., Savage, H.T., Clark, A.E. and Wun-Fogle, M. (1990) Preisach modeling of hysteresis in Terfenol. J. Appl. Phys. **67**, **No.9**, 5016–5018.

Riberio, A.L. (1990) AC-bias recording and Preisach diagrams. J. Appl. Phys. **67**, **No.9**, 5382–5384

Rivas, J., Zamarro, L.M. Martin, E. and Pereira, C. (1981) Simple approximation for magnetization curves and hysteresis loops. IEEE Trans. Magn. **MAG-17**, **No.4**, 1498–1502.

Sablik, M.J. and Jiles, D.C. (1993) Coupled Magnetoelastic Theory of Magnetic and Magnetostrictive Hysteresis. IEEE Trans. Magn. **29**, **No.3**, 2113–2123.

Saito, Y. (1982) Three-dimensional analysis of magnetodynamic fields in electromagnetic devices taken into account the dynamic hysteresis loops. IEEE. Trans. Magn. **18**, **No.3**, 546–551.

Sebestyén, L.G. and Takács, J. (1961) Magnetic recording; theory of tape magnetisation. Electronic Technology Aug, 274–278.

Singleton, E.W. and Handjipanayis, G.C. (1990) Magnetic viscosity studies in hard magnetic materials. J. Appl. Phys. **67**. **No.9**, 4759–4761.

Snoek, J.L. (1938) Time effects in magnetization. Physica **5**, 663–688.

Snoek, J.L. (1941) Effect of small quantities of C and N on elastic and plastic properties of Fe. Physica **8**, 711–733.

Snoek, J.L. (1941) A mechanical counterpart to the Rayleigh law of ferromagnetic hysteresis. Physica **8**, 745–747.

Speliotis, D.E. (1990) On remanence loops and recording performance. J. Appl. Phys. **67**, **No.9**, 5358–5360.

Steinmetz, C. (1891). Note on the law of hysteresis. The Electrician. **No.659**, **XXVI**, 261–262. Stoner E. C. and Wohlfarth E. P. (1948) A mechanism of magnetic hysteresis in heterogeneous alloys. Phys. Trans. Roy. Soc. A **24**, 599–642.

Street, R. and Woolley, J.C. (1949) A study of magnetic viscosity. Proc. Phys. Soc. A **62**, 562–572.

Takács, J. (2001) A phenomenological mathematical model of hysteresis. COMPEL Int. J. Comp. Math. E. E. Eng. **20**, **No.4**, 1002–1014.

Takács, J. (2003) Fourier analysis of hysteretic distortions. COMPEL Int. J. Comp. Math. E. E. Eng. **22**, **No.2**, 273–284.

Takács, J. Laplace transforms of wave forms with hysteretic distortion. (To be published)

Takács, J. (1953) A Fourier amplitúdók meghatározása operatorszámitással. Magy. Hir. Techn. **4**, **No.7–8**, 93–96.

Takács, J. (1961) Notes on "Fourier Series Derivation" Proc. IEEE. **49**, **No.9**, 1446.

Taniguchi, S. (1956) Sci. Rept. Res. Inst. Tokohu Univ. A **8**, 173.

Taratorin, A., Cheng, D. and Marinero, E. (2000) Media Noise, Nonlinear Distortions and Thermal Stability in High Density Recording. IEEE Trans. Magn. **36**, **No.1**, 80–85.

Teape, J.W., Simpson, R.R.S., Slater, R.D. and Wood, W.S. (1974) Representation of characteristic, including hysteresis, by exponential series. Proc. IEE **121**, **No.9**, 1019–1020.

Toomin, H. and Wildfeuer, D. (1944) The Mechanism of Supersonic Frequencies as Applied to Magnetic Recording., Proc. Inst. Radio Eng. **32**, 664–668.

Trutt, F.C., Erdélyi, E.A. and Hopkins, R.E. (1968). Representation of the magnetization characteristic of DC machines for computer use. IEEE Trans. Power A Sys. **87**, **No.3**, 665–669.

Udpa, S.S. and Lord, W. (1985) A Fourier description model of hysteresis loop phenomena. IEEE Trans. Magn. **21**, **No.6**, 2370–2373.

Vajda, F., Della Torre, E., Pardávi-Horváth, M. and Vértesy, G. (1993) A variable variance Preisach model. IEEE Trans. Magn. **MAG-29**, 3793–3795.

Vajda, F. and Della Torre, E. (1994) Identification of parameters in an accommodation model. IEEE Trans. Magn. **20**, **No.6**, 4371–4373.

Vajda, F., Oti, J. and Della Torre, E. (1990) Rotational properties of vector phenomenological models of magnetic media. J. Appl. Phys. **67**, **No.9**, 5376–5378.

Warburg, E. (1881) Magnetische Untersuchungen. Ann. Physik. **13**, 141–164.

Weber, W. (1852) Über den Zuzammenhang der Lehre vom Diamagnetismus mit der Lehre von dem Magnetismus und der Elektricitat. Ann. Phys. Chem. (Pogg. Ann). **LXXXVII**, **No.10**, 145–189.

Wecker, J., Katter, M., Schnitzke, K. and Schultz, L. (1990) Magnetic hardening of Sm-Fe-Ti alloys. J. Appl. Phys. **67**, **No.9**, 4951–4953.

Weiss, P.E. (1906). La variacion du ferromagnetisme avec la temperature. Comptes Rendus **143**, 1136–1139

Weiss, P.E. (1907). L'hypothese du champ moleculare et la propriete ferromagnetique. J. Phys. **VI**, 661–690.

Weiss, P.E. (1910) Absolute value of intensity of magnetization at saturation. J. Phys. **9**, 373–393.

Westmijze, W.K. (1953) Studies on magnetic recording. Phillips Res. Rep. **8**.

Wetzel, W.W. (1947) Review of the present status of magnetic recording theory. Audio Eng., Nov. 31, 12–16. Dec. 31, 14–17. Jan. (1948). 32, 26–30.

Widger, G.F.T. (1969) Representation of magnetisation curves over extensive range by rational fraction approximations. Proc. IEE **116**, 156.

Wiegert, R.F. and Levy, M. (1990) Effects of gas exposure on the surface-acoustic-wave attenuation and magnetoresistance of nickel thin films. J. Appl. Phys. **67**, **No.9**, 4992–4994.

Willcock, S.N.M. and Tanner, B.K. (1983) Harmonic analysis of B-H loops. IEEE. Trans. Magn. **19**, **No.5**, 2265–2270.

Williams, H.J. and Goertz, M. (1952) Domain Structure of Perminvar having a rectangular hysteresis loop. J. Appl. Phys. **23**, **No.3**, 316–323.

Wlodarski, Z. and Wlodarska, J. (2001) Simplified analysis of circuits containing ferromagnetic cores without air gaps. COMPEL Int. J. Comp. Math. E. E. Eng. **20**, **No.4**, 914–922.

Wohlfarth, E.P. (1984) The coefficient of magnetic viscosity. J. Phys. F: Met. Phys. **14**, **1**, 155–159.

Woodward, J.G. and Della Tore, E. (1959) Magnetic Characteristics of Recording Tapes and the Mechanism of the Recording Process. J. Audio Eng. Soc. **7**, **No.4**, 189–195.

Zener, C. (1946) An elasticity in metals. Trans. Am. Soc. Mining. Met. Eng. **167**, 155–189.

Zirka, S.E. and Moroz, Y.I. (1995) Hysteresis modeling based on transplantation. IEEE Trans. Magn. **31**, 3509–3511

Zirka, S.E. and Moroz, Y.I. (1999) Hysteresis modeling based on similarity. IEEE Trans. Magn. **35**, **No.4**, 2090–2096.

Zolotariov, N.A. (1989) Matematichescoe modelirovanie magnitnogo gisterezisa. Electrichestvo **No.6**, 21–26.

Author Index

Mathematics of Hysteretic Phenomena. Jeno Takács

ISBN: 3-527-40401-5

Subject Index

Mathematics of Hysteretic Phenomena. Jeno Takács

ISBN: 3-527-40401-5